République Algérienne Démocratique et Populaire

Ministère de l'Enseignement Supérieure et de la Recherche Scientifique

Université Echahid Hamma Lakhdar d'El-Oued

Faculté de Sciences et de La Technologies Filière: Genie Electrique

Mémoire de fin d'étude

Présenté pour l'obtention du diplôme de

MASTER ACADEMIQUE

Domaine: Sciences et Technologie

Filière: Télécommunication

Spécialité: Systèmes de Télécommunication

Réalisé par: ZERROUD Youcef, KHALDI Oussama

Thème

Conception and electric simulation of solar cell

Devant le jury composé de:

Mr.	**Université Echahid Hamma Lakhdar**	**Président**
Mr.	**Université Echahid Hamma Lakhdar**	**Examinateur**
Mr.KATEB Mohamed Nadjib	**Université Echahid Hamma Lakhdar**	**Encadreur**

2023-2024

Abstract

In this work, we aimed to achieve the highest possible yield from perovskite solar cells by varying the thickness of the layers. Additionally, we explored semiconductors, solar radiation, and the different types and features of solar cells. From previous studies, We discovered that TiO_2 results in reduced cell performance. Consequently, we proposed using ZnO as an alternative due to its superior properties. Our results showed that incorporating ZnO increased the yield of the perovskite solar cells. Therefore, we believe that ZnO has great potential and should receive significant attention in future research and development.

Keywords: solar cell, Perovskite, SCAPS 1D.

ملخص

في هذا العمل، هدفنا إلى تحقيق أعلى عائد ممكن من خلايا الطاقة الشمسية البيروفسكايتية من خلال تغيير سمك الطبقات. بالإضافة إلى ذلك، استكشفنا أشباه الموصلات والإشعاع الشمسي وأنواع وخصائص الخلايا الشمسية المختلفة. من الدراسات السابقة، اكتشفنا أن TiO_2 يؤدي إلى تقليل أداء الخلية. لذلك، اقترحنا استخدام ZnO كبديل بسبب خصائصه المتفوقة. أظهرت نتائجنا أن دمج ZnO زاد من عائد خلايا الطاقة الشمسية البيروفسكايتية. وبالتالي، نعتقد أن ZnO لديه إمكانيات كبيرة ويجب أن يحظى باهتمام كبير في الأبحاث والتطوير المستقبلية .

الكلمات المفتاحية: خلية شمسية، بيروفسكايت، .SCAPS 1D.

Résumé

Dans ce travail, nous avons visé à obtenir le rendement le plus élevé possible des cellules solaires à pérovskite en variant l'épaisseur des couches. De plus, nous avons exploré les semi-conducteurs, le rayonnement solaire, ainsi que les différents types et caractéristiques des cellules solaires. D'après des études antérieures, nous avons découvert que le TiO_2 réduit les performances des cellules. Par conséquent, nous avons proposé d'utiliser le ZnO comme alternative en raison de ses propriétés supérieures. Nos résultats ont montré que l'incorporation du ZnO a augmenté le rendement des cellules solaires à pérovskite. Par conséquent, nous pensons que le ZnO a un grand potentiel et devrait recevoir une attention significative dans les recherches et développements futurs.

Mots-clés : cellule solaire, pérovskite, SCAPS 1D.

Dedication

This humble work is dedicated to my dear parents ,whose love ,appreciation dedication ,and respect I hold in the highest regard.

Nowords can truly express the depth of my gratitude for the countless efforts you made day and night ,for my education and well-being.

Thes work stands as a testament to the sacrifices you made for my education and training.

To my brothers ,my sisters ,my entire family ,and my friends ,I extend my heartfelt thanks and appreciation .

Acknowledgments

First and foremost, I would like to thank **God Almighty** for giving me the strength, knowledge, ability and opportunity to undertake this research study and to persevere and complete it satisfactorily. Without his blessings, this achievement would not .have been possible

I would like to thank the following people for helping with this research project: I express my gratitude to**Dr KATEB Mohamed Nadjib** as supervisor of this work, by his,knowledge, time, dedication, guidance support, encouragement and invaluableadvises.throughout of this work to achieve the Master degree

Table of contents

Table of figures

List of tables

Abbreviations list

F_{cc}	face-centred Cubic
TCO	Transparent Conductive Oxide
E_F	Fermi energy
K	Boltzmann constant
T	Temperature
N	The density of free electrons
N_c	Conduction Band Density
N_D	Donor Density
N_v	Valence Band Density
E_i	intrinsic level
n_i	intrinsic carrier density
E_A	Acceptor level
E_D	Donor level
ETA	Efficinecy
E_g	Energy Band
E_v	Valence Band
E_c	Conduction Band
FF	Fill Factor
I	current
V	voltage
I_{max}	Maximum current
I_{ph}	Photon Current
I_{sc}	Shor Circuit Current
PV	Photovoltaic
P_{max}	Maximum Power Point
R_s	Series Resistance
R_{sh}	Shunt Resistance
V_{oc}	Open Circuit Voltage
V_{max}	Maximum Voltage
V_{th}	Thermodynamics Voltage
PSC	Perovskite Solar Cell

PCE power conversion efficiency

NiO_x Nitric Oxide

ZnO Zinc oxide

TiO_2 Titanium dioxide

$CH_3NH_3PbI_3$ Methylammonium lead iodide

General Introduction

Ever since the discovery of electricity, the overriding concern has been how to generate it in the most efficient manner possible. Traditional methods of electricity generation, such as coal, natural gas, and nuclear energy, have dominated the energy landscape for decades [1] [2]. However, these sources have significant drawbacks, including environmental degradation, pollution, and the depletion of non-renewable resources [3] [4]. Therefore, it is crucial to develop and adopt alternative sources of energy that can meet the growing demand while ensuring sustainable development and environmental preservation.

Renewable energy sources such as solar, wind, hydro, geothermal, hydrokinetic, bioenergy, and hydrogen are gaining attention for their potential to provide clean, sustainable, and inexhaustible power [5][6]. These sources are considered environmentally friendly and are essential for reducing the carbon footprint and mitigating the effects of climate change.

Among these renewable sources, photovoltaic (PV) energy, which involves the use of solar cells, stands out as one of the leading environmentally friendly options. Solar energy is particularly accessible and cost-effective compared to other renewable sources[7][8]. Solar cells, based on semiconductor technology, convert sunlight into electricity. This conversion process is clean and sustainable, making solar energy an inexhaustible power source [9] [10].

The first chapter provides an overview of the basic properties and characteristics of semiconductors. It covers topics such as crystal structures, classification of materials into conductors, insulators and semiconductors, intrinsic and extrinsic semiconductors, and the emerging perovskite materials with their unique structure and potential applications in solar cells.

The second chapter covers the fundamentals of how solar cells work - detailing the properties of solar radiation, photon absorption to generate charge carriers in semiconductors, recombination mechanisms, and modeling the ideal and practical solar cell behavior. It also overviews three generations of solar cell technologies aimed at improving efficiency and lowering costs.

The third chapter focuses on introducing the SCAPS-1D solar cell simulation program. It explains the fundamental semiconductor equations used by SCAPS,

describes the user interface and various panels/functions for defining the solar cell structure, setting parameters, running different types of simulations (single, batch, etc.), and visualizing the results such as energy band diagrams, I-V curves, and other characteristics.

The fourth chapter we will optimize perovskite solar cell by changing the thickness of the absorber layer, we will compare between different TOC results.

Finally, we will end this thesis with a conclusion that resume our work and the main results we will obtain from simulation

Chapter 1:

Basic properties of Semiconductor

1.1 Introduction

Semiconductors are the cornerstone of modern electronics, featuring prominently in a range of devices from computers to solar cells. These materials, which include elemental semiconductors like silicon (Si) and germanium (Ge), as well as compound semiconductors such as gallium arsenide (GaAs), possess unique electrical properties due to their crystal structures. The diamond lattice of Si and Ge, and the zinc blende lattice of GaAs, allow for controlled conductivity, crucial for electronic applications. This introduction explores the fundamental characteristics of semiconductors, highlighting their crystal structures, conduction mechanisms, and the role of doping in modifying their electrical properties. Additionally, the promising perovskite structures, known for their potential in solar technology, are briefly discussed. Understanding these basic principles is essential for advancing semiconductor technologies and their diverse applications.

1.2 Crystal structure

The semiconductors that are most commonly utilized are single crystals with a diamond (with Si and Ge) or zinc Blende (with GaAs and other compound semiconductors) lattice type as showing in Fig.1.1.

The composition of both lattices can be viewed as two interpenetrating face-centred Cubic (fcc) sublattices that are displaced by one quarter of the distance along the diagonal of The cube. All atoms in the diamond lattice are identical, while the two fcc sublattices are built Of different atoms in the case of III–V compounds such as GaAs. Each atom is surrounded by four close neighbours belonging to the other fcc sublattice [13].

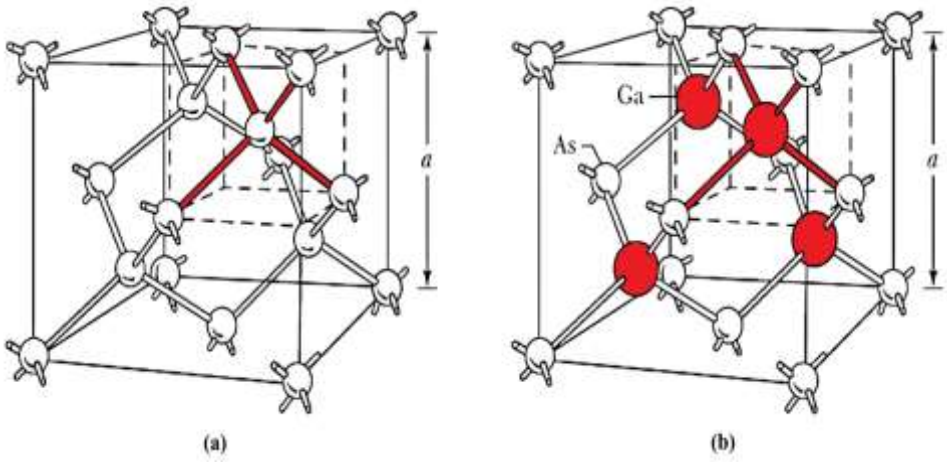

Figure 1.1 (a) Diamond lattice, (b) Zinc blende lattice [13].

1.3 Element semiconductors

In the early 19th century, the study of semiconductor materials began. Many semiconductors have been studied over the years. A portion of the periodic table related to semiconductors is shown in Table 1.1. Silicon (Si) and germanium (Ge) are two semiconductor elements composed of a single species of atoms found in Column IV. During the early 1950s, germanium was the primary semiconductor material. Since the early 1960s silicon has become a practical substitute and has now virtually supplanted germanium as a semiconductor Material. The main reasons we now use silicon are that silicon devices exhibit better properties at room temperature, and high-quality silicon dioxide can be grown thermally. There are also economic considerations. Device-grade silicon costs much less than any other semiconductor material. Silicon in the form of silica and silicates comprises 25% of the Earth's crust, and silicon is second only to oxygen in abundance. Currently, silicon is one of the most studied elements in the periodic table, and silicon technology is by far the most advanced among all semiconductor technologies [12].

Column / Period	II	III	IV	V	VI
2		5 B Boron 10.81	6 C Carbon 12.011	7 N Nitrogen 14.007	8 O Oxygen 15.999
3	12 Mg Magnesium 24.32	13 Al Aluminium 26.98	14 Si Silicon 28.085	15 P Phosphorus 30.97	16 S Sulfur 32.065
4	51 Zn Antimony 121.76	31 Ga Gallium 69.72	32 Ge Germanium 72.63	33 As Arsenic 74.92	34 Se Selenium 74.92
5	48 Cd Cadmium 112.411	49 In Indium 114.82	50 Sn Tin 118.71	51 Sb Antimony 121,76	52 Te Tellurium 127,6
6	80 Hg Mercury 200.59		82 Pb Lead 207.2		

Table 1.1 Portion periodic table related to semiconductors.

1.4 Conduction in metals, semiconductors, and insulators

The vast difference in how well metals, semiconductors, and insulators conduct electricity can be explained by looking at their energy bands. These bands represent the allowed energy levels for electrons within a material. Figure 1.2 shows the energy band diagrams of three classes of solids: metals, semiconductors, and insulators [14] [15].

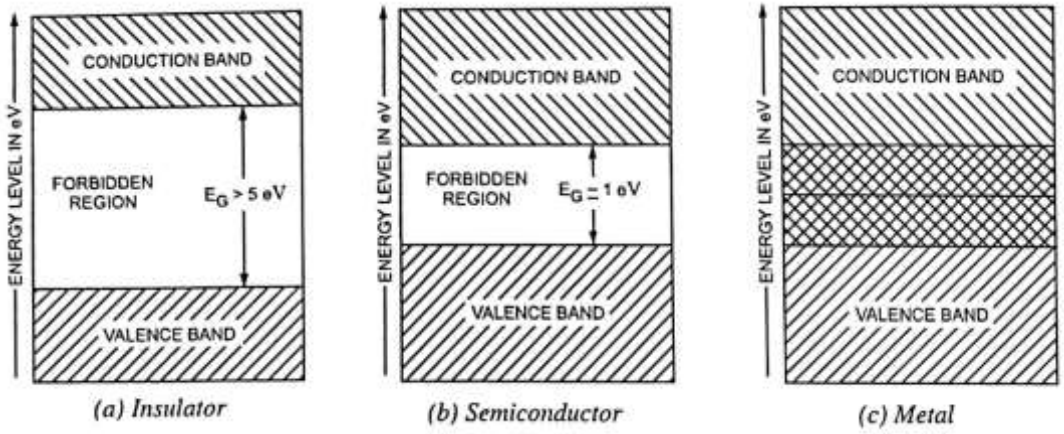

Figure 1.2 Schematic energy band representations of (c) a conductor (the overlapping bands), (b) a semiconductor, (a) an insulator.

a) Insulators

In case of insulators, there is practically no electron in the conduction band, and the valence band is filled. For an insulator, the valence and conduction bands are so apart (more than 5 eV) that at normal temperature (25°C) the energy which can be supplied to an electron from an applied field is too small to carry a particle from the filled band into the vacant band. Since the electron cannot acquire externally applied energy, conduction is impossible. Only at very high temperature or under high external electric field, an electron can jump the gap. This is called the breakdown of the insulating material [14].

b) Semiconductor

For semiconductors at a temperature of absolute zero (-273.15°C) the valence band is usually full and there may be no electron in the conduction band. It means that no current can flow in the semiconductors and, therefore, the Energy Band Diagram of Semiconductors behaves as insulators at absolute zero temperature. However, in semiconductor materials, both bands are so close (about 1 eV apart) that an electron can be lifted from the valence band to the conduction band by imparting

some energy to it. This energy must be more than energy gap E_G. If the energy imparted to the electron is less than E_G, it cannot be lifted from valence band to conduction band because no permissible energy level exists between the two bands. The energy imparted by the heat at room temperature is sufficient to lift electrons from the valence band to the conduction band. Some electrons do jump the gap and get into the conduction band. Thus, Energy Band Diagram of Semiconductors is capable of conducting some electric current, even at normal ambient temperature [2].

c) Metal

In case of conducting materials (metals), there is no forbidden gap, and the valence and conduction bands overlap each other, as illustrated in Fig. 1.2 (c). The orbits in the conduction band are very large. An electron in the conduction band experiences almost negligible nuclear attraction. In fact, an electron in the conduction band does not belong to any particular atom. But it moves randomly throughout the solid. This is the reason that electrons in the conduction band are called the free electrons. Due to overlapping of valence and conduction bands, a slight potential difference across the conductor causes the free electrons to constitute electric current.

1.5 Intrinsic semiconductors

Intrinsic semiconductors contain no (in practice, very few) impurities compared with the number of thermally generated electrons and holes. For this condition we shall attempt to estimate the number of free charge carriers (electrons and holes) under equilibrium conditions. The occupation probability for an electronic state is given by the Fermi Dirac function [1].

$$f(E) = \frac{1}{1+\exp\left(\frac{E-E_F}{k*T}\right)} \tag{1.1}$$

Where E_F, the Fermi energy, is the energy at which the occupation probability of a (possible) state is one half, k is the Boltzmann constant and T is the absolute temperature.

The density of free electrons n is obtained by integrating the carrier concentration (Fig. 1.3(d)) given by the product of the density of states N (Fig.1.3 (b)) and the occupation probability $F_n(E)$ (Fig. 1.3(c)) over the conduction band:

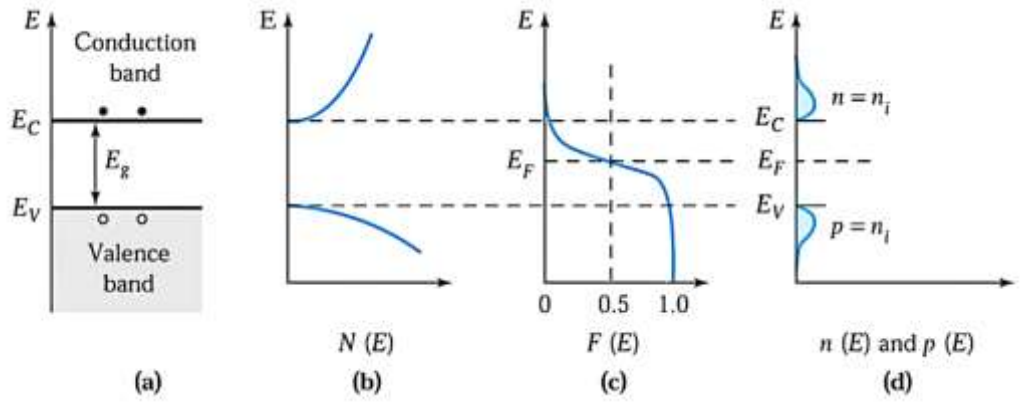

Figure 1.3 Intrinsic semiconductor: (a) Schematic band diagram, (b) Density of states, (c) Fermi distribution function, (d) Carrier concentration.

$$n = 2\left(\frac{2\pi m_n kT}{h^2}\right)^{\frac{3}{2}} e^{-\frac{E_C - E_F}{kT}} = N_C e^{-\frac{E_C - E_F}{kT}} \quad (1.2(a))$$

Similarity for holes, we have:

$$p = 2\left(\frac{2\pi m_p kT}{h^2}\right)^{\frac{3}{2}} e^{-\frac{E_F - E_V}{kT}} = N_V e^{-\frac{E_F - E_V}{kT}} \quad (1.2(b))$$

N_C And N_V are the effective densities of states in the conduction and valence bands respectively. The product of electron and hole concentration, given by $\cdot p = N_C N_V e^{-\frac{E_C - E_V}{kT}}$, depends on the band gap $E_G = E_C - E_V$ and is thus independent of the Fermi level E_F.

So far the value of the Fermi level E_F has not been specified and equations (1.1) to (1.2) will also be valid for extrinsic semiconductors (to be dealt with in the following chapter). The Fermi level for intrinsic semiconductors E_i can be found from the requirement that the numbers of electrons and holes are equal: $n = p = n_i$. One thus finds that:

$$n_i = \sqrt{N_C N_V} e^{-\frac{E_C - E_V}{2kT}} = \sqrt{N_C N_V} e^{-\frac{E_G}{2kT}} \quad (1.3)$$

And

$$E_i = \frac{E_C + E_V}{2} + \frac{3kT}{4} \ln\left(\frac{m_p}{m_n}\right) \quad (1.4)$$

Where E_i is the Fermi level close to the middle of the band gap, the deviation being due to the unequal effective masses of electrons and holes.

Introducing the intrinsic carrier density n_i and the intrinsic level E_i, one may reformulate the more generally valid (1.2) in the useful form:

$$n = n_i e^{\frac{E_F - E_i}{kT}} \qquad p = n_i e^{\frac{E_i - E_F}{kT}} \tag{1.5}$$

1.6 Extrinsic semiconductors

Intrinsic semiconductors are rarely used in semiconductor devices since it is extremely difficult to obtain sufficient purity in the material. Moreover, in most cases one intentionally alters the property of the material by adding small fractions of specific impurities. This procedure, which can be performed either during crystal growth or later in selected regions of the crystal, is called doping. Depending on the type of added material, one obtains n-type semiconductors with an excess of electrons in the conduction band or p-type with additional holes in the valence band. We will look at extrinsic semiconductors through the simple bond representation and also through a band model [13].

Figure 1.4(a) shows a two-dimensional schematic bond representation of a silicon crystal with one silicon atom replaced by an arsenic atom with five valence electrons. Only four are used for the formation of covalent bonds with neighboring atoms, while the fifth is not bound to a specific atom but is free for conduction. It should be stressed that the crystal as a whole remains uncharged, since the charge of the free electron is compensated for by the excess charge of the arsenic nucleus bound in the crystal lattice [13].

If a silicon atom is replaced by an atom with only three valence electrons (Fig. 1.4(b)) one electron is missing in the covalent bonds and a hole is thus created. This hole may be filled by an electron from a neighboring atom, this being equivalent to a movement of the hole. The hole is free for conduction. (That the moving hole is more than a missing electron whose place is filled by a neighboring electron follows from quantum mechanical considerations and is experimentally verified in the Hall experiment [13].

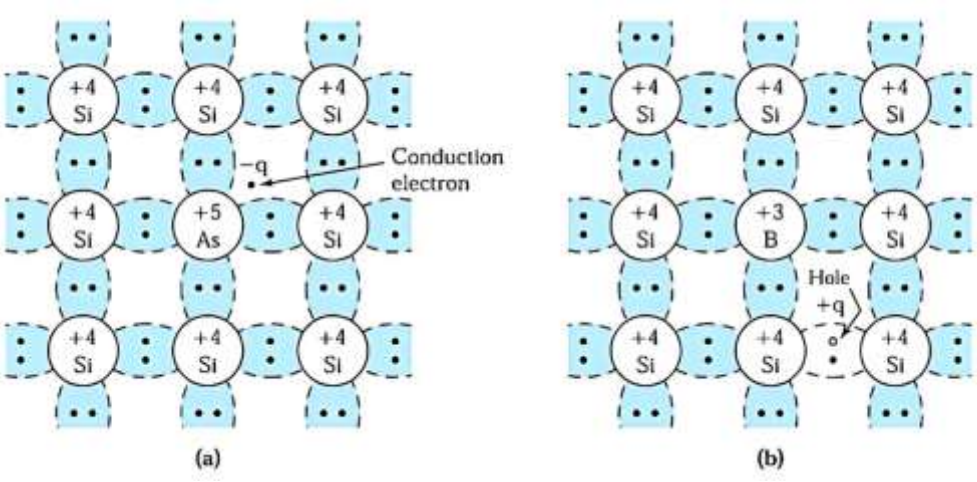

Figure 1.4 Schematic bond pictures for (a) n-type Si with donor (arsenic) and (b) p type Si with acceptor (boron).

Looking at the situation in the band model, we can state that the replacement of a proper atom of the lattice by a different atom is accompanied by the creation of localized energy levels in the band gap. These energy levels may be of the donor (E_D) or acceptor (E_A) type. If donor levels E_D are close to the conduction band, as is the case for phosphorous ($E_C - E_D = 0.045$ eV) or arsenic ($E_C - E_D = 0.054$ eV) atoms in silicon, for instance, these states will transported to the conduction band (Fig. 1.5 a). This is due to the many states with similar energy level nearby in the conduction band, with which the donor states have to share their electrons.

Equivalent considerations hold for acceptor-type states, e.g. boron in silicon ($E_A - E_V = 0.045$ eV). These states will be filled almost completely and holes will be created in the valence band (Fig. 1.5 b).

The situation that the donor levels are almost completely ionized can be described by a movement of the Fermi level E_F from the intrinsic level E_i towards the conduction band. Up to fairly high doping concentrations, the value of E_F follows from (1.2) by setting the electron concentration in the conduction band *n* equal to the donor concentration N_D, thus:

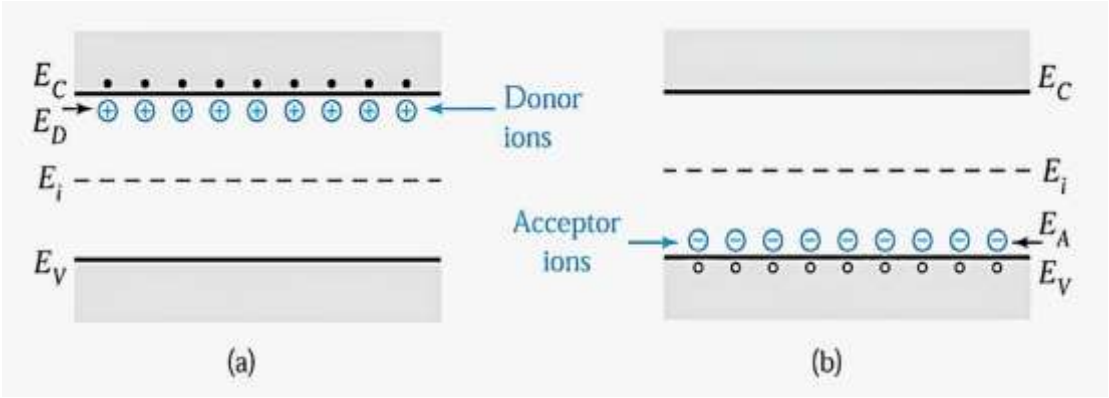

Figure 1.5 (a) Schematic energy band representation of extrinsic n-type, (b) p-type semiconductors.

$$E_C - E_F = kT \ln \frac{N_C}{N_D} \tag{1.6}$$

Similarity one obtains for p-type material and acceptor concentration N_A:

$$E_F - E_V = kT \ln \frac{N_V}{N_A} \tag{1.7}$$

A somewhat more complicated treatment is required for the simultaneous presence of donors and acceptors and for very high doping concentrations. It may also be mentioned in this context that the number of donor or acceptor states does not necessarily equal the number of corresponding impurity atoms, since in order to become electrically active doping atoms they have to be properly built into the crystal lattice [13].

Using the results of the previous section, the density of free electrons n is

$$n = n_i e^{\frac{E_F - E_i}{kT}} \tag{1.8(a)}$$

The density of free holes p is

$$p = n_i e^{\frac{E_i - E_F}{kT}} \tag{1.8(b)}$$

The increase of majority carriers (electrons in the case of n-type material) is accompanied by a decrease of minority carriers according to the mass-action law

$$n \cdot p = n_i^2 \tag{1.9}$$

In agreement with (1.8)

1.7 Perovskite structure

The terms "perovskite" and "perovskite structure" are often used interchangeably. Technically, a perovskite is a type of mineral that was first found in the Ural Mountains and named after Lev Perovski (who was the founder of the Russian

Geographical Society). A perovskite structure is any compound that has the same structure as the perovskite mineral [18].

True perovskite (the mineral) is composed of calcium, titanium and oxygen in the form CaTiO3. Meanwhile, a perovskite structure is anything that has the generic form ABX3 and the same crystallographic structure as perovskite (the mineral). However, since most people in the solar cell world aren't involved with minerals and geology, perovskite and perovskite structure are used interchangeably.

The perovskite unit cell is demonstrated below. As with many structures in crystallography, it can be represented in multiple ways. The simplest way to think about a perovskite is as a large atomic or molecular cation (positively-charged) of type A in the centre of a cube. The corners of the cube are then occupied by atoms represented by B (also positively-charged cations) and the faces of the cube are occupied by a smaller atom X with negative charge (anion).

Depending on which atoms/molecules are used in the structure, perovskites can have an impressive array of interesting properties, including superconductivity, giant magnetoresistance, spin-dependent transport (spintronics) and catalytic properties. Perovskites therefore represent an exciting playground for physicists, chemists and material scientists [17].

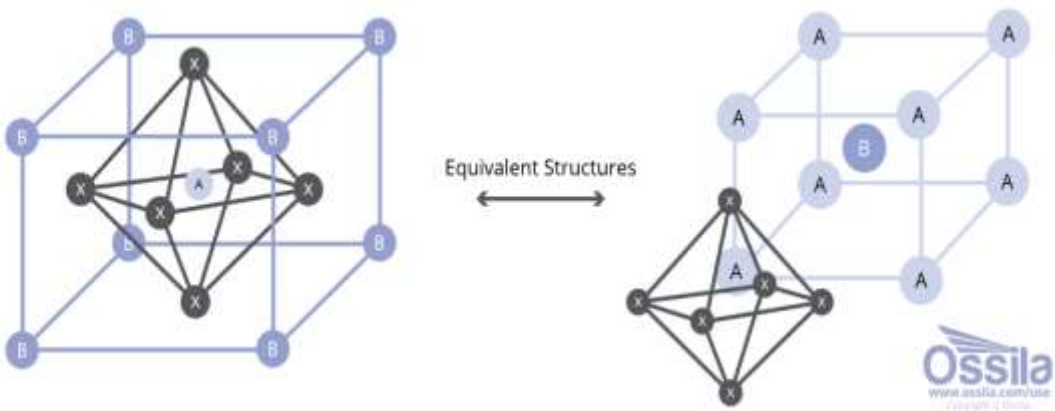

Figure 1.6: A generic perovskite crystal structure of the form ABX3 [17].

Perovskites were first successfully used in solid-state solar cells in 2012 and since then most cells have used the following combination of materials in the usual perovskite form ABX3:

- A = An organic cation - methylammonium ($CH_3NH_3^+$) or formamidinium ($NH_2CHNH_2^+$)

- B = A big inorganic cation - usually lead(II) (Pb^{2+})
- X_3= A slightly smaller halogen anion – usually chloride (Cl^-) or iodide (I^-)

1.8 Challenges

The biggest issue in the field of perovskites currently is long-term instability. This has been shown to be due to degradation pathways involving external factors, such as water, light, and oxygen, and also as a result of intrinsic instability, such as degradation upon heating, because of the properties of the material [19].

1.9 Conclusion

In this chapter, we explored the fundamental properties of semiconductors, examining their crystal structures and how their conduction mechanisms differ from metals and insulators. Metals conduct electricity due to free electrons, while insulators lack these carriers, and semiconductors exhibit conditional conductivity. We distinguished between intrinsic semiconductors, which rely on thermal excitation, and extrinsic semiconductors, enhanced by doping to create n-type or p-type materials. Additionally, we discussed perovskites, noting their promising optoelectronic properties and potential in solar cells due to their flexible structure, high absorption, and tunable bandgaps. This foundational understanding sets the stage for exploring advanced semiconductor technologies and applications.

Chapter 2:

The Properties and Characteristics Of solar cell

2.1 Introduction

Solar energy is the most available energy source for human society. Since the total solar energy absorbed by the Earth reaches 4 × 106 EJ/year, it represents ten times the energy consumed in the world in 2007. For example, if 50 percent of the sunlight shining in New Mexico was converted into useful energy, this could meet all the energy needs of the United States of America [20]. Harnessing this immense energy requires efficient solar cells, which convert sunlight directly into electricity through the photovoltaic effect in semiconductor materials. This chapter explores the fundamental principles behind solar cells, including solar radiation characteristics, photon absorption, energy transfer processes, and the various types of solar cells developed across different generations. It also delves into advanced technologies like perovskite solar cells, which promise higher efficiencies and lower production costs, driving the future of renewable energy solutions.

2.2 Solar radiation

AM1.5 represents the spectrum of solar light that remains after the light passes at an angle through approximately one and a half Earth atmospheres (Fig. 2.1). AM1.5 is used as the standard spectral distribution of light to measure a solar cell's efficiency. Generally, 99% of the light that reaches the Earth's surface is at wavelengths of less than 2500 nm in the AM1.5 spectrum, and 88% is less than 1350nm. To be efficient, a solar cell should be able to absorb the largest number of photons possible. Fig. 2.1 compares the AM0 and AM1.5 spectra [21].

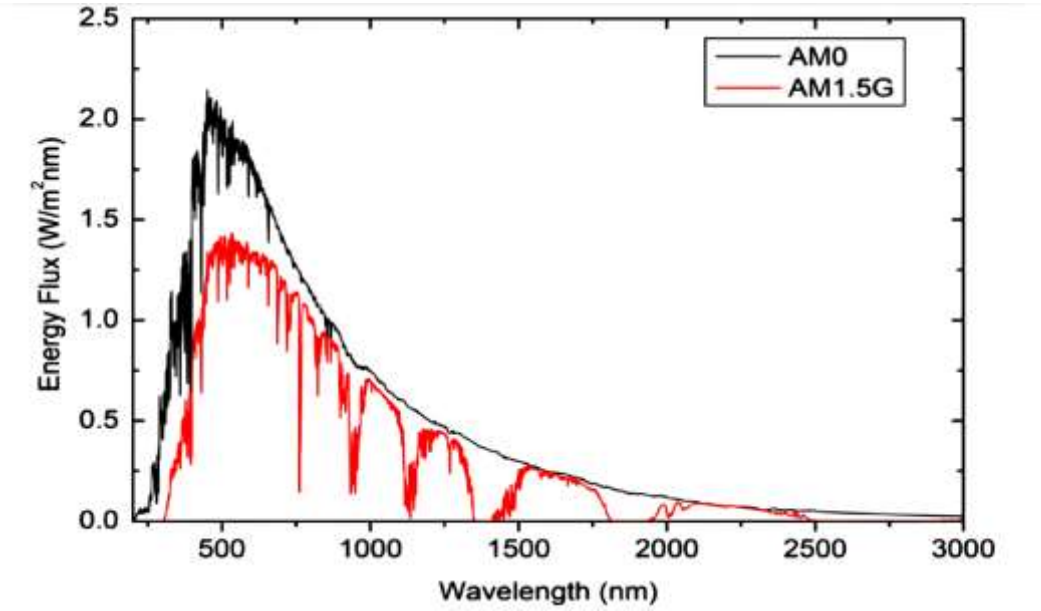

Figure 2.1:AM0 and AM1.5 solar irradiance spectra **[**8].

2.3 Transfer of energy from the photon to the electron

There are two pre-requisites for luminescence: (1) the luminescent material must have a semiconductor structure with a nonzero band gap Eg (e.g. metals do not luminesce since they have no band gap); (2) energy must be imparted to this material before luminescence can take place. The mechanism of photoluminescence in semiconductors is schematically illustrated in Figure 2.2, which plots the E-k diagrams for a direct band gap material (left) and an indirect gap material (right), where E and k are respectively the kinetic energy and wave vector (or "momentum vector") of the electron or hole ($E = k^2\bar{h}^2/2m_*, where\ \bar{h} \equiv h/2\pi$ is the Planck constant h divided by 2π, and m_* is the electron or hole effective mass). The direct and indirect gap materials are distinguished by their relative positions of the conduction band minimum and the valence band maximum in the Brillouin zone (the volume of k space containing all the values of k up to π / a where a is the unit lattice cell dimension). In a direct gap material, both the conduction band minimum and the valence band maximum occur at the zone center where k = 0. In an indirect gap material, however, the conduction band minimum does not occur at k = 0, but rather at some other values of k which is usually at the zone edge or close to it [22].

2.4 Generation of excess carriers by light

The principle is based on the interaction of light and matter in semiconductors.

The energy of the photon corresponding to a given radiation is related to its wavelength by the relation:

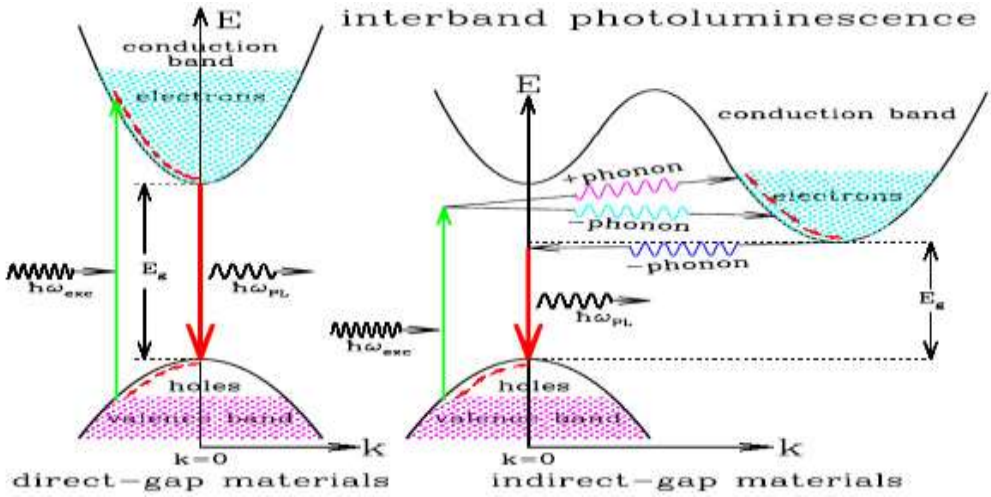

Figure 2.2: Schematic band diagrams for the photo luminescence processes in a directgap material (left) and an indirect gap material (right) [22].

$$E_p = h\nu = \frac{hc}{\lambda} = \frac{1.24}{\lambda}$$

Where ν is the frequency of the radiation, λ the wavelength of the radiation in μm, c the speed of light, E_p the photon energy in eV and h is the Plank constant.

A luminous radiation encountering a semiconductor is absorbed according to LambertBouguer's law:

$$I(x) = I\,(1-R)\,exp(-\alpha x) = I_o exp(-\alpha x)$$

Where x is the depth of absorption of the beam in the material from the surface of the semiconductor, R is the reflection coefficient, represents the part of the incident light energy I, reflected on the surface of the material, and α is the absorption coefficient.

The optical behavior of the material is fully described by its optical constants. These are the refractive index n and the extinction coefficient k, which together form the complex refractive index N. n and k depend on the wavelength of the incident light. The refractive index n is related to the propagation speed of the light wave and the coefficient k is a unit of measurement for the wave damping. The complex refractive index is defined as:

$$N = n(\lambda) + ik(\lambda)$$

The optical absorption coefficient α is given by:

$$\alpha = \frac{4\pi k}{\lambda}$$

Figure 2.3 gives the absorption spectra of some materials. The minimum energy required for the incident photon to cause the electronic transition depends on the band gap E_g of the material.

The calculation of the generation rate of electron-hole pairs G(x) ($cm^{-3}s^{-1}$) is carried out as follows. Calling I_o, the flux of photons ($cm^{-2}s^{-1}$) incident on the illuminated side of the material and α(cm^{-1}) the absorption coefficient of light by the material. At depth x, this generation rate is:

$$G(x) = \alpha(1-R)I_o e^{-\alpha x}$$

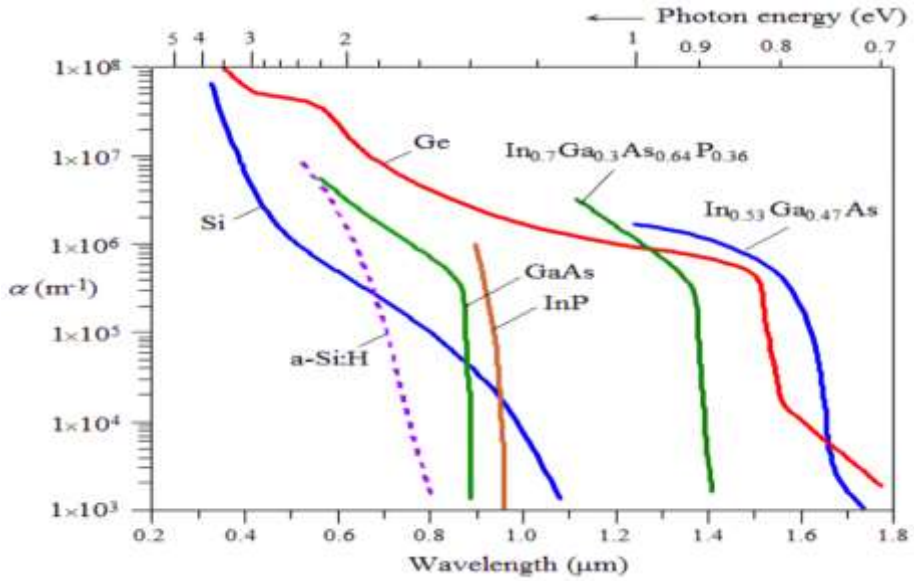

Figure 2.3 Absorption spectra of the most commonly used semiconductor materials in solar cells.

2.5 Recombination mechanisms of excess carriers

By recombination we refer to the loss of mobile electrons or holes by any of a number of removal mechanisms. Unlike generation, where one mechanism is dominant, several different recombination mechanisms are important for the photovoltaic device.[24]

2.5.1 Band – to – band recombination

Band-to-band recombination refers to the annihilation of an e – h pair followed by the emission of a photon of corresponding energy. These unavoidable recombination (in the sense that, unlike other recombination mechanisms, they must occur in any PV cell) are particularly effective indirect band gap materials, such as GaAs.

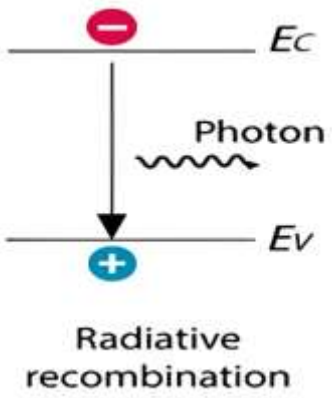

Figure 2.4: Scheme of the main recombination processes Radiative [25].

2.5.2 Auger recombination

Auger recombination refers to a three-particle mechanism where the energy of an electron in the CB (or, alternatively, the energy of a hole in the VB) is transferred to another electron (or hole). The excess energy is rapidly dissipated as heat in the crystalline network.

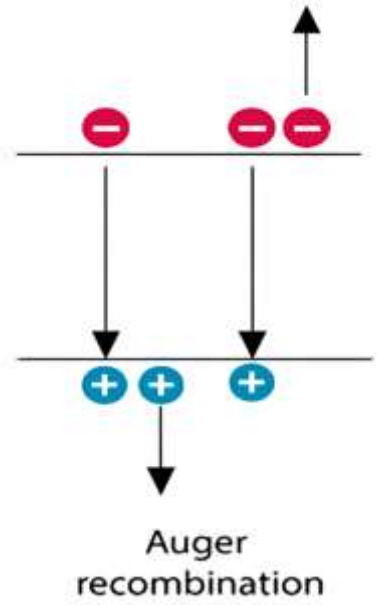

Figure 2.5: Scheme of the main recombination processes Auger [25].

2.5.3 Shockley Read Hall (SRH) recombination

Recombination involves impurities or defects in the crystalline structure, giving rise to unwanted energy levels acting like traps in the forbidden gap: annihilation of an e – h pair may occur if both a free electron in the CB, and a hole in the VB, simultaneously fall into an impurity trap [25].

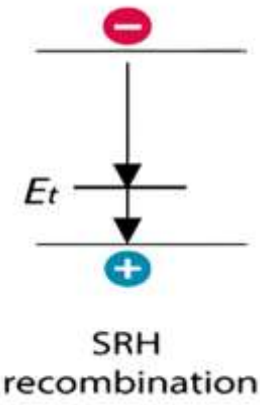

Figure 2.6: Scheme of the main recombination processes Shockley – Read – Hall. [11].

SRH recombination is often strong in many semiconductor materials, and a particular care should be brought toward minimizing the defect density in the PV cell through appropriate fabrication and doping conditions. Trap states are also likely to appear at the surface of the cell because of material discontinuities. These recombination mechanisms, known as surface recombination, may be minimized with high-quality surface passivation.

2.5.4 Surface recombination

Surface recombination velocity is an important parameter which affects the dark saturation current and the quantum efficiency of solar cells. Similarly to dislocations and planar defects such as grain boundaries, surfaces (and interfaces in general) introduce band of electronic states in the band gap which can be ascribed to broken (or strained) bonds and impurities. A complete characterisation of surface recombination must also take into account the surface charge which may give rise to band bending. To achieve optimal operation, surface recombination is reduced by a passivating or window layer which prevents minority carriers from reaching the surface. Passivation of silicon surface by an oxide layer, or the deposition of a thin 'window' layer of GaAlAs on GaAs solar cells are just two examples of such practice [26].

2.6 Operating principle of a solar cell

The photovoltaic effect used in solar cells makes it possible to directly convert the light energy of the sun's rays into electricity through the production and transport in a semiconductor material of positive and negative electrical charges under the effect of light. This material has two parts, one with an excess of electrons and the other with a deficit in electrons, respectively called n-type doped and p-type doped. When the first is brought into contact with the second, the excess electrons in the material n diffuse into the material p. The initially n-doped area becomes positively charged, and the initially p-doped area becomes negatively charged. An electric field is therefore created between them which tends to push the electrons into the n zone and the holes towards the p zone. A PN junction is therefore formed. By adding metal contacts to areas n and p, a diode is obtained. When the junction is illuminated, the photons of energy equal to or greater than the width of the forbidden band give up their energy to the atoms, each one passes an electron from the valence band into the conduction band and also leaves a hole capable of move, thus generating an electron-hole pair. If

a charge is placed across the cell, the electrons from zone n join the holes in zone p via the external connection, giving rise to a potential difference and an electric current flow.

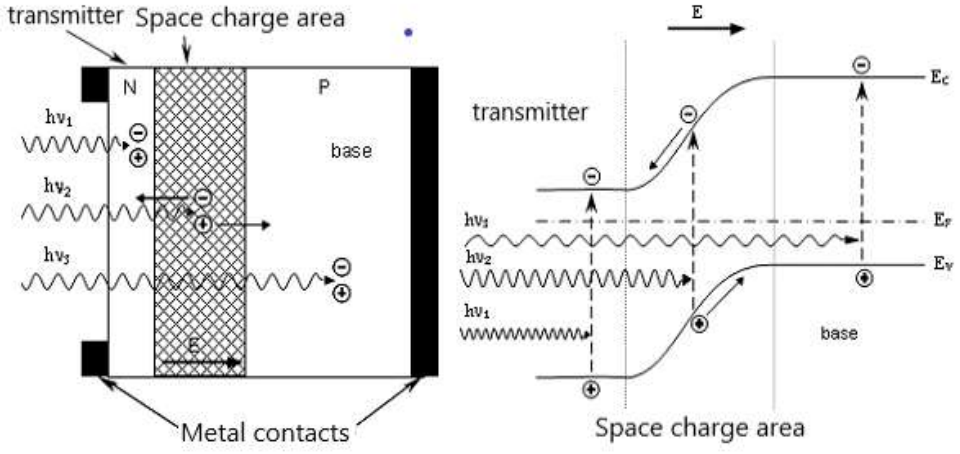

Figure 2.7: Structure and band diagram of a photovoltaic cell.

The operating principle of a solar cell is illustrated in Figure 2.3 .The incident photons create carriers in the N, P regions and the space charge region. The behavior of these free carriers differs depending on the location of their creation. In the electrically neutral zones P and N, the minority photocarriers diffuse. Those that reach the space charge region are propelled by the electric field towards the region where they become the majority. These photocarriers therefore contribute or current through their diffusion, they create a diffusion photocurrent. In the space charge zone, the electron-hole pairs created by the photons are dissociated by the electric field, the electron is propelled towards the N-type region and the hole towards the P-type region. The carriers give rise to a generation photocurrent. These two contributions add to create a resulting photocurrent I_{ph} which contributes to the reverse current of the diode [27].

2.7 The ideal solar cell

The equivalent circuit of a solar cell consists of an ideal current generator in parallel with a diode in reverse bias, both of which are connected to a load. The generated current is directly proportional to light intensity. This highlights how important it is to accurately replicate the solar spectrum when testing solar cells. [28]

This model does not take into account the internal losses of the current. The output current (I) of the ideal solar cell model with single diode connected in module is obtained by Kirchhoff law [29]:

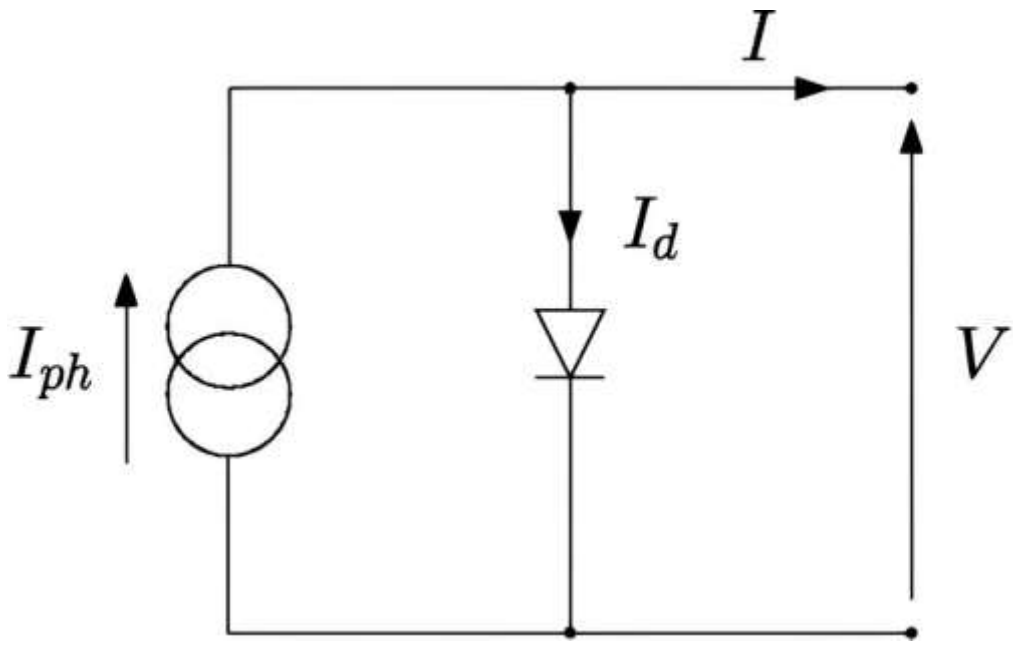

Figure 2.8: Equivalent circuit diagram of an ideal solar cell.

From this ideal circuit diagram, we can extract equations to describe and model solar cells. This also helps us define some of the most important metrics we use to describe solar cells. In its simplest form, we can describe current through the load as the amount of current generated minus the current that flows through the diodes [28].

$$I = I_{ph} + I_d$$

Where I_{ph} is the photo generated current, I_d is the diode current and it's expressed by:

$$I_d = I_0(e^{\frac{qV_d}{kT}} - 1)$$

In which I_0 is the reverse saturation current, q is the electron charge, k = Boltzmann's constant, and T is the diode junction temperature [30].

Fig. 2.8 shows the IV (current – voltage) curve of a solar cell that follows Eq. (2.8). The photo generated current shifts the IV curve up, enhancing the available power to be extracted. Under low-voltage values, the output current remains close to the short-circuit value. However, as the voltage increases, the dark current grows exponentially and the output current decreases [25].

The open-circuit voltage, which corresponds to the point of the IV curve where the dark current and the photo generated current compensate each other, leading to an output current equal to zero, can simply be derived from Eq. (2.8):

$$V_{oc} = \frac{kT}{q} \ln\left(1 + \frac{I_{ph}}{I_0}\right)$$

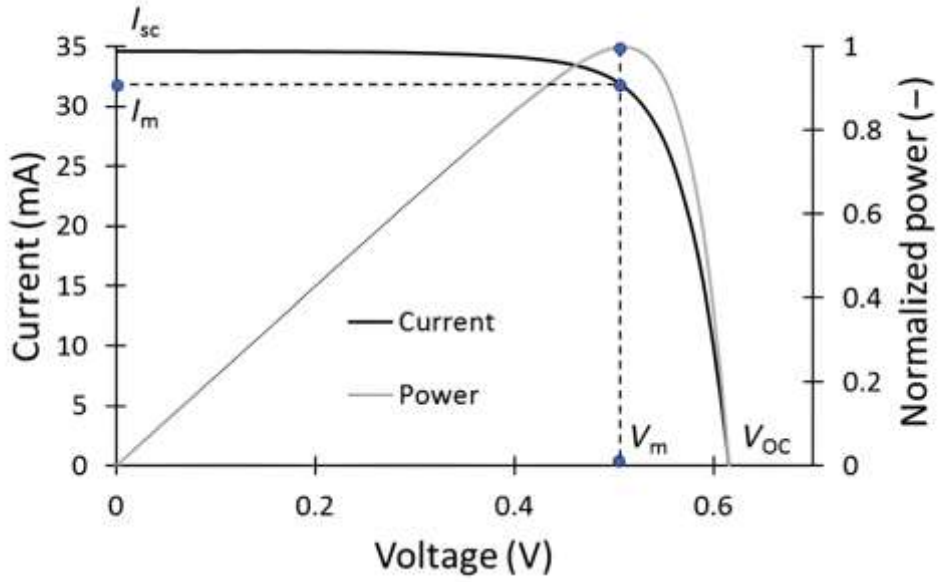

Figure 2.9: IV Curve of a photovoltaic (PV) cell, showing the main solar cell Parameters [25].

The power P = IV produced by the cell is shown in Figure 2.8The cell generates the maximum power P_{max} at a voltage V_m and current I_m and it is convenient to define the fill factor FF by

$$FF = \frac{I_m V_m}{I_{sc} V_{oc}} = \frac{P_{max}}{I_{sc} V_{oc}}$$

The fill factor FF of a solar cell with the ideal characteristic will be furnished by the subscript 0. It cannot be determined analytically but it can be shown that FF_o depends only on the ratio $v_{oc} = V_{oc}/kT$. FF_o is determined, to an excellent accuracy, by the approximate expression

$$FF_O \frac{v_{oc} - \ln(v_{oc} + 0.72)}{V_{oc} + 1}$$

2.8 Solar Cell in practice:

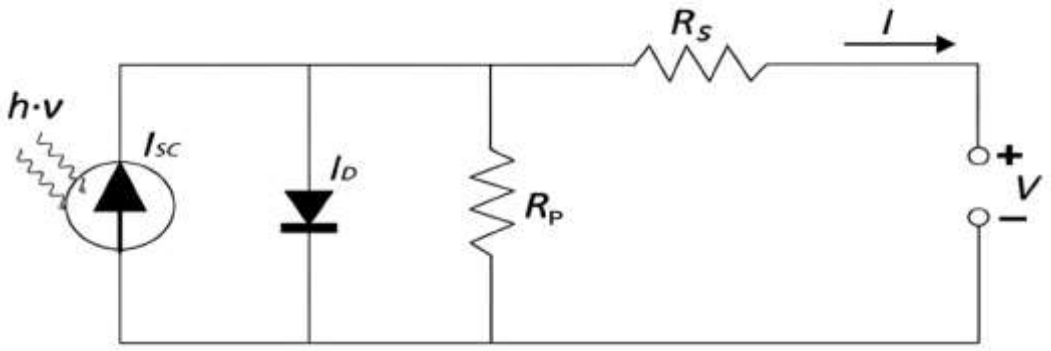

Figure 2.9: Equivalent circuit of a solar cell in practice.

The I-V characteristic of a solar cell in practice usually differs to some extent from the ideal characteristic .The solar cell (or circuit) may also contain series (R_s) and parallel (or shunt, R_P) resistances, leading to a characteristic of the form [26].

$$I = I_{ph} - I_o\left\{e^{\left(\frac{V+IR_s}{2kT}\right)} - 1\right\} - \frac{V + IR_s}{R_P}$$

Where the light-generated current I_{ph} may, in some instances, depend on the voltage. These features are shown in the equivalent circuit of Figure 2.9. The effect of the series and parallel resistances on the I–V characteristic of the solar cell is shown in Figures 2.10. The effect of the series resistance on the fill factor can be writing as:

$$FF = FF_0(1 - r_s)$$

Where $r_s = R_s I_{SC}/V_{OC}$ An analogous expression exists also for the parallel resistance.

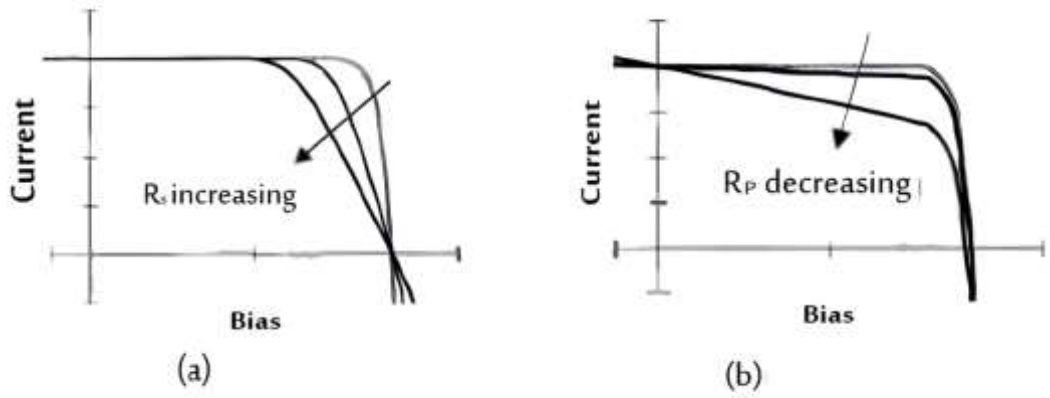

Figure 2.10: Effect of (a) increasing series and (b) reducing parallel resistances. In each case the outer curve has $R_s = 0$ and $R_P = \infty$. In each case the effect of the resistances is to reduce the area of the maximum power rectangle.

2.9 Types of solar cells:

It relies mainly on semiconductors similar to the formation of the P-N junction, as these solar cells are divided into three different generations, classified according to the materials used and how they are manufactured, and they all convert light energy into electrical conductivity [31].

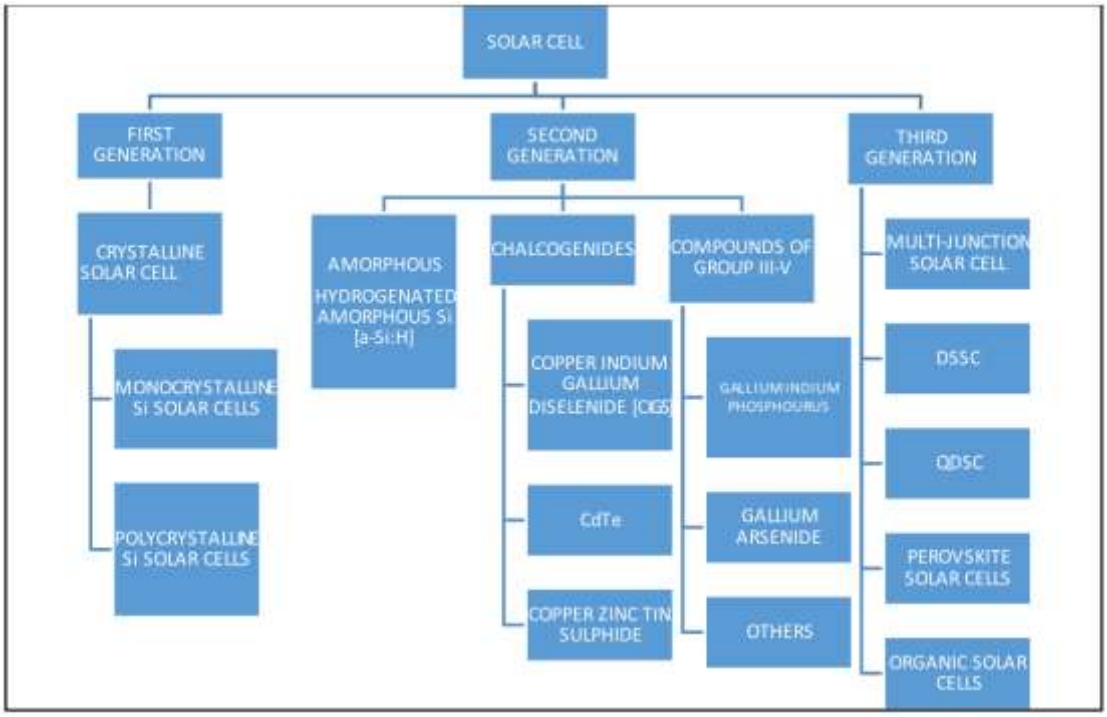

Figure 2.12: Various types of solar cells and current advancements [31].

2.9.1 First generation solar cells

These are solar cells based on crystalline Si wafers. Manufactured from Crystalline Si, thus most costly technique of obtaining pure Silicon crystal is involved in this technology. These solar cells are used worldwide and these have highest commercial efficiency [11]. About 80% solar cell market is based on single crystalline solar cells. It was reported by Zhao et al (1998) that polycrystalline solar cells having honeycomb like structure have efficiency of about 19.8%. Polycrystalline solar cells are less efficient as compared to the crystalline solar cells.

1. Single crystalline solar cells
2. Polycrystalline solar cells

2.9.2 Second generation solar cell Technology (Thin film solar cell technology)

Si crystal wafer technology is costly as it uses mostly pure crystalline Si. Obtaining pure Si is a complex and costly process. Cost of solar cells can be reduced if thin films of Si (1μm) can be deposited. Very little amount of Silicon is used by thin film technology as compared to wafer based technology. R. Chittick developed amorphous Si deposited thin films first. Then his co-workers published a report on first systematic and explenatory study on plasma enhanced chemical vapour deposition technique [32].

2.9.3 Third generation solar cell technology

Third generation PV cell technology refers to single junction solar cell which can overcome Shockley–Queisser limit of 31–41% power efficiency. C-Si solar cells (First generation) and thin film solar cells are having some limitations for achieving higher efficiency and to be established as Photovoltaic technology to fulfil all conditions as per golden triangle. Third generation solar cell technology consists of the following types of solar cells.

1. CZTS solar cells including materials CZTSe and CZTSSe
2. Dye sensitized solar cells
3. Quantum Dot solar cells
4. Perovskite solar cells
5. Organic solar cells

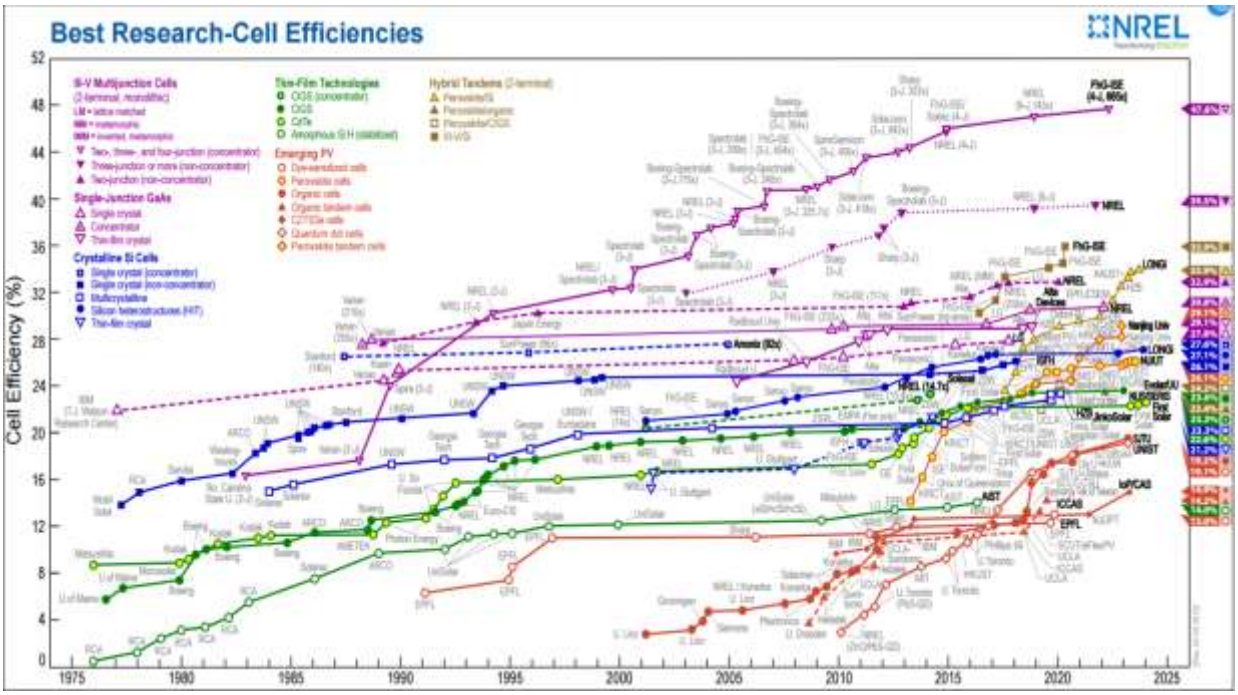

Figure 2.13: Best Research-Cell Efficiency Chart [33]

2.10 Perovskite solar cells

Perovskite solar cells (PSCs) are thin-film semiconductor-type solar cells that are similar to practical solar cells using compound semiconductors (GaAs, CdTe, etc.) and amorphous Si in photovoltaic (PV) industries. The advantage of these thin-film cells over the most popular crystalline Si solar cells is their processability into lightweight, thin, flexible devices. Lightweight and mechanical flexibility are significant added values sought for next-generation PV devices. Flexibility enables

the device to be attached to curved surfaces of outdoor and indoor structures. Lightweight is particularly advantageous for mounting the device on mobile objects including cars and people [34].

2.11 Absorption spectra of perovskite:

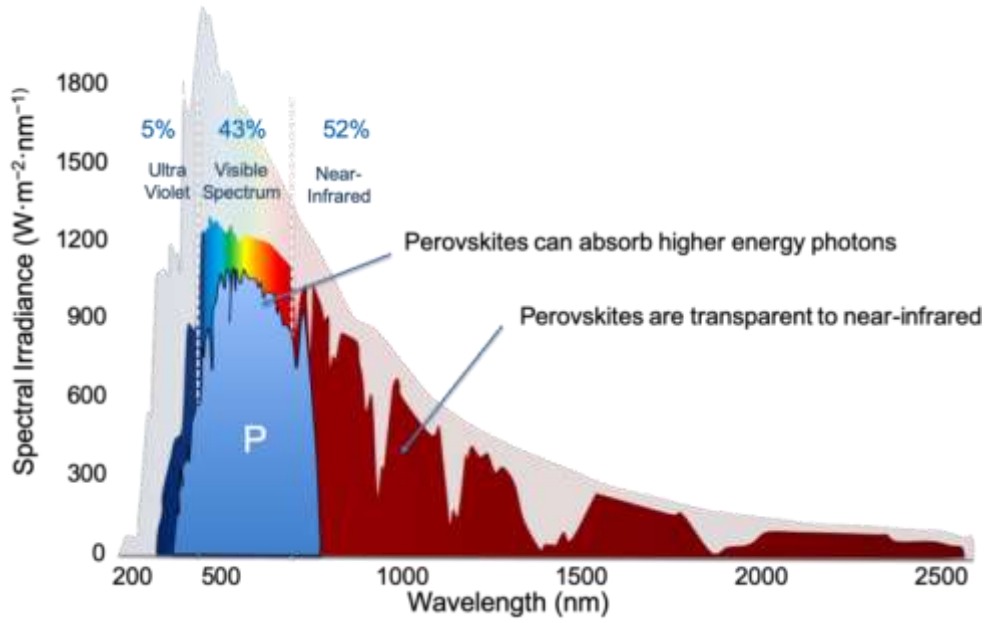

Figure 2.14: Material absorption curve [35].

Peroskites are very efficient at absorbing high-energy photons in the ultraviolet and visible spectrum. Absorption quickly drops off at 780 nm, making perovskites essentially transparent to the near-infrared spectrum where more than half of the total available energy is located.

2.12 Fabrication of Perovskite Solar Cells

Perovskite materials have been considered to be simpler and easier to fabricate than semiconductor silicon.

The perovskite film itself is typically processed by either vacuum or solution methods. Film quality is very important. Initially, vacuum-deposited films gave the best devices, but this process requires the co-evaporation of the organic (methylammonium) component at the same time as the inorganic (lead halide) components, necessitating specialist evaporation chambers that are not available to many researchers. As a result, there have been significant efforts into improving solution-processed devices, as these are simpler and allow for low-temperature processing, and these now equal vacuum-deposited cells in terms of efficiency.

Typically, the active layer of a perovskite solar cell is deposited via either a one or two-step process. In the one-step process, a precursor solution (such as a mix of CH_3NH_3I and PbI_2) is coated that then converts to the perovskite film upon heating. A variation on this is the 'antisolvent' method, in which the precursor solution is coated in a polar solvent, and then quenched during the spin coating process by a non-polar solvent. Precise timings of the quench and volumes of the quenching solvents is required to give the optimal performance.

In the two-step process, the metal halide (such as PbI_2) and organic components (such as CH_3NH_3I) are spin-coated in separate, subsequent films. Alternatively, metal halide films can be coated and annealed in a chamber filled with the organic component vapour, known as 'vacuum-assisted solution process' (VASP).

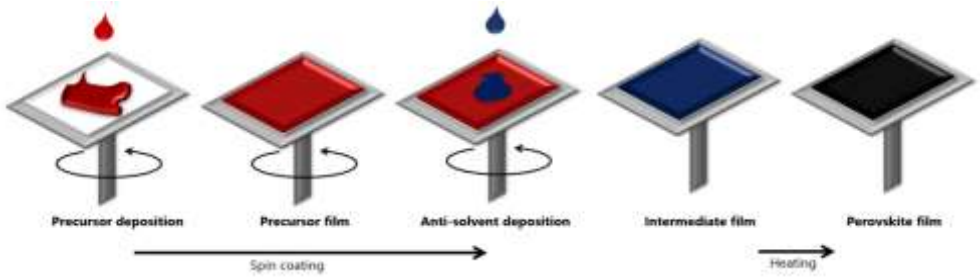

Figure 2.15: An approximation of the anti-solvent quenching method often used to coat perovskites in a one-step process from a precursor solution [14].

2.13 Conclusion

Solar cells convert the abundant energy from sunlight into electricity through the photovoltaic effect in semiconductor materials. This chapter covered the fundamental working principles, including the properties of solar radiation, photon absorption and photoelectric energy generation, and various recombination mechanisms that impact efficiency. The ideal solar cell was modeled as a current source with parallel diode, though practical devices exhibit parasitic resistances. Three generations of technologies were discussed - first generation crystalline silicon cells are efficient but expensive, second generation thin-films reduce cost but sacrifice some efficiency, while third generation architectures like perovskites, organics, and multi-junctions aim to exceed traditional limits at low cost. Continued research into new materials, cell designs, and manufacturing is important for making solar cells an even more viable renewable energy solution by enhancing efficiency and lowering costs to meet growing global energy demands sustainably.

Chapter 3:

SCAPS-1D program

3.1 Introduction

SCAPS (Solar Cell Capacitance Simulator) is a one dimensional solar cell simulation program developed at the department of Electronics and Information Systems (ELIS) of the University Of Gent, Belgium. Several researchers have contributed to it's development: Alex Niemegeers, Marc Burgelman, Koen Decock, Johan Verschraegen, Stefaan Degrave. A description of the program, and the algorithms it uses.

3.2 SCAPS-1D program

The program is freely available to the PV research community (universities and research institutes). It runs on PC under Windows 95, 98, NT, 2000, XP, Vista, Windows 7, and occupies about 50 MB of disk space.

SCAPS is originally developed for cell structures of the CuInSe2 and the CdTe family. Several extensions however have improved its capabilities so that it is also applicable to crystalline solar cells (Si and GaAs family) and amorphous cells (a-Si and micromorphous Si). An overview of its main features is given below:

- Up to 7 semiconductor layers
- Almost all parameters can be graded (i.e. dependent on the ocal composition or on the depth in the cell): Eg, χ, ε, N_C, N_V, v_{thn}, v_{thp}, μ_n, μ_p, N_A, N_D, all traps (defects) N_t
- Recombination mechanisms: band-to-band (direct), Auger, SRH-type
- Defect levels: in bulk or at interface; their charge state and recombination is accounted for
- Defect levels, charge type: no charge (idealisation), monovalent (single donor, acceptor), divalent (double donor, double acceptor, amphoteric), multivalent (user defined)
- Defect levels, energetic distributions: single level, uniform, Gauss, tail, or combinations
- Defect levels, optical property: direct excitation with light possible (impurity photovoltaic effect, IPV)
- Defect levels, metastable transitions between defects
- Contacts: work function or flat-band; optical property (reflection of transmission filter) filter

- Tunneling: intra-band tunneling (within a conduction band or within a valence band); tunneling to and from interface states
- Generation: either from internal calculation or from user supplied g(x) file
- Illumination: a variety of standard and other spectra included (AM0, AM1.5D, AM1.5G, AM1.5Gedition2, monochromatic, white,...)
- Illumination: from either the p-side or the n-side; spectrum cut-off and attenuation
- Working point for calculations: voltage, frequency, temperature
- The program calculates energy bands, concentrations and currents at a given working point, J-V characteristics, ac characteristics (C and G as function of V and/or f), spectral response (also with bias light or voltage)
- Batch calculations possible; presentation of results and settings as a function of batch parameters
- Loading and saving of all settings; start-up of SCAPS in a personalised configuration; a script language including a free user function
- Very intuitive user interface
- A script language facility to run SCAPS from a 'script file'; all internal variables can be accessed and plotted via the script.
- A built-in curve fitting facility
- A panel for the interpretation of admittance measurements

3.3 Fundamental equations in semiconductors

Semiconductors physics is an area very rich in modeling and mathematics problems. It consists of a fundamental set of equations that bring together electrostatic potential and load carriers in a very specific field of simulation. These equations, which are resolved via specific software for simulating semiconductor-based devices, are derived from Maxwell equations. [37]

They are mainly: Poisson's equation and continuity equations for both electrons and holes given by the following equations, which are used by SCAPS:

$$\frac{\partial^2 \psi}{\partial x^2} + \frac{q}{\varepsilon}\left[p(x) - n(x) + N_D - N_A + \rho_p - \rho_n\right] = 0$$

$$\frac{1}{q}\frac{dJ_p}{dx} = G_{op}(x) - R(x)$$

$$\frac{1}{q}\frac{dJ_n}{dx} = -G_{op}(x) + R(x)$$

Ɛ: the dielectric constant

q: the electron charge

N_A: acceptor density

N_D: donor density

ψ: the electrostatic potential

p: hole concentration

n: electron concentration

ρ_p: hole distribution

ρ_n: electron distribution

J_p: current densities of hole

J_n: current densities of electron

G_{op}: the optical generation rate

R: the net recombination from direct and indirect recombination.

3.4 SCAPS interface

SCAPS is a Windows-oriented program, developed with LabWindows/CVI of National Instruments. Scaps use the LW/CVI terminology of a 'Panel' (names used in other software's are: a window, a page, a popup…). SCAPS opens with the 'Action Panel'.

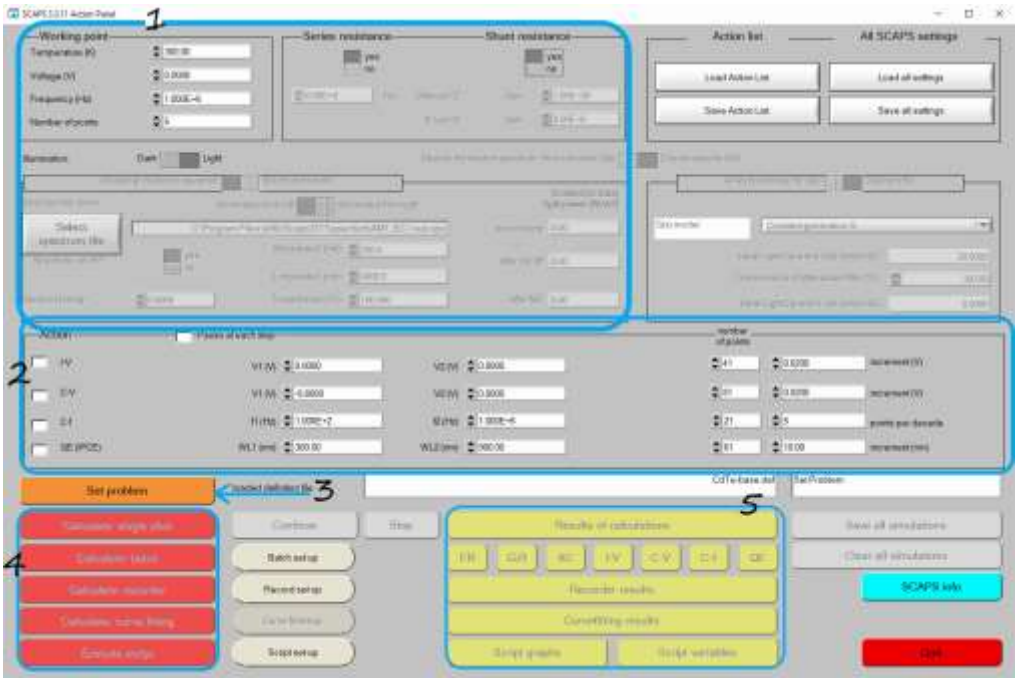

Figure 3.1: SCAPS the Action panel or main panel.

The action panel consists of 5 parts

1. Working point
2. Indicate what you will calculate, i.e. which measurement you will simulate
3. Set problem (define the problem)
4. Start the calculation(s)
5. Display the simulated curves

3.5 Define the working point

The working point specifies the parameters which are not varied in a measurement simulation, and which are relevant to that measurement. Thus

- The temperature T: relevant for all measurements. Note: in SCAPS, only $N_C(T)$, $N_V(T)$, the thermal velocities, the thermal voltage kT and all their derivatives are the only variables which have an explicit temperature dependence; you must input for each T the corresponding materials parameters yourself.
- The voltage V: is discarded in I-V and C-V simulation. It is the dc-bias voltage in C-f simulation and in QE(λ) simulation. SCAPS always starts at 0 V, and proceeds at the working point voltage in a number of steps that you also should specify.
- The frequency f: is discarded in I-V, QE(λ) and C-f simulation. It is the frequency at which the C-V measurement is simulated.
- The illumination: is used for all measurements. For the QE(λ) measurement, it determines the bias light conditions. The basis settings are: dark or light, choice of the illuminated side, choice of the spectrum. A one sun (= 1000 W/m^2) illumination with the 'air mass 1.5, global' spectrum is the default, but you have a large choice of monochromatic light and spectra for your specialized simulations. If you have an optical simulator at your disposal you can immediately load a generation profile as well instead of using a spectrum.

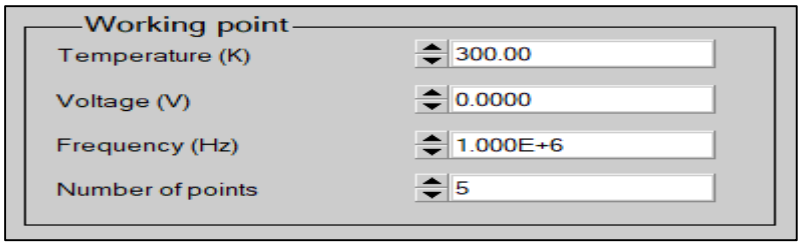

Figure 3.2: SCAPS working point

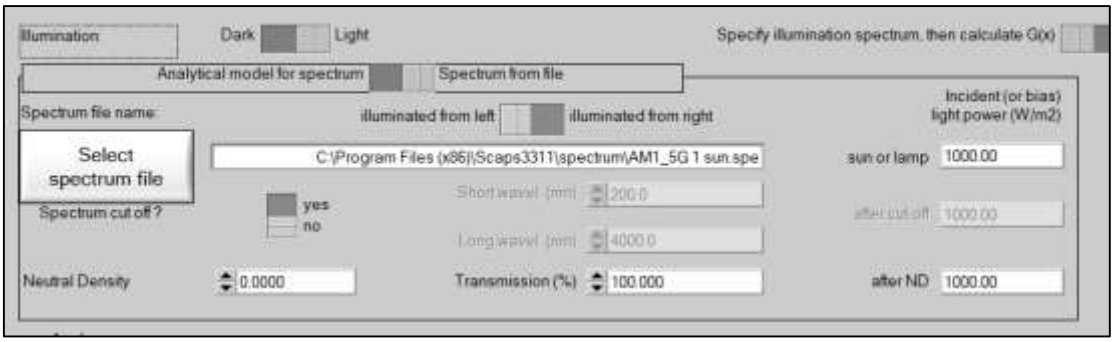

Figure 3.3: SCAPS spectrum and illumination

3.6 Spectrum and illumination:

Choose if you are simulating in dark or light, and select spectrum file you can find many files in SCAPS data base.

3.7 Select the measurement(s) to simulate

In the action-part of the Action Panel, you can select one or more of the following measurements to simulate: I-V, C-V, C-f and QE(λ). Adjust if necessary the start and end values of the argument, and the number of steps. Initially, do one simulation at a time, and use rather coarse steps: your computer and/or the SCAPS program might be less fast than you hope, or your problem could be really tough... A hint: in a C-V simulation, the I-V curve is calculated as well; no need then to specify it separately.

3.8 Define the problem

When clicking the 'Set Problem'-button on the action panel, the 'Solar cell definition'-panel is displayed. This panel allows to create/edit solar cell structures and to save those to or load from definition files. These definition files are standard ASCII-files with extension '*.def' which can be read with e.g. notepad. Even though the format of these files seems self-explaining it is however strongly advised not to alter them manually. You can design your solar cell and change different layers by clicking on add layer and modify properties such us thickness, band gap

Figure 3.4: SCAPS solar cell definition panel

3.9 Change parameters

By clicking on a layer, you can alter its thickness and band gap, among other factors.

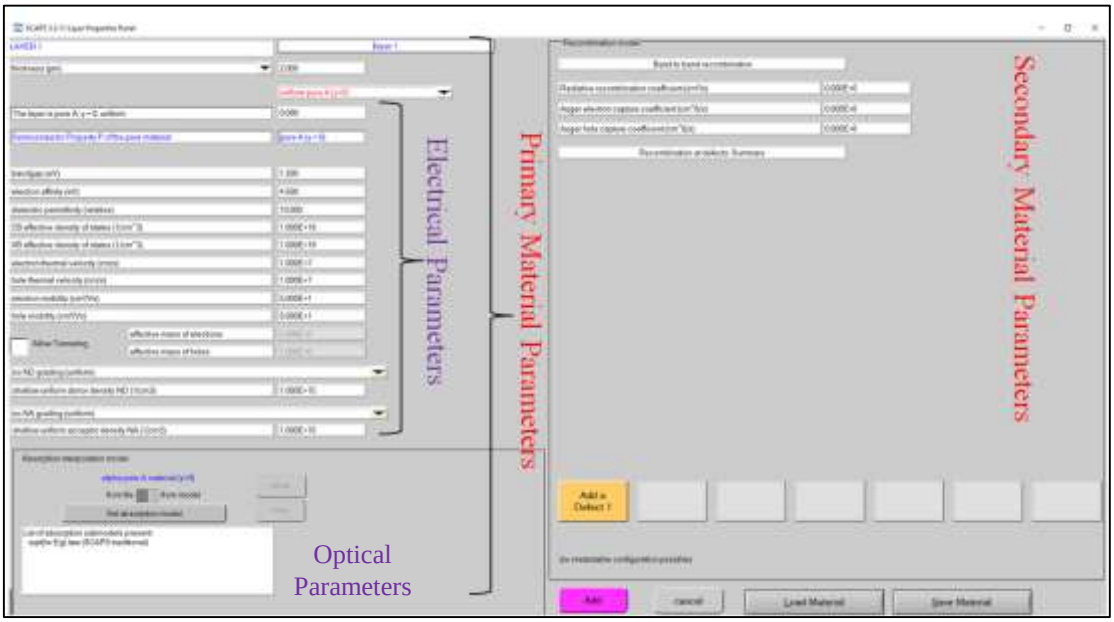

Figure 3.5: Parameters of the layer

3.10 Start the calculation(s)

We have 3 different types of calculation single shot, batch and recorder:

- **Single shot calculation:** when clicking on the button (calculate: single shot) the calculations start. At the bottom of the Panel, you see a status line, e.g. “iv from 0.000 to 0.800 Volt: V = 0.550 Volt”, showing you how the simulation proceeds. Meanwhile, SCAPS stands you a free movie how the conduction and valence bands, the Fermi levels and the whole caboodle are evolving.

When you see the hated divergence message, you're entitled to get into a bad mood, but don't exaggerate. Anyway, you did not lose the I-V points already calculated.

- **Batch calculation:** When you want to explore the influence of one or a few parameters to the solar cell characteristics, you can take profit of the batch option. When you click Batch set-up, a panel opens where you can choose which parameter to vary, over which range, and in which mode (Lin, Log or custom). You can also define more than one parameter, and vary all of them (in a nested way or 'simultaneous'), but be modest to start. A batch calculation is launched when calculate: batch is clicked.

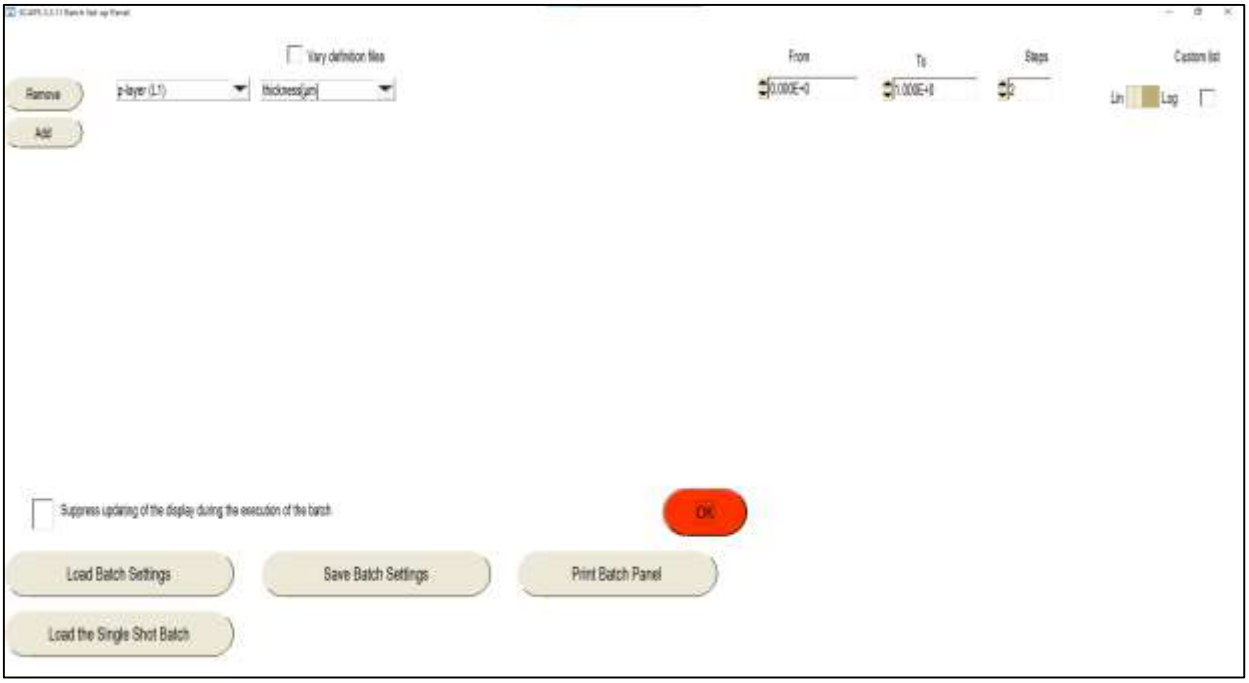

Figure 3.6: Batch set-up panel

3.11 Display the simulated curves

After the calculation(s), SCAPS switches to the Energy band panel (or the AC-band panel). You can now look at your ease to the band diagrams; carrier densities, current densities, at the last bias point calculated (stop your calculations earlier, or use the pause button on the Action Panel if you want to look at an intermediate state at ease). You can output the results (buttons print, save graphs, show (then the numbers are shown on screen; cut & paste to e.g. Excel is possible), or save (then the numbers are

saved to a file). You can switch to one of the specialized output Panels (if you have already simulated at least one corresponding measurement). We only show the example of the IV Panel

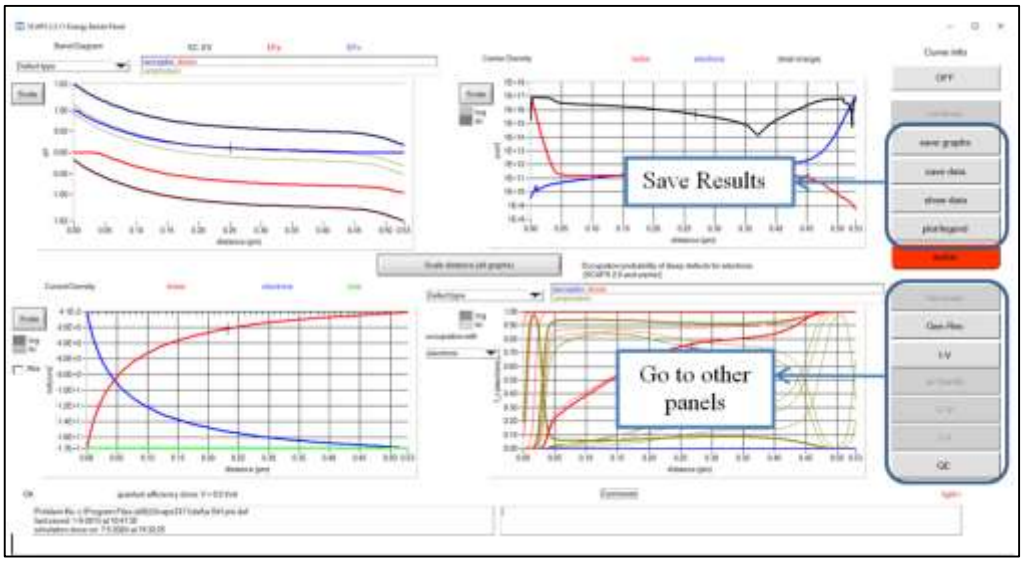

Figure 3.7: SCAPS energy band panel

3.12 Conclusion

In this chapter, we described SCAPS-1D simulation program. We started with introducing the fundamental equations in semiconductors which are used by SCAPS. We explained how to use necessary functions in this program and how to start simulating and finding results.

Chapter 4: Simulation and Results

4.1 Introduction:

The most promising option for third-generation solar cell technology is the Organic Inorganic Perovskite Solar Cell (PSC), which can be economically fabricated and has good electrical and optical features. Recent years have witnessed remarkable advancements in PSC research, leading to improved performance relative to cost.

Simple 1D simulation based study is presented in this work for $CH_3NH_3PbI_3$ (also known as $MAPbI_3$) based PSC with all inorganic metal oxide transport layers in a p–I–n configuration. NiO_x, a high bandgap p-type oxide is chosen as HTM to provide better optical transparency for incoming light. On the other hand, ETMs as TiO_2.

4.2 Describe the structure of a perovskite single junction solar cell:

The schematic diagram of the solar cell, shown in Figure, illustrates the typical p-i-n structure of a. The Thickness of $CH_3NH_3PbI_3$ ($MAPbI_3$) perovskite layer is 350 nm and it's positioned between the HTM and ETM layers, NiOx is used as the HTM in all structures with a thickness of 80 nm. For the ETM layer, two different metal oxides—TiO_2, ZnO—are alternately utilized, each also having a thickness of 80 nm, and their performances are compared.

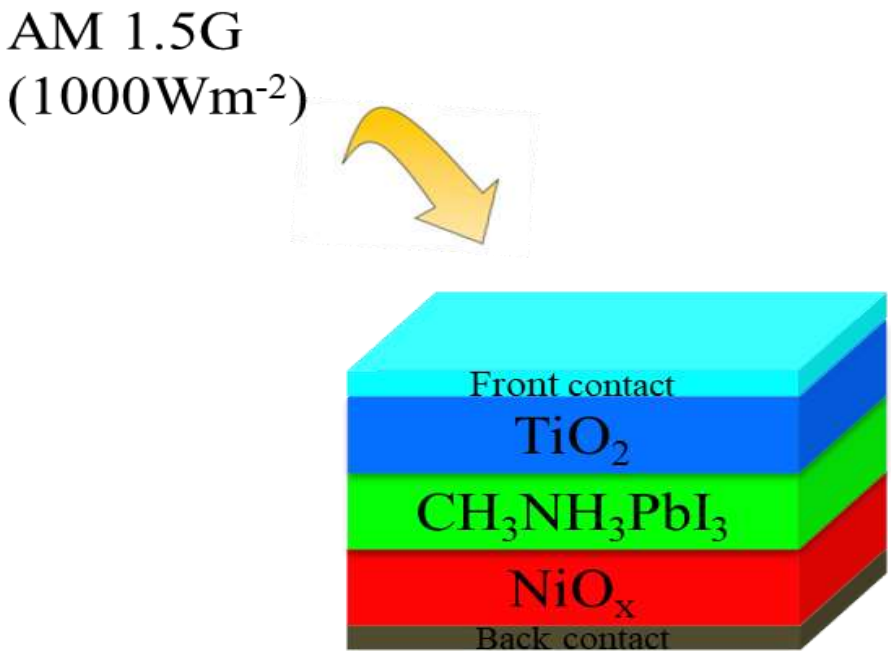

Figure .41: Schematic diagram of p-i-n $CH_3NH_3PbI_3$ (MAPbI3) PSC Structure used in the simulation.

4.3 Selection of Material Parameters

Characteristics	**NiOx**	**$MAPbI_3$**	**TiO_2**	**ZnO**
Thickness(nm)	80	350	80	80
Bandgap(eV)Eg	3.75	1.56	3.3	3.2
Electron affinity(ev)	2.1	3.9	4.2	4.10
Dielectric permittivity	10.7	10	10	8.1
CB effective density of states(1/cm^3)	2.8×10^{19}	2.76×10^{18}	3.16×10^{18}	4.5×10^{18}
VB effective density of states(1/cm^3)	1.8×10^{19}	3.9×10^{18}	2.5×10^{19}	1×10^{18}
Electron thermal velocity(cm/s)	1×10^{7}	1×10^{7}	1×10^{17}	1×10^{7}
Hole thermal velocity(cm/s)	1×10^{7}	1×10^{7}	1×10^{17}	1×10^{7}
Electron mobility(cm^2/Vs)	12	15	0.1	300
Hole mobility(cm^2/Vs)	25	15	0.1	1
Shallow uniform donor density ND ($1/cm^3$)	0	0	1×10^{19}	1×10^{19}
Shallow uniform acceptor density NA ($1/cm^3$)	1×10^{15}	1×10^{11}	0	0

Table 4.1: Electrical and optical properties of different layer used in SCAPS [38][39][40].

Figure .42: simulated structure of the p-i-n $CH_3NH_3PbI_3$ (MAPbI3) PSC in SCAPS.

4.4 The basic perovskite solar cell results

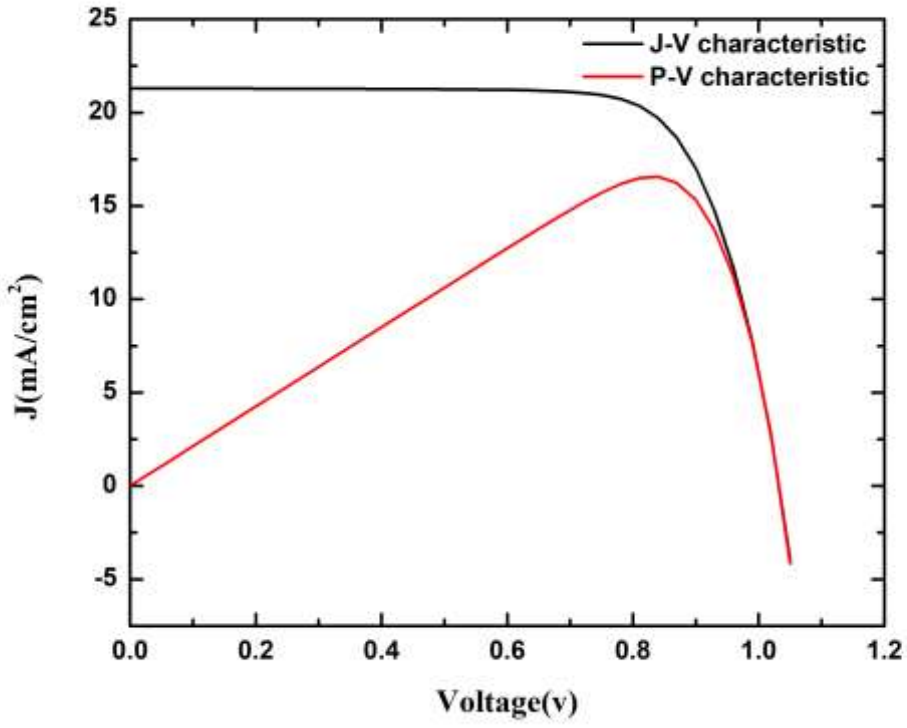

Figure 4.3: J-V and P-V characteristic curves of perovskite solar cell (figure 4.1).

Parameter	**Result with TiO_2**
V_{OC} (v)	**1.033044**
J_{SC} (mA/cm²)	**21.2995813**
FF (%)	**75.321**
Eta (%)	**16.5733**

Table 4.2: I-V characteristic resulted from PSC simulation of (figure 4.1).

4.5 Analysis with the Variation of Absorber ($MAPbI_3$) Thickness

To observe the effect of absorber ($MAPbI_3$) layer thickness on solar cell performance, the thickness is varied from 350 nm to 1000 nm keeping all other parameters same as before for TiO_2 structures.

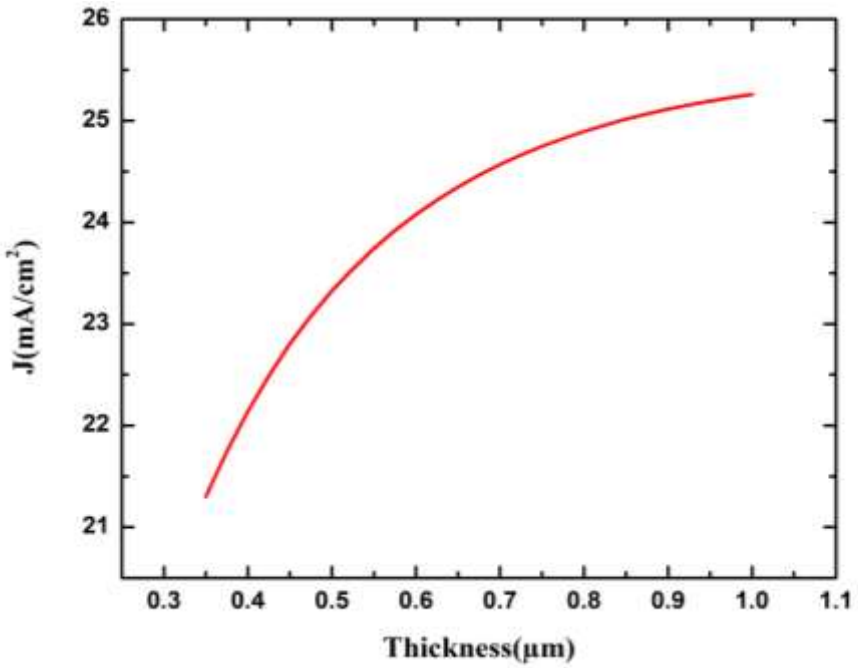

Figure .44: J–V characteristics for difference thickness of $MAPbI_3$.

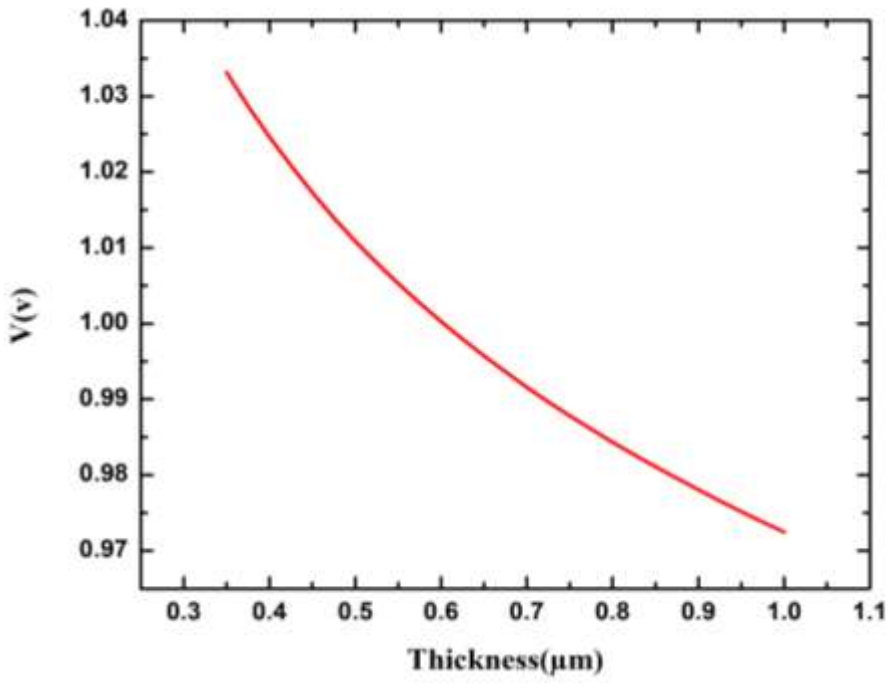

Figure .45: Open circuit Voltage as function of thickness of $MAPbI_3$.

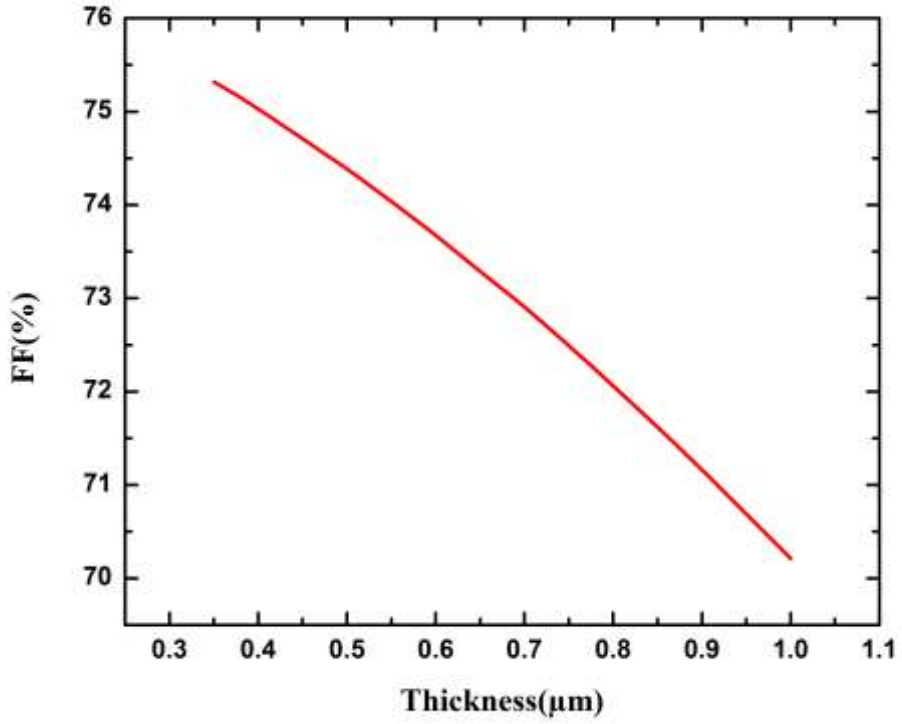

Figure .46: Fill factor curve as function of thickness of $MAPbI_3$.

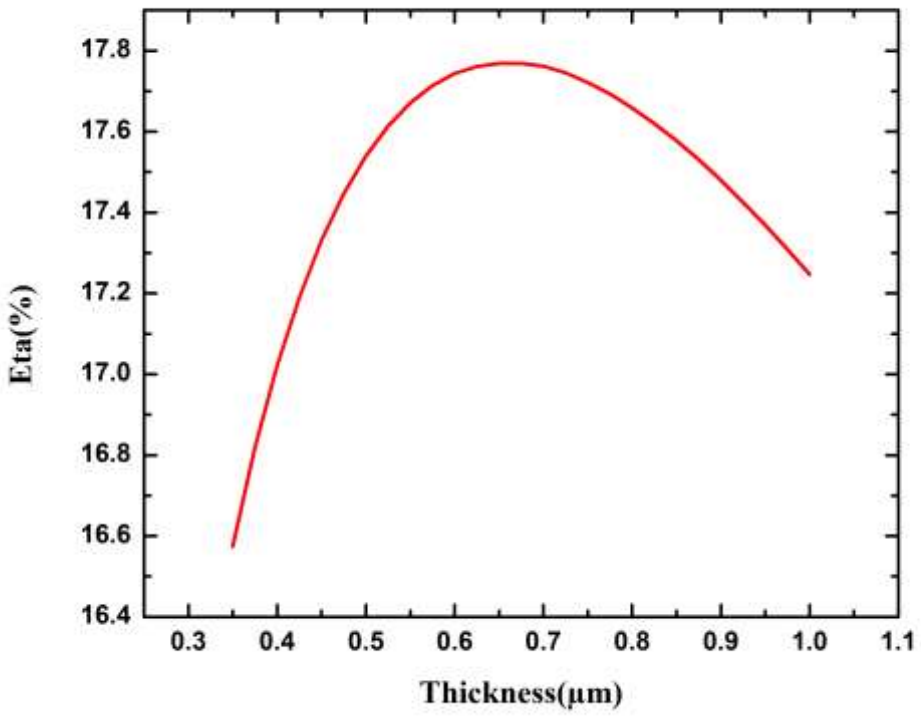

Figure .47: Effect of variation of $MAPbI_3$ thickness on Efficiency.

Thickness(μm)	V_{OC} (V)	J_{SC} (mA/cm^2)	FF (%)	Eta%
0.35	1.03316	21.29958	75.31858	16.57445
0.4	1.02462	22.1426	75.02768	17.02203
0.45	1.01729	22.80321	74.71211	17.33138
0.5	1.01088	23.32573	74.38731	17.54022
0.55	1.00528	23.74253	74.03865	17.67141
0.6	1.00029	24.07741	73.67423	17.74395
0.65	0.99572	24.34837	73.29024	17.76865
0.7	0.99159	24.56857	72.90676	17.76156
0.75	0.98782	24.74828	72.48972	17.72139
0.8	0.98434	24.89532	72.06075	17.65885
0.85	0.98112	25.01575	71.618	17.57745
0.9	0.97806	25.11432	71.16132	17.47959
0.95	0.97518	25.19477	70.69243	17.36866
1	0.97246	25.26007	70.20934	17.24659

Table 4.3: The effect of changing the thickness of $MAPbI_3$ on solar cell performance.

Figure 4 showing the increase in short-circuit current density (J_{sc}) with increasing thickness, is from a study on perovskite solar cells, specifically utilizing the $MAPbI_3$ perovskite material as the absorber layer. The upward trend in J_{sc} indicates that thicker perovskite layers, despite slightly lower absorption coefficients, can enhance charge carrier extraction and improve the photocurrent generation capability, which is crucial for achieving higher power conversion efficiencies in perovskite-based photovoltaic devices.

It is observed that figure 5 shows the open-circuit voltage (V_{oc}) of a perovskite solar cell decreasing as the thickness of the $MAPbI_3$ absorber layer increases, suggesting a trade-off between improved light absorption at higher thicknesses and increased recombination losses that lower the V_{oc}. Optimal thickness is crucial to balance these competing effects for maximizing device performance.

Figure 6 shows the fill factor (FF) curve for a perovskite solar cell as a function of absorber layer thickness. The fill factor decreases linearly from about 75% to 70% as the thickness increases from 0.3 μm to 1.0 μm. This indicates that thicker absorber layers result in reduced fill factors, likely due to increased recombination losses and decreased charge collection efficiency.

From the result in figure 7 shows that the power conversion efficiency of $MAPbI_3$ perovskite solar cells follows a bell-shaped curve as a function of absorber layer thickness. Efficiency increases with thickness, peaks at around 17.76% for a thickness of 0.6-0.7 μm, and then decreases with further increases in thickness. These trends results from the balance between improved light absorption and short-circuit current in thicker layers, and higher recombination losses and lower open-circuit voltages. The optimal thickness of 0.6-0.7 μm maximizes efficiency by optimizing current collection and minimizing voltage losses, providing key insights for designing high-efficiency $MAPbI_3$-based photovoltaics.

4.6 Comparative study between TiO_2, ZnO of perovskite Transparent Conductive Oxide layers

As the justification of the simulation environment is being established, the simulation is being carried out for two ETMs (TiO_2 & ZnO) keeping the same HTM (NiOx) and the same $MAPbI_3$ thickness 650nm.

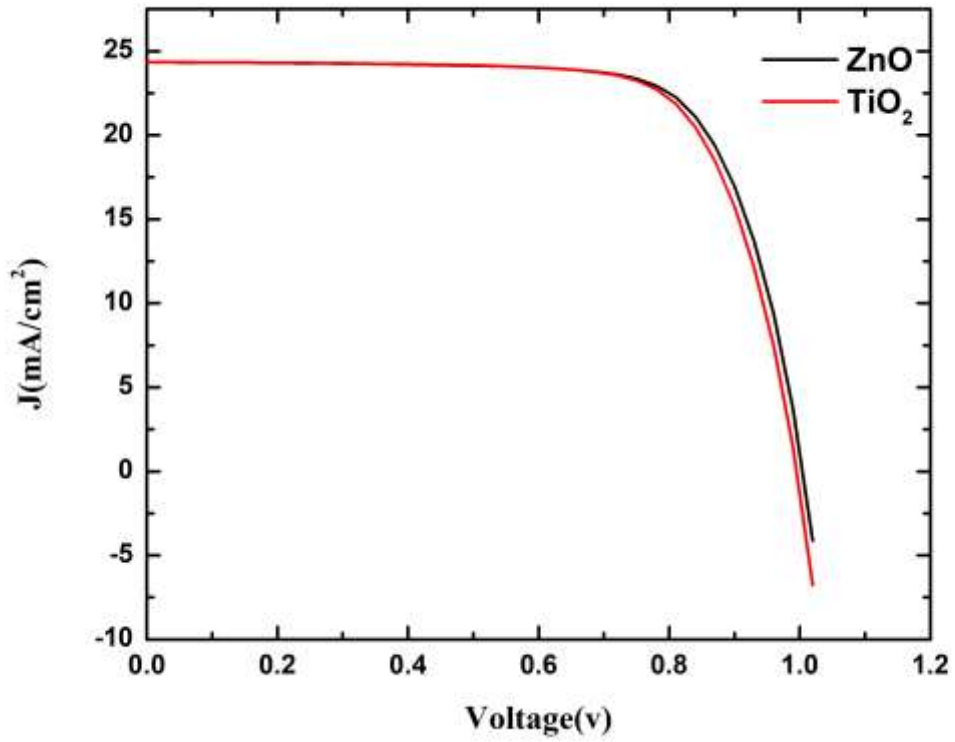

Figure .48: I-V characteristic curve for p-i-n PSC for TiO_2 and ZnO at perovskite layer thickness 650 nm

Parameter	**Result with TiO_2**	**Result with ZnO**
V_{OC} (v)	**0.995677**	**1.0051**
J_{SC} (mA/cm^2)	**24.348366**	**24.344832**
FF (%)	**73.306**	**73.6641**
Eta (%)	**17.7717**	**18.0259**

Table 4.4: I-V characteristic resulted from PSC simulation with TiO_2 and ZnO layers

4.7 Results and discussion

The p-i-n PSC structure for two different ETMs namely TiO_2 and ZnO are analyzed for same absorber ($MAPbI_3$) layer thickness (650 nm), it is observed that, ZnO have superior performance over TiO_2 which is the mostly used ETM in perovskite research so far specially for microscopic structure.

The cell containing ZnO as ETM exhibits higher Eta (0.25% increased than TiO_2)

4.8 Optimization of thicknesses of NiO_x

Figure 8 demonstrates that as the thickness of the NiO_x layer increases, the efficiency of the solar cell decreases. Based on this observation, we have decided to use a NiO_x thickness of 30 nm to achieve an optimal efficiency of 19.6%. This thickness strikes a balance between material usage and maintaining high efficiency.

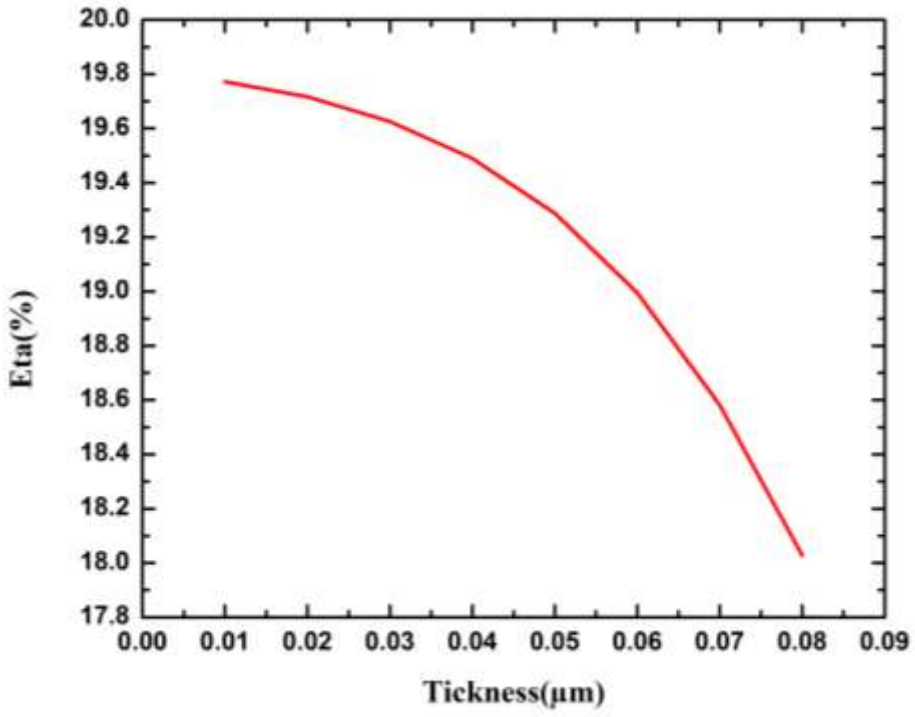

Figure .49: Effect of NiO_x thickness on Efficiency.

4.9 Conclusion

In this chapter, the effects of using inorganic transparent oxides metal (TiO_2 ,ZnO) and deferent thickness of $MAPbI_3$ on perovskite solar cell is thoroughly studied using SCAPS 1D program. The main focus is given to seek some transport material properties which are controlling key PSC performances, and optimizing the thickness of the observer to get maximum efficiency.

General Conclusion

In this work, we focused on studying and enhancing the performance of perovskite solar cells by modifying their composition. Perovskite solar cells, composed of multiple layers containing the perovskite compound, are an innovative type of solar cell. To achieve maximum efficiency in converting solar energy to electrical energy, it is essential to improve their properties and components.

Achieving the highest yield requires optimizing factors such as electrical charge conduction, light transmission, and reducing energy loss. The composition and arrangement of different layers in the cell significantly affect these factors. One issue identified in previous studies is the decreased efficiency due to TiO2, which has defects impacting cell performance. Thus, searching for alternatives is crucial.

We proposed using ZnO as a substitute for TiO2. ZnO possesses unique properties making it a strong candidate for improving perovskite solar cell performance. Based on our study, we believe that incorporating ZnO can significantly enhance the efficiency of perovskite solar cells. Therefore, ZnO should receive considerable attention in future research and development.

In summary, this work involved studying and improving perovskite solar cells by altering their structure and using ZnO instead of traditional materials. To achieve an optimal efficiency of 19.6%, the $CH_3NH_3PbI_3$ layer should be 650 nm thick and the NiO_x layer should be 30 nm thick. We believe that this approach may be an effective and promising solution for the future.

Reference

[1] Union of Concerned Scientists. (2019). How electricity is generated.

[2] International Energy Agency. (2020). Electricity information: Overview.

[3] World Health Organization. (2018). Air pollution.

[4] Intergovernmental Panel on Climate Change. (2014).

[5] International Renewable Energy Agency. (2020). Renewable energy statistics 2020.

[6] National Renewable Energy Laboratory. (2021). Renewable electricity futures study.

[7] Fraunhofer Institute for Solar Energy Systems. (2021). Photovoltaics report.

[8] National Renewable Energy Laboratory. (2020). Photovoltaic research.

[9] Solar Energy Industries Association. (2021). Solar power.

[10] EnergySage. (2020). The advantages of solar energy.

[11] Callister, W. D., & Rethwisch, D. G. (2020). Materials science and engineering: An introduction (10th ed.). John Wiley & Sons.

[12] Streetman, B. G., & Banerjee, S. K. (2015). Solid state electronic devices (7th ed.). Pearson.

[13] G. Lutz, Semiconductor radiation detectors. Springer, 2007.

[14] https://www.eeeguide.com/energy-band-diagram-of-semiconductors-insulators-and-metals/

[15] S. M. Sze and M. K. Lee, “Semiconductor devices: phys-ics and technology. 3-rd
edition.-New York, John Wiley and Sons, Inc,” 2012.

[16] Husainat, A., Ali, W., Cofie, P., Attia, J., & Fuller, J. (2019). Simulation and analysis of methylammonium lead iodide (CH3NH3PbI3) perovskite solar cell with Au contact using SCAPS 1D simulator. American Journal of Optics and Photonics, 7(2), 33.

[17] https://www.ossila.com/pages/perovskites-and-perovskite-solar-cells-an-introduction

[18] Husainat, A., Ali, W., Cofie, P., Attia, J., & Fuller, J. (2019). Simulation and analysis of methylammonium lead iodide (CH3NH3PbI3) perovskite solar cell with

Au contact using SCAPS 1D simulator. American Journal of Optics and Photonics, 7(2), 33.

[19] Correa-Baena, J. P., Saliba, M., Buonassisi, T., Grätzel, M., Abate, A., Tress, W., & Hagfeldt, A. (2017). Promises and challenges of perovskite solar cells. Science, 358(6364), 739-744.

[20] فيزياء الطاقة الشمسية سي جوليان تشن

[21] M.A.M. Al-Alwani et al. Renewable and Sustainable Energy Reviews 65 (2016) 183–213

[22] https://ned.ipac.caltech.edu/level5/Sept03/Li/Li4.html

[23] G. Barbarino, F. Barbato, and E. Nocerino, "The Semiconductor Multiplication System
for Photoelectrons in a Vacuum Silicon Photomultiplier Tube (VSiPMT) and Related Front End Electronics."

[24] J. Nelson, The Physics of Solar Cells, Imperial College Press, 2003 Sze, S. M. (1981). Physics of semiconductor devices (2nd ed.). Wiley.

[25] Thomas, S. (Ed.). (2019). Nanomaterials for solar cell applications. Elsevier

[26] Practical Handbook of Photovoltaics_ Fundamentals and Applications

[27] Kateb M.N, Mokrani Z. (2011). Conception et simulation électrique d'une cellule solaire en Si par le logiciel Tcad-Silvaco (Master's thesis).

[28] https://www.ossila.com/pages/equivalent-circuit-of-solar-cell

[29] Karim, S., Machkour, N., Zegrari, M., Aitelmahjoub, A., & Sabiri, Z. (2018). Modeling photovoltaic system using MATLAB/Simulink. Smart Application and Data Analysis for Smart Cities (SADASC'18).

[30] https://wzy.ece.iastate.edu/Courses/EE303/8_Photovoltaics.pdf

[31] Dambhare, M. V., Butey, B., & Moharil, S. V. (2021, May). Solar photovoltaic technology: A review of different types of solar cells and its future trends. In Journal of Physics: Conference Series (Vol. 1913, No. 1, p. 012053). IOP Publishing.

[32] Moon, M. M. A., Rahman, M. F., Hossain, J., & Ismail, A. B. M. (2019). Comparative study of the second generation a-Si: H, CdTe, and CIGS thin-film solar cells. Advanced Materials Research, 1154, 102-111.

[33] N. R. E. Laboratory, "Best Research-Cell Efficiency Chart." NREL Golden, CO, 2023.

[34] Tsutomu Miyasaka - Perovskite Photovoltaics and Optoelectronics_ from Fundamentals to Advanced Applications (2022, Wiley-VCH)

[35] https://qdsolarinc.com/technology/

[36] Burgelman, M., Nollet, P., & Degrave, S. (2000). SCAPS: A simulation program for the electric and optical characteristics of thin-film solar cells. University of Gent.

[37] Khelfaoui-Hala. (2022). Simulation of thin film solar cells using the SCAPS-1D program. University of Mohammed Boudiaf Msila.

[38] Rahman, M. S., Miah, S., Marma, M. S. W., & Sabrina, T. (2019, February). Simulation based investigation of inverted planar perovskite solar cell with all metal oxide inorganic transport layers. In 2019 International Conference on Electrical, Computer and Communication Engineering (ECCE) (pp. 1-6). IEEE.

[39] Haruyama, J., Sodeyama, K., Han, L., & Tateyama, Y. (2016). Surface properties of CH3NH3PbI3 for perovskite solar cells. Accounts of Chemical Research, 49(3), 554-561.

[40] BENSALAH M. N. E.I (2022). Simulation et optimisation d'une cellule solaire a base de materiaux perovskite hybride ($CH_3NH_3PbI_{3-X}Cl_X$). Université SAAD DAHLAB de BLIDA

Acknowledgments

First and foremost, I would like to thank **God almighty** for giving me the strength and perseverance as well as the ability to undertake and complete this research. It would not have been possible without God's blessings.

Second, I would also like to thank **Dr Kateb Mohamed Nadjib**, our supervisor. This work would not be done without his advice, support, guidance and invaluable knowledge.

Dedication

This humble work is dedicated to my dear parents, whose love, appreciation dedication, and respect I hold in the highest regard.

No words can truly express the depth of my gratitude for the countless efforts you made day and night as well as for my education and well-being.

This work stands as a testament to the sacrifices you made.

To my brothers, my sisters, my entire family and my friends, I extend my heartfelt thanks and appreciation.

Abstract

In this work, we aimed to achieve the highest possible yield from perovskite solar cells by varying the thickness of the layers. Additionally, we explored semiconductors, solar radiation, and the different types and features of solar cells. From previous studies, We discovered that TiO_2 results in reduced cell performance. Consequently, we proposed using ZnO as an alternative due to its superior properties. Our results showed that incorporating ZnO increased the yield of the perovskite solar cells. Therefore, we believe that ZnO has great potential and should receive significant attention in future research and development.

Keywords: solar cell, Perovskite, SCAPS 1D.

ملخص

في هذا العمل، هدفنا إلى تحقيق أعلى عائد ممكن من خلايا الطاقة الشمسية البيروفسكايتية من خلال تغيير سمك الطبقات. بالإضافة إلى ذلك، استكشفنا أشباه الموصلات والإشعاع الشمسي وأنواع وخصائص الخلايا الشمسية المختلفة. من الدراسات السابقة، اكتشفنا أن TiO_2 يؤدي إلى تقليل أداء الخلية. لذلك، اقترحنا استخدام ZnO كبديل بسبب خصائصه المتفوقة. أظهرت نتائجنا أن دمج ZnO زاد من عائد خلايا الطاقة الشمسية البيروفسكايتية. وبالتالي، نعتقد أن ZnO لديه إمكانيات كبيرة ويجب أن يحظى باهتمام كبير في الأبحاث والتطوير المستقبلية .

الكلمات المفتاحية: خلية شمسية، بيروفسكايت، .SCAPS 1D.

Résumé

Dans ce travail, nous avons visé à obtenir le rendement le plus élevé possible des cellules solaires à pérovskite en variant l'épaisseur des couches. De plus, nous avons exploré les semi-conducteurs, le rayonnement solaire, ainsi que les différents types et caractéristiques des cellules solaires. D'après des études antérieures, nous avons découvert que le TiO_2 réduit les performances des cellules. Par conséquent, nous avons proposé d'utiliser le ZnO comme alternative en raison de ses propriétés supérieures. Nos résultats ont montré que l'incorporation du ZnO a augmenté le rendement des cellules solaires à pérovskite. Par conséquent, nous pensons que le ZnO a un grand potentiel et devrait recevoir une attention significative dans les recherches et développements futurs.

Mots-clés : cellule solaire, pérovskite, SCAPS 1D.

Table of contents

Table of figures

List of tables

Abbreviations list

F_{cc}	face-centred Cubic
TCO	Transparent Conductive Oxide
E_F	Fermi energy
K	Boltzmann constant
T	Temperature
N	The density of free electrons
N_c	Conduction Band Density
N_D	Donor Density
N_v	Valence Band Density
E_i	intrinsic level
n_i	intrinsic carrier density
E_A	Acceptor level
E_D	Donor level
ETA	Efficinecy
E_g	Energy Band
E_v	Valence Band
E_c	Conduction Band
FF	Fill Factor
I	current
V	voltage
I_{max}	Maximum current
I_{ph}	Photon Current
I_{sc}	Shor Circuit Current
PV	Photovoltaic
P_{max}	Maximum Power Point
R_s	Series Resistance
R_{sh}	Shunt Resistance
V_{oc}	Open Circuit Voltage
V_{max}	Maximum Voltage
V_{th}	Thermodynamics Voltage
PSC	Perovskite Solar Cell

PCE power conversion efficiency

NiO_x Nitric Oxide

ZnO Zinc oxide

TiO_2 Titanium dioxide

$CH_3NH_3PbI_3$ Methylammonium lead iodide

General Introduction

Ever since the discovery of electricity, the overriding concern has been how to generate it in the most efficient manner possible. Traditional methods of electricity generation, such as coal, natural gas, and nuclear energy, have dominated the energy landscape for decades [1] [2]. However, these sources have significant drawbacks, including environmental degradation, pollution, and the depletion of non-renewable resources [3] [4]. Therefore, it is crucial to develop and adopt alternative sources of energy that can meet the growing demand while ensuring sustainable development and environmental preservation.

Renewable energy sources such as solar, wind, hydro, geothermal, hydrokinetic, bioenergy, and hydrogen are gaining attention for their potential to provide clean, sustainable, and inexhaustible power [5][6]. These sources are considered environmentally friendly and are essential for reducing the carbon footprint and mitigating the effects of climate change.

Among these renewable sources, photovoltaic (PV) energy, which involves the use of solar cells, stands out as one of the leading environmentally friendly options. Solar energy is particularly accessible and cost-effective compared to other renewable sources[7][8]. Solar cells, based on semiconductor technology, convert sunlight into electricity. This conversion process is clean and sustainable, making solar energy an inexhaustible power source [9] [10].

The first chapter provides an overview of the basic properties and characteristics of semiconductors. It covers topics such as crystal structures, classification of materials into conductors, insulators and semiconductors, intrinsic and extrinsic semiconductors, and the emerging perovskite materials with their unique structure and potential applications in solar cells.

The second chapter covers the fundamentals of how solar cells work - detailing the properties of solar radiation, photon absorption to generate charge carriers in semiconductors, recombination mechanisms, and modeling the ideal and practical solar cell behavior. It also overviews three generations of solar cell technologies aimed at improving efficiency and lowering costs.

The third chapter focuses on introducing the SCAPS-1D solar cell simulation program. It explains the fundamental semiconductor equations used by SCAPS,

describes the user interface and various panels/functions for defining the solar cell structure, setting parameters, running different types of simulations (single, batch, etc.), and visualizing the results such as energy band diagrams, I-V curves, and other characteristics.

The fourth chapter we will optimize perovskite solar cell by changing the thickness of the absorber layer, we will compare between different TOC results.

Finally, we will end this thesis with a conclusion that resume our work and the main results we will obtain from simulation

Chapter 1:

Basic properties of Semiconductor

1.1 Introduction

Semiconductors, with electrical conductivity between that of conductors and insulators, are essential in electronics. Their conductivity is controlled through doping, which adds impurities to create free electrons (n-type) or holes (p-type). They also change conductivity with temperature and have a specific band structure with a valence and conduction band separated by an energy gap, crucial for devices like transistors and diodes. Additionally, semiconductors can emit and absorb light, used in LEDs and solar cells. These properties—doping control, temperature sensitivity, band structure, and light interaction—make semiconductors vital in various technologies.

1.2 Crystal structure

The semiconductors that are most commonly utilized are single crystals with a diamond (with Si and Ge) or zinc Blende (with GaAs and other compound semiconductors) lattice type as showing in (Figure.1.1).

The composition of both lattices can be viewed as two interpenetrating face-centred Cubic (fcc) sublattices that are displaced by one quarter of the distance along the diagonal of The cube. All atoms in the diamond lattice are identical, while the two fcc sublattices are built Of different atoms in the case of III–V compounds such as GaAs. Each atom is surrounded by four close neighbours belonging to the other fcc sublattice [13].

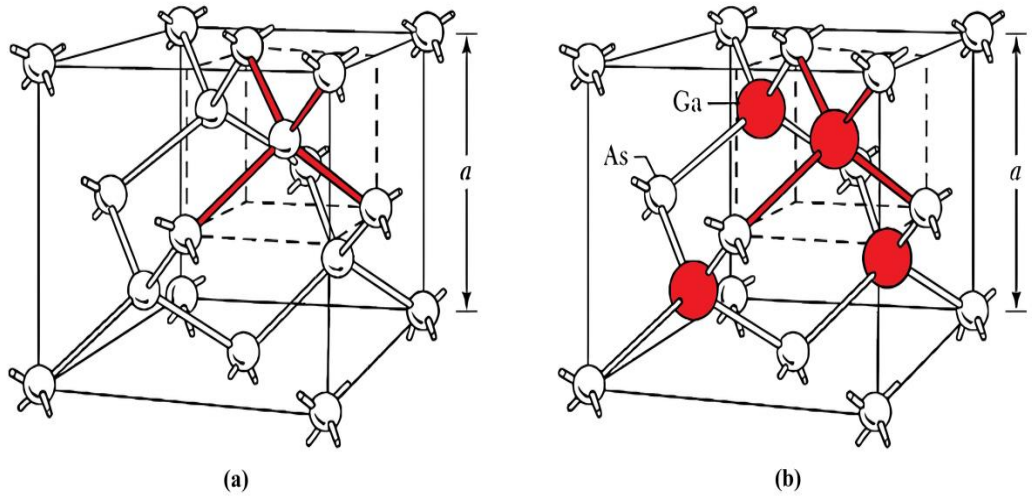

Figure 1.1 (a) Diamond lattice, (b) Zinc blende lattice [13].

1.3 Element semiconductors

In the early 19th century, the study of semiconductor materials began. Many semiconductors have been studied over the years. A portion of the periodic table related to semiconductors is shown in Table 1.1. Silicon (Si) and germanium (Ge) are two semiconductor elements composed of a single species of atoms found in Column IV. During the early 1950s, germanium was the primary semiconductor material. Since the early 1960s silicon has become a practical substitute and has now virtually supplanted germanium as a semiconductor Material. The main reasons we now use silicon are that silicon devices exhibit better properties at room temperature, and high-quality silicon dioxide can be grown thermally. There are also economic considerations. Device-grade silicon costs much less than any other semiconductor material. Silicon in the form of silica and silicates comprises 25% of the Earth's crust, and silicon is second only to oxygen in abundance. Currently, silicon is one of the most studied elements in the periodic table, and silicon technology is by far the most advanced among all semiconductor technologies [12].

Table 1.1 Portion periodic table related to semiconductors.

Column / Period	II	III	IV	V	VI
2		5 B Boron 10.81	6 C Carbon 12.011	7 N Nitrogen 14.007	8 O Oxygen 15.999
3	12 Mg Magnesium 24.32	13 Al Aluminium 26.98	14 Si Silicon 28.085	15 P Phosphorus 30.97	16 S Sulfur 32.065
4	51 Zn Antimony 121.76	31 Ga Gallium 69.72	32 Ge Germanium 72.63	33 As Arsenic 74.92	34 Se Selenium 74.92
5	48 Cd Cadmium 112,411	49 In Indium 114.82	50 Sn Tin 118.71	51 Sb Antimony 121,76	52 Te Tellurium 127,6
6	80 Hg Mercury 200.59		82 Pb Lead 207.2		

1.4 Conduction in metals, semiconductors, and insulators

The vast difference in how well metals, semiconductors, and insulators conduct electricity can be explained by looking at their energy bands. These bands represent the allowed energy levels for electrons within a material. (Figure 1.2) shows the energy band diagrams of three classes of solids: metals, semiconductors, and insulators [14] [15].

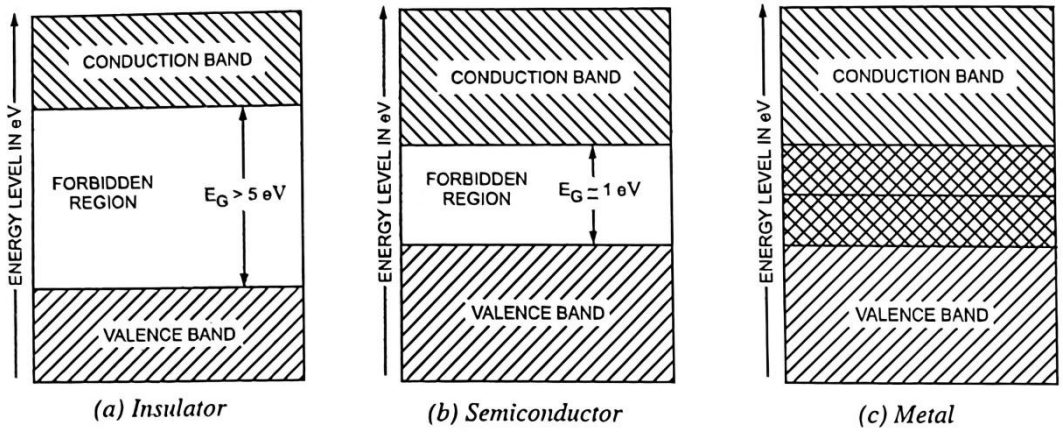

Figure 1.2 Schematic energy band representations of (c) a conductor (the overlapping bands), (b) a semiconductor, (a) an insulator.

a) Insulators

In case of insulators, there is practically no electron in the conduction band, and the valence band is filled. For an insulator, the valence and conduction bands are so apart (more than 5 eV) that at normal temperature (25°C) the energy which can be supplied to an electron from an applied field is too small to carry a particle from the filled band into the vacant band. Since the electron cannot acquire externally applied energy, conduction is impossible. Only at very high temperature or under high external electric field, an electron can jump the gap. This is called the breakdown of the insulating material [14].

b) Semiconductor

For semiconductors at a temperature of absolute zero (-273.15°C) the valence band is usually full and there may be no electron in the conduction band. It means that no current can flow in the semiconductors and, therefore, the Energy Band Diagram of Semiconductors behaves as insulators at absolute zero temperature. However, in semiconductor materials, both bands are so close (about 1 eV apart) that an electron can be lifted from the valence band to the conduction band by imparting

some energy to it. This energy must be more than energy gap E_G. If the energy imparted to the electron is less than E_G, it cannot be lifted from valence band to conduction band because no permissible energy level exists between the two bands. The energy imparted by the heat at room temperature is sufficient to lift electrons from the valence band to the conduction band. Some electrons do jump the gap and get into the conduction band. Thus, Energy Band Diagram of Semiconductors is capable of conducting some electric current, even at normal ambient temperature [2].

c) Metal

In case of conducting materials (metals), there is no forbidden gap, and the valence and conduction bands overlap each other, as illustrated in (Figure. 1.2 (c)). The orbits in the conduction band are very large. An electron in the conduction band experiences almost negligible nuclear attraction. In fact, an electron in the conduction band does not belong to any particular atom. But it moves randomly throughout the solid. This is the reason that electrons in the conduction band are called the free electrons. Due to overlapping of valence and conduction bands, a slight potential difference across the conductor causes the free electrons to constitute electric current.

1.5 Intrinsic semiconductors

Intrinsic semiconductors contain no (in practice, very few) impurities compared with the number of thermally generated electrons and holes. For this condition we shall attempt to estimate the number of free charge carriers (electrons and holes) under equilibrium conditions. The occupation probability for an electronic state is given by the Fermi Dirac function [1].

$$f(E) = \frac{1}{1+\exp\left(\frac{E-E_F}{k*T}\right)} \tag{1.1}$$

Where E_F, the Fermi energy, is the energy at which the occupation probability of a (possible) state is one half, k is the Boltzmann constant and T is the absolute temperature.

The density of free electrons n is obtained by integrating the carrier concentration (Figure. 1.3(d)) given by the product of the density of states N (Figure.1.3 (b)) and the occupation probability $F_n(E)$ (Figure. 1.3(c)) over the conduction band:

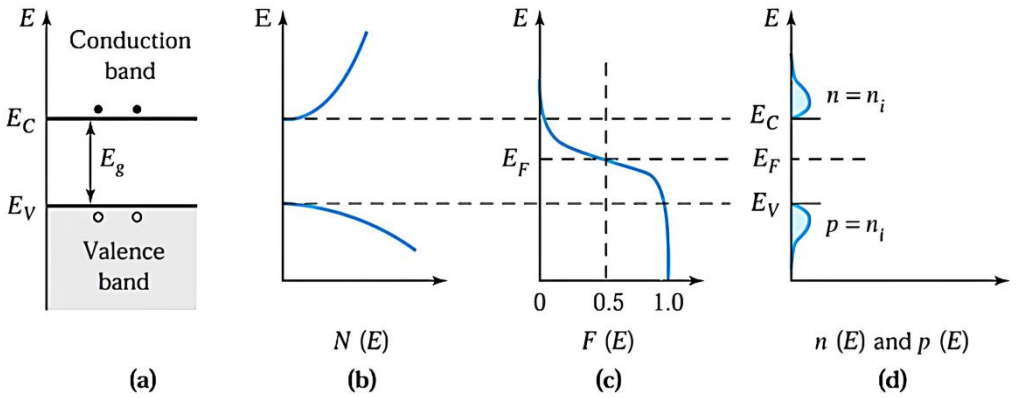

Figure 1.3 Intrinsic semiconductor: (a) Schematic band diagram, (b) Density of states, (c) Fermi distribution function, (d) Carrier concentration.

$$n = 2\left(\frac{2\pi m_n kT}{h^2}\right)^{\frac{3}{2}} e^{-\frac{E_C - E_F}{kT}} = N_C e^{-\frac{E_C - E_F}{kT}} \quad (1.2(a))$$

Similarity for holes, we have:

$$p = 2\left(\frac{2\pi m_p kT}{h^2}\right)^{\frac{3}{2}} e^{-\frac{E_F - E_V}{kT}} = N_V e^{-\frac{E_F - E_V}{kT}} \quad (1.2(b))$$

N_C And N_V are the effective densities of states in the conduction and valence bands respectively. The product of electron and hole concentration, given by $\cdot p = N_C N_V e^{-\frac{E_C - E_V}{kT}}$, depends on the band gap $E_G = E_C - E_V$ and is thus independent of the Fermi level E_F.

So far the value of the Fermi level E_F has not been specified and equations (1.1) to (1.2) will also be valid for extrinsic semiconductors (to be dealt with in the following chapter). The Fermi level for intrinsic semiconductors E_i can be found from the requirement that the numbers of electrons and holes are equal: $n = p = n_i$. One thus finds that:

$$n_i = \sqrt{N_C N_V} e^{-\frac{E_C - E_V}{2kT}} = \sqrt{N_C N_V} e^{-\frac{E_G}{2kT}} \quad (1.3)$$

And

$$E_i = \frac{E_C + E_V}{2} + \frac{3kT}{4} \ln\left(\frac{m_p}{m_n}\right) \quad (1.4)$$

Where E_i is the Fermi level close to the middle of the band gap, the deviation being due to the unequal effective masses of electrons and holes.

Introducing the intrinsic carrier density n_i and the intrinsic level E_i, one may reformulate the more generally valid (1.2) in the useful form:

$$n = n_i e^{\frac{E_F - E_i}{kT}} \qquad p = n_i e^{\frac{E_i - E_F}{kT}} \tag{1.5}$$

1.6 Extrinsic semiconductors

Intrinsic semiconductors are rarely used in semiconductor devices since it is extremely difficult to obtain sufficient purity in the material. Moreover, in most cases one intentionally alters the property of the material by adding small fractions of specific impurities. This procedure, which can be performed either during crystal growth or later in selected regions of the crystal, is called doping. Depending on the type of added material, one obtains n-type semiconductors with an excess of electrons in the conduction band or p-type with additional holes in the valence band. We will look at extrinsic semiconductors through the simple bond representation and also through a band model [13].

(Figure 1.4(a)) shows a two-dimensional schematic bond representation of a silicon crystal with one silicon atom replaced by an arsenic atom with five valence electrons. Only four are used for the formation of covalent bonds with neighboring atoms, while the fifth is not bound to a specific atom but is free for conduction. It should be stressed that the crystal as a whole remains uncharged, since the charge of the free electron is compensated for by the excess charge of the arsenic nucleus bound in the crystal lattice [13].

If a silicon atom is replaced by an atom with only three valence electrons (Figure 1.4(b)) one electron is missing in the covalent bonds and a hole is thus created. This hole may be filled by an electron from a neighboring atom, this being equivalent to a movement of the hole. The hole is free for conduction. (That the moving hole is more than a missing electron whose place is filled by a neighboring electron follows from quantum mechanical considerations and is experimentally verified in the Hall experiment [13].

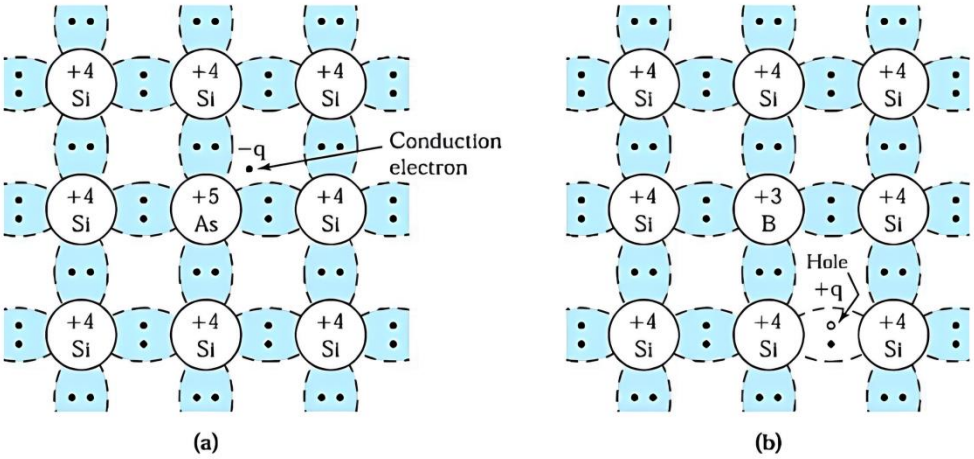

Figure 1.4 Schematic bond pictures for (a) n-type Si with donor (arsenic) and (b) p type Si with acceptor (boron).

Looking at the situation in the band model, we can state that the replacement of a proper atom of the lattice by a different atom is accompanied by the creation of localized energy levels in the band gap. These energy levels may be of the donor (E_D) or acceptor (E_A) type. If donor levels E_D are close to the conduction band, as is the case for phosphorous ($E_C - E_D = 0.045$ eV) or arsenic ($E_C - E_D = 0.054$ eV) atoms in silicon, for instance, these states will transported to the conduction band (Fig. 1.5 a). This is due to the many states with similar energy level nearby in the conduction band, with which the donor states have to share their electrons.

Equivalent considerations hold for acceptor-type states, e.g. boron in silicon ($E_A - E_V = 0.045$ eV). These states will be filled almost completely and holes will be created in the valence band (Figure 1.5 b).

The situation that the donor levels are almost completely ionized can be described by a movement of the Fermi level E_F from the intrinsic level E_i towards the conduction band. Up to fairly high doping concentrations, the value of E_F follows from (1.2) by setting the electron concentration in the conduction band *n* equal to the donor concentration N_D, thus:

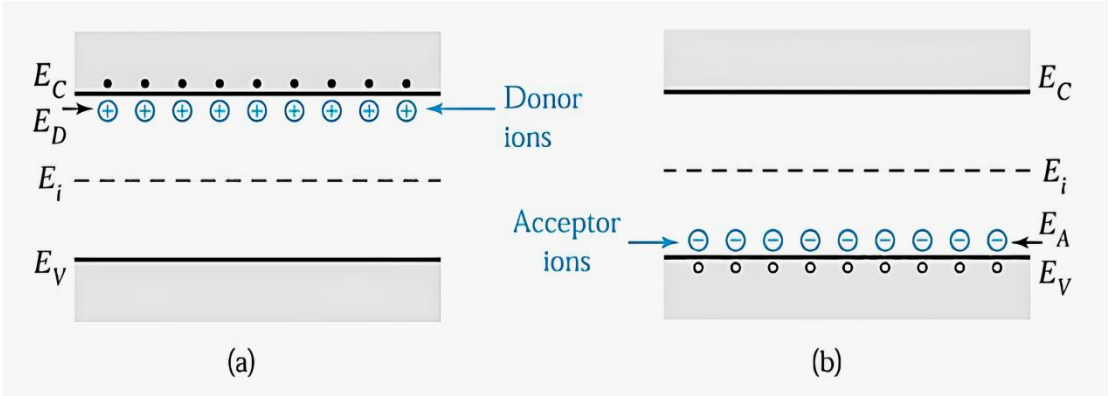

Figure 1.5 (a) Schematic energy band representation of extrinsic n-type, (b) p-type semiconductors.

$$E_C - E_F = kT \ln \frac{N_C}{N_D} \tag{1.6}$$

Similarity one obtains for p-type material and acceptor concentration N_A:

$$E_F - E_V = kT \ln \frac{N_V}{N_A} \tag{1.7}$$

A somewhat more complicated treatment is required for the simultaneous presence of donors and acceptors and for very high doping concentrations. It may also be mentioned in this context that the number of donor or acceptor states does not necessarily equal the number of corresponding impurity atoms, since in order to become electrically active doping atoms they have to be properly built into the crystal lattice [13].

Using the results of the previous section, the density of free electrons n is

$$n = n_i e^{\frac{E_F - E_i}{kT}} \tag{1.8(a)}$$

The density of free holes p is

$$p = n_i e^{\frac{E_i - E_F}{kT}} \tag{1.8(b)}$$

The increase of majority carriers (electrons in the case of n-type material) is accompanied by a decrease of minority carriers according to the mass-action law

$$n \cdot p = n_i^2 \tag{1.9}$$

In agreement with (1.8)

1.7 Perovskite structure

The terms "perovskite" and "perovskite structure" are often used interchangeably. Technically, a perovskite is a type of mineral that was first found in the Ural Mountains and named after Lev Perovski (who was the founder of the Russian

Geographical Society). A perovskite structure is any compound that has the same structure as the perovskite mineral [18].

True perovskite (the mineral) is composed of calcium, titanium and oxygen in the form CaTiO3. Meanwhile, a perovskite structure is anything that has the generic form ABX3 and the same crystallographic structure as perovskite (the mineral). However, since most people in the solar cell world aren't involved with minerals and geology, perovskite and perovskite structure are used interchangeably.

The perovskite unit cell is demonstrated below. As with many structures in crystallography, it can be represented in multiple ways. The simplest way to think about a perovskite is as a large atomic or molecular cation (positively-charged) of type A in the centre of a cube. The corners of the cube are then occupied by atoms represented by B (also positively-charged cations) and the faces of the cube are occupied by a smaller atom X with negative charge (anion).

Depending on which atoms/molecules are used in the structure, perovskites can have an impressive array of interesting properties, including superconductivity, giant magnetoresistance, spin-dependent transport (spintronics) and catalytic properties. Perovskites therefore represent an exciting playground for physicists, chemists and material scientists [17].

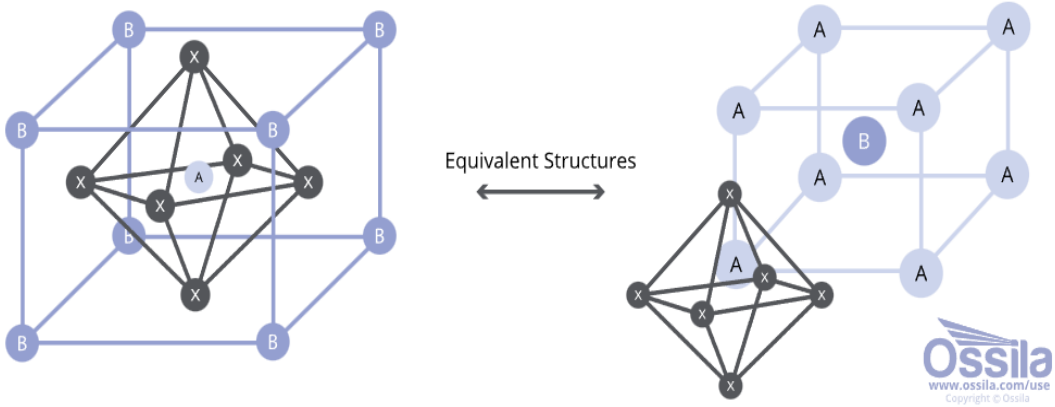

Figure 1.6: A generic perovskite crystal structure of the form ABX3 [17].

Perovskites were first successfully used in solid-state solar cells in 2012 and since then most cells have used the following combination of materials in the usual perovskite form ABX3:

- A = An organic cation - methylammonium ($CH_3NH_3^+$) or formamidinium ($NH_2CHNH_2^+$)

- B = A big inorganic cation - usually lead(II) (Pb^{2+})
- X_3= A slightly smaller halogen anion – usually chloride (Cl^-) or iodide (I^-)

1.8 Challenges

The biggest issue in the field of perovskites currently is long-term instability. This has been shown to be due to degradation pathways involving external factors, such as water, light, and oxygen, and also as a result of intrinsic instability, such as degradation upon heating, because of the properties of the material [19].

1.9 Conclusion

In this chapter, we explored the fundamental properties of semiconductors, examining their crystal structures and how their conduction mechanisms differ from metals and insulators. Metals conduct electricity due to free electrons, while insulators lack these carriers, and semiconductors exhibit conditional conductivity. We distinguished between intrinsic semiconductors, which rely on thermal excitation, and extrinsic semiconductors, enhanced by doping to create n-type or p-type materials. Additionally, we discussed perovskites, noting their promising optoelectronic properties and potential in solar cells due to their flexible structure, high absorption, and tunable bandgaps. This foundational understanding sets the stage for exploring advanced semiconductor technologies and applications.

Chapter 2:

The Properties and Characteristics Of solar cell

2.1 Introduction

Solar cells are photoconverters that convert direct sunlight into electricity. Light from the sun is a stream of pure energy particles called photons. In this chapter, we will learn about the working principle of solar cells and the types of solar cells.

2.2 Solar radiation

Solar energy is the most available energy source for human society. Since the total solar energy absorbed by the Earth reaches 4×10^6 EJ/year, it represents ten times the energy consumed in the world in 2007. For example, if 50 percent of the sunlight shining in New Mexico was converted into useful energy, this could meet all the energy needs of the United States of America [20].

AM1.5 represents the spectrum of solar light that remains after the light passes at an angle through approximately one and a half Earth atmospheres (Figure 2.1). AM1.5 is used as the standard spectral distribution of light to measure a solar cell's efficiency. Generally, 99% of the light that reaches the Earth's surface is at wavelengths of less than 2500 nm in the AM1.5 spectrum, and 88% is less than 1350nm. To be efficient, a solar cell should be able to absorb the largest number of photons possible; otherwise, the cells will lose their energy because the absorptionspectrum is limited by the semiconductor band. Therefore, researchers suggest small band gap materials to increasesolar cell performance. Regardless, only photons withenergies greater than the band gap will be absorbed. (Figure 2.1) compares the AM0 and AM1.5 spectra [21].

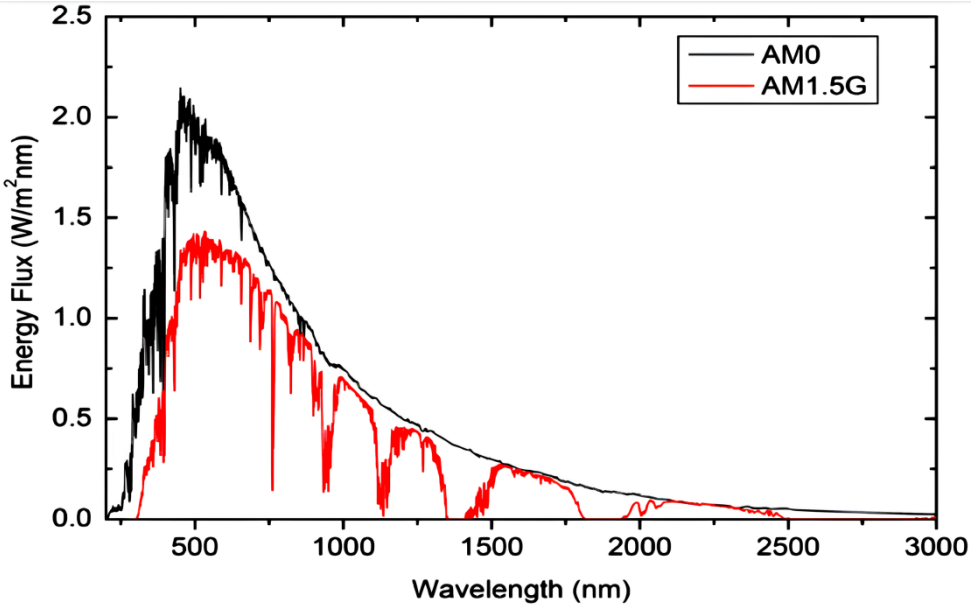

Figure 2.1:AM0 and AM1.5 solar irradiance spectra **[**8].

2.3 Transfer of energy from the photon to the electron

There are two pre-requisites for luminescence: (1) the luminescent material must have a semiconductor structure with a nonzero band gap Eg (e.g. metals do not luminesce since they have no band gap); (2) energy must be imparted to this material before luminescence can take place. The mechanism of photoluminescence in semiconductors is schematically illustrated in (Figure 2.2), which plots the E-k diagrams for a direct band gap material (left) and an indirect gap material (right), where E and k are respectively the kinetic energy and wave vector (or "momentum vector") of the electron or hole ($E = k^2\bar{h}^2/2m_*, where\ \bar{h} \equiv h/2\pi$ is the Planck constant h divided by 2π, and m_* is the electron or hole effective mass). The direct and indirect gap materials are distinguished by their relative positions of the conduction band minimum and the valence band maximum in the Brillouin zone (the volume of k space containing all the values of k up to π / a where a is the unit lattice cell dimension). In a direct gap material, both the conduction band minimum and the valence band maximum occur at the zone center where k = 0. In an indirect gap material, however, the conduction band minimum does not occur at k = 0, but rather at some other values of k which is usually at the zone edge or close to it [22].

2.4 Generation of excess carriers by light

The principle is based on the interaction of light and matter in semiconductors.

The energy of the photon corresponding to a given radiation is related to its wavelength by the relation:

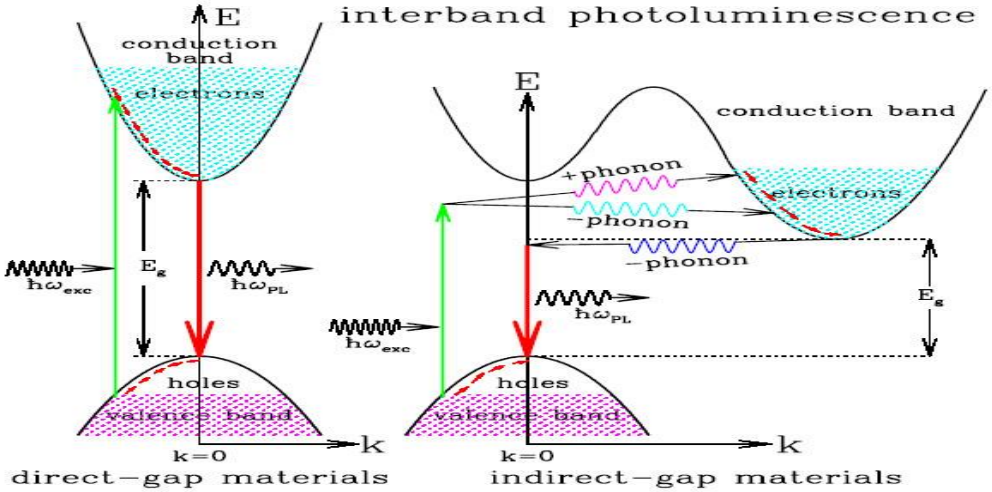

Figure 2.2: Schematic band diagrams for the photo luminescence processes in a directgap material (left) and an indirect gap material (right) [22].

$$E_p = h\nu = \frac{hc}{\lambda} = \frac{1.24}{\lambda} \quad (2.1)$$

Where ν is the frequency of the radiation, λ the wavelength of the radiation in μm, c the speed of light, E_p the photon energy in eV and h is the Plank constant.
A luminous radiation encountering a semiconductor is absorbed according to LambertBouguer's law:

$$I(x) = I(1-R)\exp(-\alpha x) = I_o \exp(-\alpha x) \quad (2.2)$$

Where x is the depth of absorption of the beam in the material from the surface of the semiconductor, R is the reflection coefficient, represents the part of the incident light energy I, reflected on the surface of the material, and α is the absorption coefficient.

The optical behavior of the material is fully described by its optical constants. These are the refractive index n and the extinction coefficient k, which together form the complex refractive index N. n and k depend on the wavelength of the incident light. The refractive index n is related to the propagation speed of the light wave and the coefficient k is a unit of measurement for the wave damping. The complex refractive index is defined as:

$$N = n(\lambda) + ik(\lambda) \quad (2.3)$$

The optical absorption coefficient α is given by:

$$\alpha = \frac{4\pi k}{\lambda} \quad (2.4)$$

(Figure 2.3) gives the absorption spectra of some materials. The minimum energy required for the incident photon to cause the electronic transition depends on the band gap E_g of the material.

The calculation of the generation rate of electron-hole pairs G(x) ($cm^{-3}s^{-1}$) is carried out as follows. Calling I_o, the flux of photons ($cm^{-2}s^{-}1$) incident on the illuminated side of the material and α(cm^{-1}) the absorption coefficient of light by the material. At depth x, this generation rate is:

$$G(x) = \alpha(1 - R)I_o e^{-\alpha x} \quad (2.5)$$

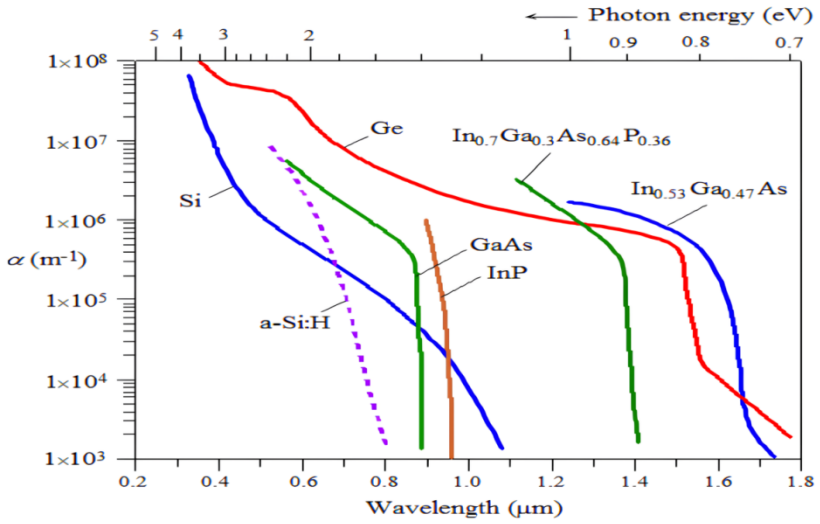

Figure 2.3 Absorption spectra of the most commonly used semiconductor materials in solar cells.

2.5 Recombination mechanisms of excess carriers

By recombination we refer to the loss of mobile electrons or holes by any of a number of removal mechanisms. Unlike generation, where one mechanism is dominant, several different recombination mechanisms are important for the photovoltaic device. [24]

2.5.1 Band – to – band recombination

Band-to-band recombination refers to the annihilation of an e – h pair followed by the emission of a photon of corresponding energy. These unavoidable recombination (in the sense that, unlike other recombination mechanisms, they must occur in any PV cell) are particularly effective indirect band gap materials, such as GaAs.

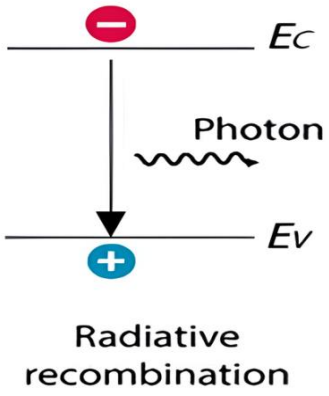

Figure 2.4: Scheme of the main recombination processes Radiative [25].

2.5.2 Auger recombination

Auger recombination refers to a three-particle mechanism where the energy of an electron in the CB (or, alternatively, the energy of a hole in the VB) is transferred to another electron (or hole). The excess energy is rapidly dissipated as heat in the crystalline network.

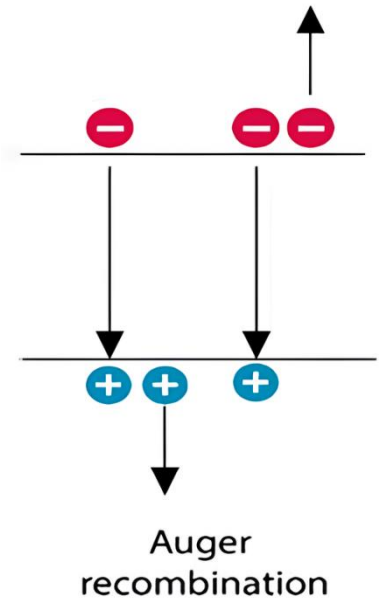

Figure 2.5: Scheme of the main recombination processes Auger [25].

2.5.3 Shockley Read Hall (SRH) recombination

Recombination involves impurities or defects in the crystalline structure, giving rise to unwanted energy levels acting like traps in the forbidden gap: annihilation of an e – h pair may occur if both a free electron in the CB, and a hole in the VB, simultaneously fall into an impurity trap [25].

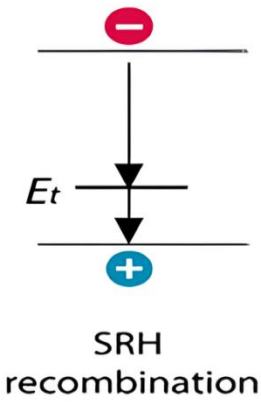

Figure 2.6: Scheme of the main recombination processes Shockley – Read – Hall. [11].

SRH recombination is often strong in many semiconductor materials, and a particular care should be brought toward minimizing the defect density in the PV cell through appropriate fabrication and doping conditions. Trap states are also likely to appear at the surface of the cell because of material discontinuities. These recombination mechanisms, known as surface recombination, may be minimized with high-quality surface passivation.

2.5.4 Surface recombination

Surface recombination velocity is an important parameter which affects the dark saturation current and the quantum efficiency of solar cells. Similarly to dislocations and planar defects such as grain boundaries, surfaces (and interfaces in general) introduce band of electronic states in the band gap which can be ascribed to broken (or strained) bonds and impurities. A complete characterisation of surface recombination must also take into account the surface charge which may give rise to band bending. To achieve optimal operation, surface recombination is reduced by a passivating or window layer which prevents minority carriers from reaching the surface. Passivation of silicon surface by an oxide layer, or the deposition of a thin 'window' layer of GaAlAs on GaAs solar cells are just two examples of such practice [26].

2.6 Operating principle of a solar cell

The photovoltaic effect used in solar cells makes it possible to directly convert the light energy of the sun's rays into electricity through the production and transport in a semiconductor material of positive and negative electrical charges under the effect of light. This material has two parts, one with an excess of electrons and the other with a deficit in electrons, respectively called n-type doped and p-type doped. When the first is brought into contact with the second, the excess electrons in the material n diffuse into the material p. The initially n-doped area becomes positively charged, and the initially p-doped area becomes negatively charged. An electric field is therefore created between them which tends to push the electrons into the n zone and the holes towards the p zone. A PN junction is therefore formed. By adding metal contacts to areas n and p, a diode is obtained. When the junction is illuminated, the photons of energy equal to or greater than the width of the forbidden band give up their energy to the atoms, each one passes an electron from the valence band into the conduction band and also leaves a hole capable of move, thus generating an electron-hole pair. If

a charge is placed across the cell, the electrons from zone n join the holes in zone p via the external connection, giving rise to a potential difference and an electric current flow.

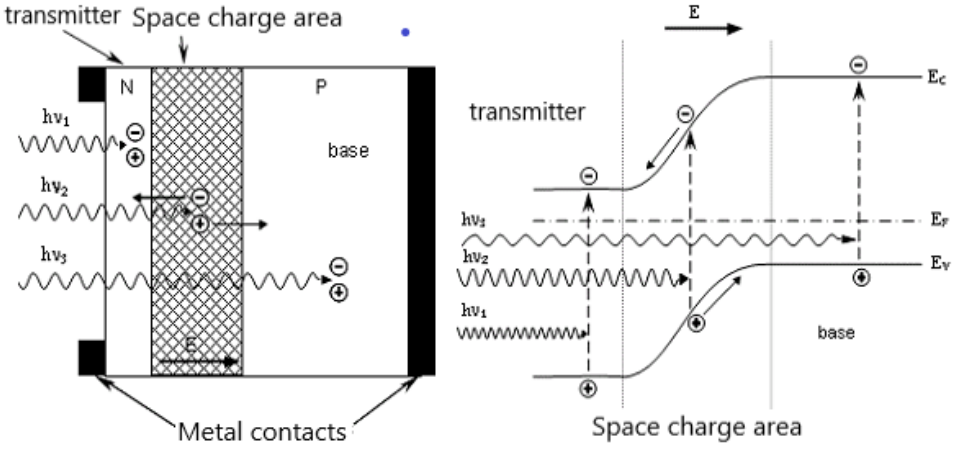

Figure 2.7: Structure and band diagram of a photovoltaic cell.

The operating principle of a solar cell is illustrated in (Figure 2.7) .The incident photons create carriers in the N, P regions and the space charge region. The behavior of these free carriers differs depending on the location of their creation. In the electrically neutral zones P and N, the minority photocarriers diffuse. Those that reach the space charge region are propelled by the electric field towards the region where they become the majority. These photocarriers therefore contribute or current through their diffusion, they create a diffusion photocurrent. In the space charge zone, the electron-hole pairs created by the photons are dissociated by the electric field, the electron is propelled towards the N-type region and the hole towards the P-type region. The carriers give rise to a generation photocurrent. These two contributions add to create a resulting photocurrent I_{ph} which contributes to the reverse current of the diode [27].

2.7 The ideal solar cell

The equivalent circuit of a solar cell consists of an ideal current generator in parallel with a diode in reverse bias, both of which are connected to a load. The generated current is directly proportional to light intensity. This highlights how important it is to accurately replicate the solar spectrum when testing solar cells. [28]

This model does not take into account the internal losses of the current. The output current (I) of the ideal solar cell model with single diode connected in module is obtained by Kirchhoff law [29]:

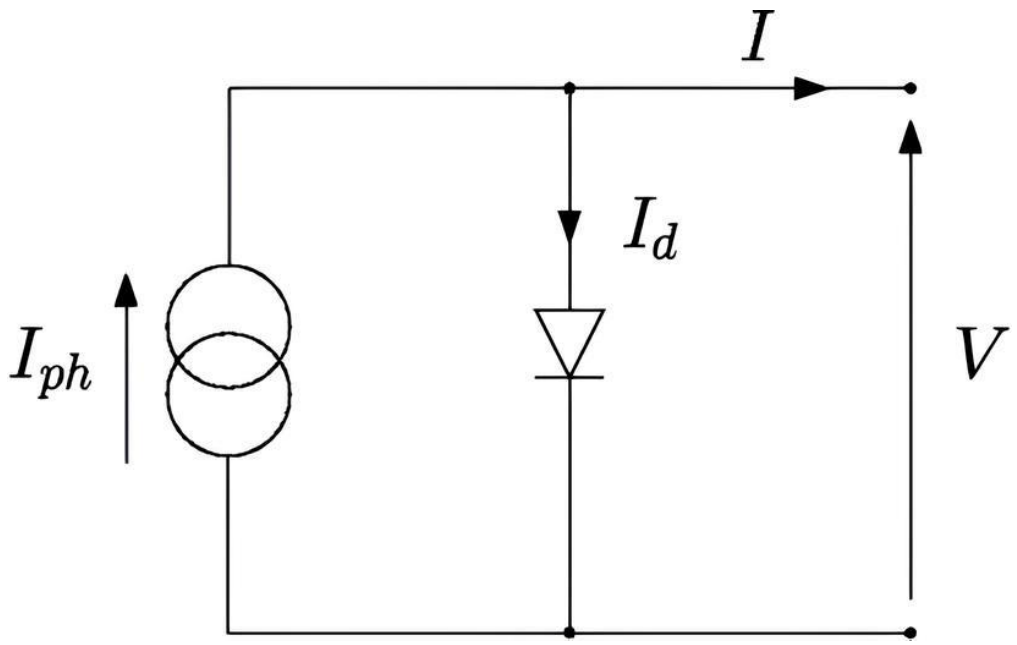

Figure 2.8: Equivalent circuit diagram of an ideal solar cell.

From this ideal circuit diagram, we can extract equations to describe and model solar cells. This also helps us define some of the most important metrics we use to describe solar cells. In its simplest form, we can describe current through the load as the amount of current generated minus the current that flows through the diodes [28].

$$I = I_{ph} + I_d \tag{2.6}$$

Where I_{ph} is the photo generated current, I_d is the diode current and it's expressed by:

$$I_d = I_0(e^{\frac{qV_d}{kT}} - 1) \tag{2.7}$$

In which I_0 is the reverse saturation current, q is the electron charge, k = Boltzmann's constant, and T is the diode junction temperature [30].

(Figure. 2.8) shows the IV (current – voltage) curve of a solar cell that follows Eq. The photo generated current shifts the IV curve up, enhancing the available power to be extracted. Under low-voltage values, the output current remains close to the short-circuit value. However, as the voltage increases, the dark current grows exponentially and the output current decreases [25].

The open-circuit voltage, which corresponds to the point of the IV curve where the dark current and the photo generated current compensate each other, leading to an output current equal to zero, can simply be derived from Eq. (2.8):

$$V_{oc} = \frac{kT}{q}\ln\left(1 + \frac{I_{ph}}{I_0}\right) \tag{2.8}$$

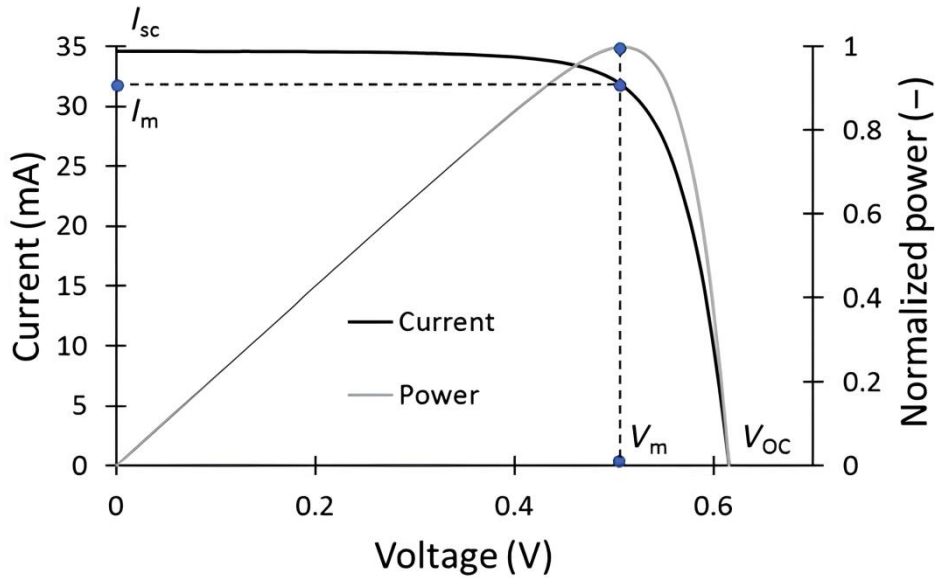

Figure 2.9: IV Curve of a photovoltaic (PV) cell, showing the main solar cell Parameters [25].

The power P = IV produced by the cell is shown in (Figure 2.8) the cell generates the maximum power P_{max} at a voltage V_m and current I_m and it is convenient to define the fill factor FF by

$$FF = \frac{I_m V_m}{I_{sc} V_{oc}} = \frac{P_{max}}{I_{sc} V_{oc}} \quad (2.9)$$

The fill factor FF of a solar cell with the ideal characteristic will be furnished by the subscript 0. It cannot be determined analytically but it can be shown that FF_o depends only on the ratio $v_{oc} = V_{oc}/kT$. FF_o is determined, to an excellent accuracy, by the approximate expression

$$FF_O \frac{v_{oc} - \ln(v_{oc} + 0.72)}{V_{oc} + 1} \quad (2.10)$$

2.8 Solar Cell in practice:

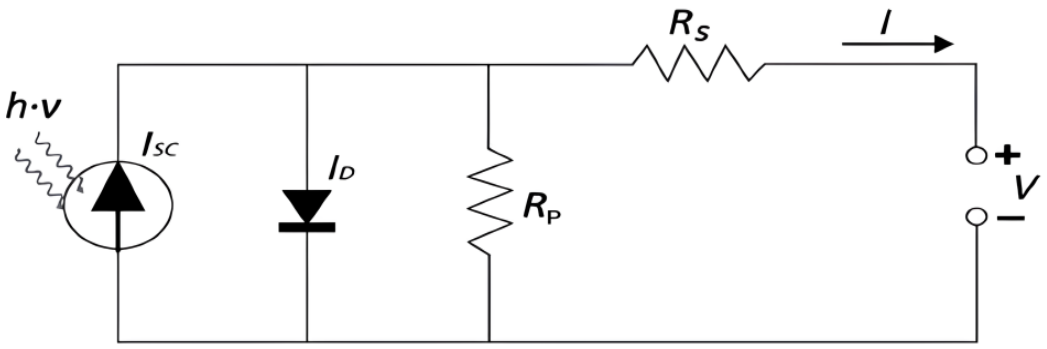

Figure 2.9: Equivalent circuit of a solar cell in practice.

The I-V characteristic of a solar cell in practice usually differs to some extent from the ideal characteristic .The solar cell (or circuit) may also contain series (R_s) and parallel (or shunt, R_P) resistances, leading to a characteristic of the form [26].

$$I = I_{ph} - I_o\left\{e^{\left(\frac{V+IR_S}{2kT}\right)} - 1\right\} - \frac{V+IR_S}{R_P} \quad (2.11)$$

Where the light-generated current I_{ph} may, in some instances, depend on the voltage. These features are shown in the equivalent circuit of (Figure 2.9). The effect of the series and parallel resistances on the I–V characteristic of the solar cell is shown in (Figures 2.10). The effect of the series resistance on the fill factor can be writing as:

$$FF = FF_0(1 - r_s) \quad (2.12)$$

Where $r_s = R_s I_{SC}/V_{OC}$ An analogous expression exists also for the parallel resistance.

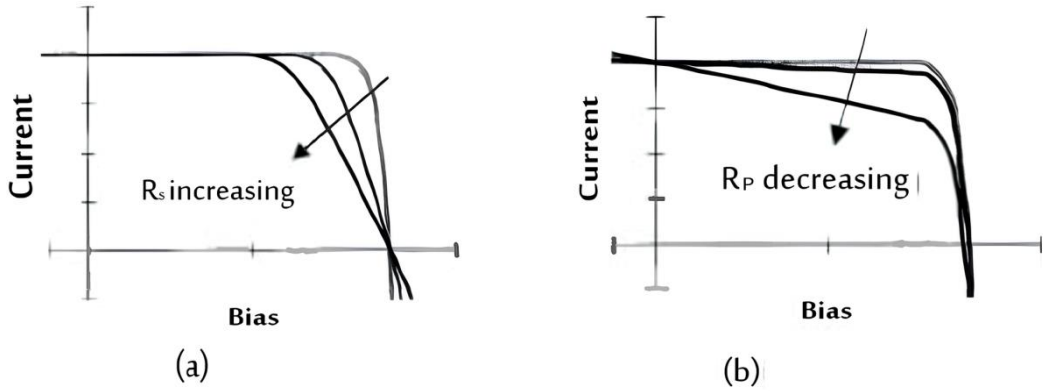

Figure 2.10: Effect of (a) increasing series and (b) reducing parallel resistances. In each case the outer curve has $R_s = 0$ and $R_P = \infty$. In each case the effect of the resistances is to reduce the area of the maximum power rectangle.

2.9 Types of solar cells:

It relies mainly on semiconductors similar to the formation of the P-N junction, as these solar cells are divided into three different generations, classified according to the materials used and how they are manufactured, and they all convert light energy into electrical conductivity [31].

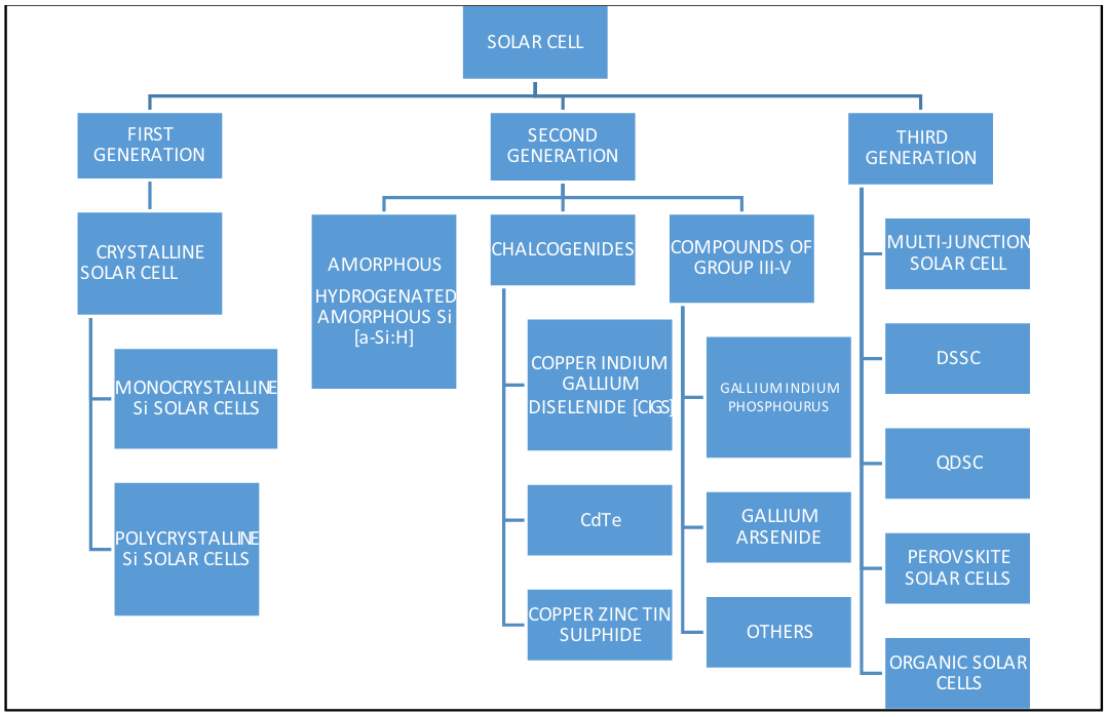

Figure 2.12: Various types of solar cells and current advancements [31].

2.9.1 First generation solar cells

These are solar cells based on crystalline Si wafers. Manufactured from Crystalline Si, thus most costly technique of obtaining pure Silicon crystal is involved in this technology. These solar cells are used worldwide and these have highest commercial efficiency [11]. About 80% solar cell market is based on single crystalline solar cells. It was reported by Zhao et al (1998) that polycrystalline solar cells having honeycomb like structure have efficiency of about 19.8%. Polycrystalline solar cells are less efficient as compared to the crystalline solar cells.

1. Single crystalline solar cells
2. Polycrystalline solar cells

2.9.2 Second generation solar cell Technology (Thin film solar cell technology)

Si crystal wafer technology is costly as it uses mostly pure crystalline Si. Obtaining pure Si is a complex and costly process. Cost of solar cells can be reduced if thin films of Si (1µm) can be deposited. Very little amount of Silicon is used by thin film technology as compared to wafer based technology. R. Chittick developed amorphous Si deposited thin films first. Then his co-workers published a report on first systematic and explenatory study on plasma enhanced chemical vapour deposition technique [32].

2.9.3 Third generation solar cell technology

Third generation PV cell technology refers to single junction solar cell which can overcome Shockley–Queisser limit of 31–41% power efficiency. C-Si solar cells (First generation) and thin film solar cells are having some limitations for achieving higher efficiency and to be established as Photovoltaic technology to fulfil all conditions as per golden triangle. Third generation solar cell technology consists of the following types of solar cells.

1. CZTS solar cells including materials CZTSe and CZTSSe
2. Dye sensitized solar cells
3. Quantum Dot solar cells
4. Perovskite solar cells
5. Organic solar cells

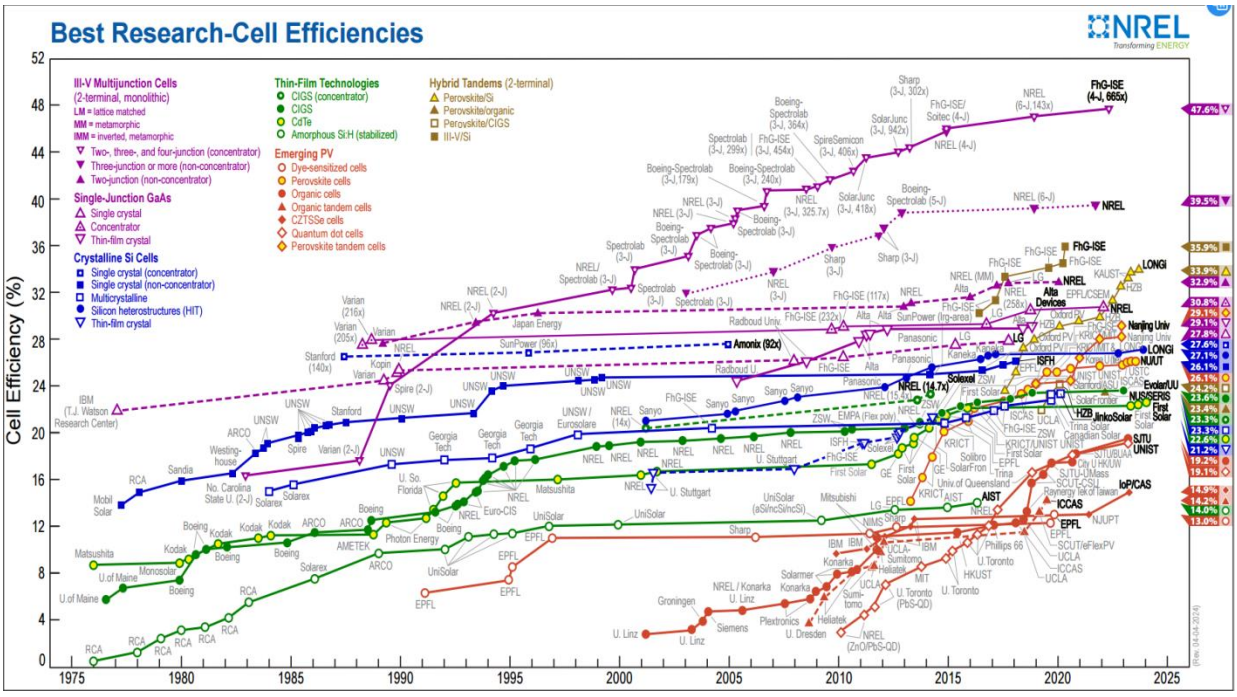

Figure 2.13: Best Research-Cell Efficiency Chart [33]

2.10 Perovskite solar cells

Perovskite solar cells (PSCs) are thin-film semiconductor-type solar cells that are similar to practical solar cells using compound semiconductors (GaAs, CdTe, etc.) and amorphous Si in photovoltaic (PV) industries. The advantage of these thin-film cells over the most popular crystalline Si solar cells is their processability into lightweight, thin, flexible devices. Lightweight and mechanical flexibility are significant added values sought for next-generation PV devices. Flexibility enables

the device to be attached to curved surfaces of outdoor and indoor structures. Lightweight is particularly advantageous for mounting the device on mobile objects including cars and people [34].

2.11 Absorption spectra of perovskite:

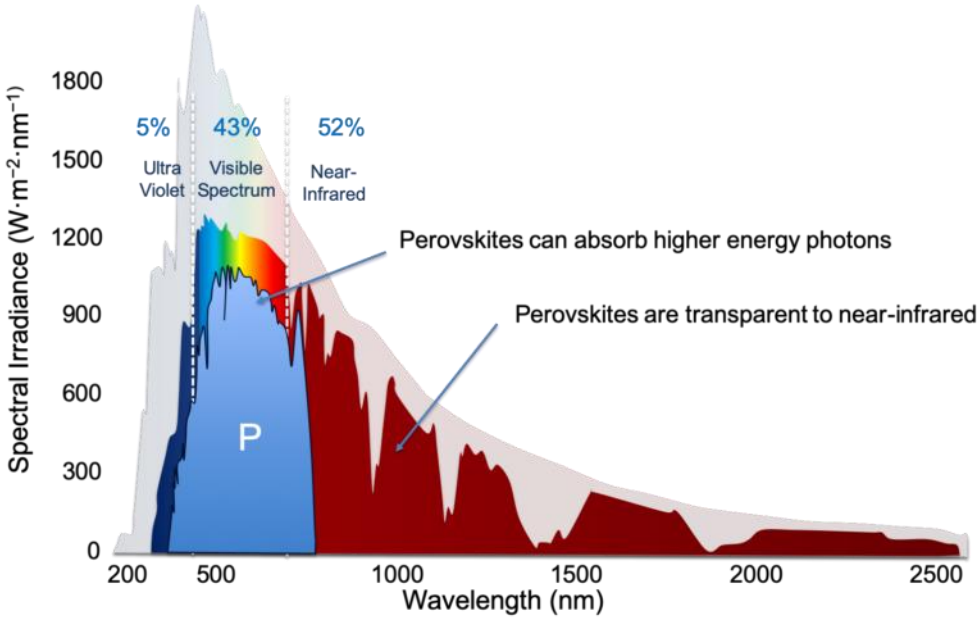

Figure 2.14: Material absorption curve [35].

Peroskites are very efficient at absorbing high-energy photons in the ultraviolet and visible spectrum. Absorption quickly drops off at 780 nm, making perovskites essentially transparent to the near-infrared spectrum where more than half of the total available energy is located.

2.12 Fabrication of Perovskite Solar Cells:

Perovskite materials have been considered to be simpler and easier to fabricate than semiconductor silicon.

The perovskite film itself is typically processed by either vacuum or solution methods. Film quality is very important. Initially, vacuum-deposited films gave the best devices, but this process requires the co-evaporation of the organic (methylammonium) component at the same time as the inorganic (lead halide) components, necessitating specialist evaporation chambers that are not available to many researchers. As a result, there have been significant efforts into improving solution-processed devices, as these are simpler and allow for low-temperature processing, and these now equal vacuum-deposited cells in terms of efficiency.

Typically, the active layer of a perovskite solar cell is deposited via either a one or two-step process. In the one-step process, a precursor solution (such as a mix of CH_3NH_3I and PbI_2) is coated that then converts to the perovskite film upon heating. A variation on this is the 'antisolvent' method, in which the precursor solution is coated in a polar solvent, and then quenched during the spin coating process by a non-polar solvent. Precise timings of the quench and volumes of the quenching solvents is required to give the optimal performance.

In the two-step process, the metal halide (such as PbI_2) and organic components (such as CH_3NH_3I) are spin-coated in separate, subsequent films. Alternatively, metal halide films can be coated and annealed in a chamber filled with the organic component vapour, known as 'vacuum-assisted solution process' (VASP).

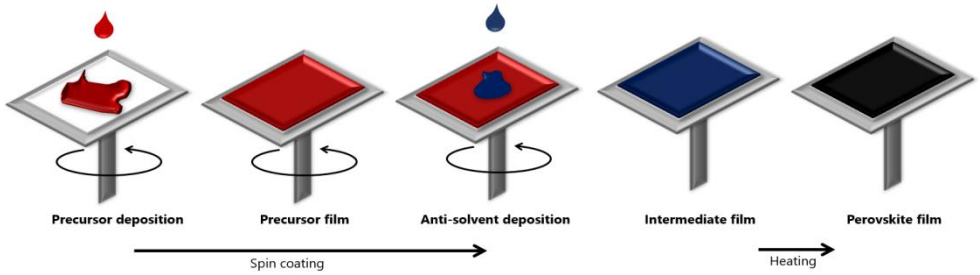

Figure 2.15: An approximation of the anti-solvent quenching method often used to coat perovskites in a one-step process from a precursor solution [14].

2.13 Conclusion

Solar cells convert the abundant energy from sunlight into electricity through the photovoltaic effect in semiconductor materials. This chapter covered the fundamental working principles, including the properties of solar radiation, photon absorption and photoelectric energy generation, and various recombination mechanisms that impact efficiency. The ideal solar cell was modeled as a current source with parallel diode, though practical devices exhibit parasitic resistances. Three generations of technologies were discussed - first generation crystalline silicon cells are efficient but expensive, second generation thin-films reduce cost but sacrifice some efficiency, while third generation architectures like perovskites, organics, and multi-junctions aim to exceed traditional limits at low cost. Continued research into new materials, cell designs, and manufacturing is important for making solar cells an even more viable renewable energy solution by enhancing efficiency and lowering costs to meet growing global energy demands sustainably.

Chapter 3:

SCAPS-1D program

3.1 Introduction

SCAPS (Solar Cell Capacitance Simulator) is a one dimensional solar cell simulation program developed at the department of Electronics and Information Systems (ELIS) of the University Of Gent, Belgium. Several researchers have contributed to it's development: Alex Niemegeers, Marc Burgelman, Koen Decock, Johan Verschraegen, Stefaan Degrave. A description of the program, and the algorithms it uses.

3.2 SCAPS-1D program

The program is freely available to the PV research community (universities and research institutes). It runs on PC under Windows 95, 98, NT, 2000, XP, Vista, Windows 7, and occupies about 50 MB of disk space.

SCAPS is originally developed for cell structures of the CuInSe2 and the CdTe family. Several extensions however have improved its capabilities so that it is also applicable to crystalline solar cells (Si and GaAs family) and amorphous cells (a-Si and micromorphous Si). An overview of its main features is given below:

- Up to 7 semiconductor layers
- Almost all parameters can be graded (i.e. dependent on the ocal composition or on the depth in the cell): Eg, χ, ε, N_C, N_V, v_{thn}, v_{thp}, μ_n, μ_p, N_A, N_D, all traps (defects) N_t
- Recombination mechanisms: band-to-band (direct), Auger, SRH-type
- Defect levels: in bulk or at interface; their charge state and recombination is accounted for
- Defect levels, charge type: no charge (idealisation), monovalent (single donor, acceptor), divalent (double donor, double acceptor, amphoteric), multivalent (user defined)
- Defect levels, energetic distributions: single level, uniform, Gauss, tail, or combinations
- Defect levels, optical property: direct excitation with light possible (impurity photovoltaic effect, IPV)
- Defect levels, metastable transitions between defects
- Contacts: work function or flat-band; optical property (reflection of transmission filter) filter

- Tunneling: intra-band tunneling (within a conduction band or within a valence band); tunneling to and from interface states
- Generation: either from internal calculation or from user supplied g(x) file
- Illumination: a variety of standard and other spectra included (AM0, AM1.5D, AM1.5G, AM1.5Gedition2, monochromatic, white,...)
- Illumination: from either the p-side or the n-side; spectrum cut-off and attenuation
- Working point for calculations: voltage, frequency, temperature
- The program calculates energy bands, concentrations and currents at a given working point, J-V characteristics, ac characteristics (C and G as function of V and/or f), spectral response (also with bias light or voltage)
- Batch calculations possible; presentation of results and settings as a function of batch parameters
- Loading and saving of all settings; start-up of SCAPS in a personalised configuration; a script language including a free user function
- Very intuitive user interface
- A script language facility to run SCAPS from a 'script file'; all internal variables can be accessed and plotted via the script.
- A built-in curve fitting facility
- A panel for the interpretation of admittance measurements

3.3 Fundamental equations in semiconductors:

Semiconductors physics is an area very rich in modeling and mathematics problems. It consists of a fundamental set of equations that bring together electrostatic potential and load carriers in a very specific field of simulation. These equations, which are resolved via specific software for simulating semiconductor-based devices, are derived from Maxwell equations. [37]

They are mainly: Poisson's equation and continuity equations for both electrons and holes given by the following equations, which are used by SCAPS:

$$\frac{\partial^2 \psi}{\partial x^2} + \frac{q}{\varepsilon}\left[p(x) - n(x) + N_D - N_A + \rho_p - \rho_n\right] = 0 \quad (3.1)$$

$$\frac{1}{q}\frac{dJ_p}{dx} = G_{op}(x) - R(x) \quad (3.2)$$

$$\frac{1}{q}\frac{dJ_n}{dx} = -G_{op}(x) + R(x) \quad (3.3)$$

Ɛ: the dielectric constant

q: the electron charge

N_A: acceptor density

N_D: donor density

ψ: the electrostatic potential

p: hole concentration

n: electron concentration

ρ_p: hole distribution

ρ_n: electron distribution

J_p: current densities of hole

J_n: current densities of electron

G_{op}: the optical generation rate

R: the net recombination from direct and indirect recombination.

3.4 SCAPS interface

SCAPS is a Windows-oriented program, developed with LabWindows/CVI of National Instruments. Scaps use the LW/CVI terminology of a 'Panel' (names used in other software's are: a window, a page, a popup…). SCAPS opens with the 'Action Panel'.

Figure 3.1: SCAPS the Action panel or main panel.

The action panel consists of 5 parts

1. Working point
2. Indicate what you will calculate, i.e. which measurement you will simulate
3. Set problem (define the problem)
4. Start the calculation(s)
5. Display the simulated curves

3.5 Define the working point

The working point specifies the parameters which are not varied in a measurement simulation, and which are relevant to that measurement. Thus

- The temperature T: relevant for all measurements. Note: in SCAPS, only $N_C(T)$, $N_V(T)$, the thermal velocities, the thermal voltage kT and all their derivatives are the only variables which have an explicit temperature dependence; you must input for each T the corresponding materials parameters yourself.
- The voltage V: is discarded in I-V and C-V simulation. It is the dc-bias voltage in C-f simulation and in QE(λ) simulation. SCAPS always starts at 0 V, and proceeds at the working point voltage in a number of steps that you also should specify.
- The frequency f: is discarded in I-V, QE(λ) and C-f simulation. It is the frequency at which the C-V measurement is simulated.
- The illumination: is used for all measurements. For the QE(λ) measurement, it determines the bias light conditions. The basis settings are: dark or light, choice of the illuminated side, choice of the spectrum. A one sun (= 1000 W/m^2) illumination with the 'air mass 1.5, global' spectrum is the default, but you have a large choice of monochromatic light and spectra for your specialized simulations. If you have an optical simulator at your disposal you can immediately load a generation profile as well instead of using a spectrum.

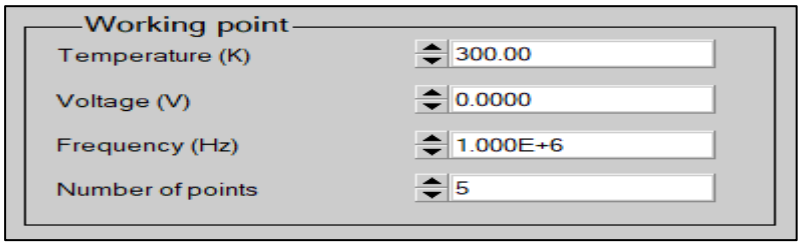

Figure 3.2: SCAPS working point

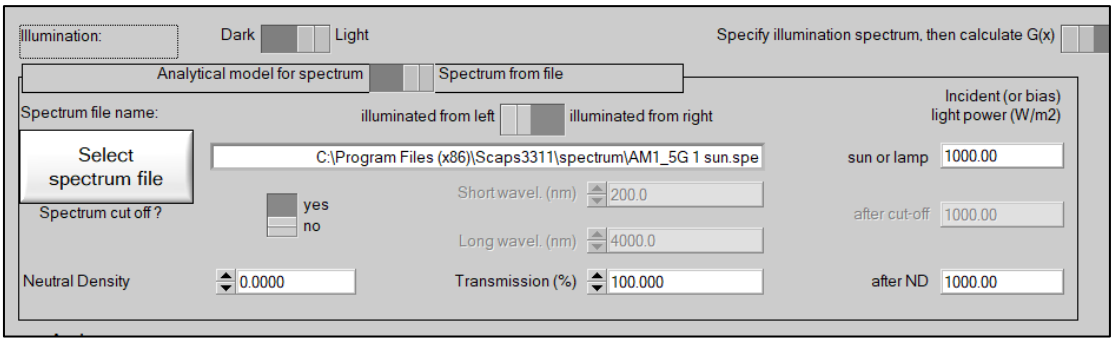

Figure 3.3: SCAPS spectrum and illumination

3.6 Spectrum and illumination:

Choose if you are simulating in dark or light, and select spectrum file you can find many files in SCAPS data base.

3.7 Select the measurement(s) to simulate

In the action-part of the Action Panel, you can select one or more of the following measurements to simulate: I-V, C-V, C-f and QE(λ). Adjust if necessary the start and end values of the argument, and the number of steps. Initially, do one simulation at a time, and use rather coarse steps: your computer and/or the SCAPS program might be less fast than you hope, or your problem could be really tough... A hint: in a C-V simulation, the I-V curve is calculated as well; no need then to specify it separately.

3.8 Define the problem:

When clicking the 'Set Problem'-button on the action panel, the 'Solar cell definition'-panel is displayed. This panel allows to create/edit solar cell structures and to save those to or load from definition files. These definition files are standard ASCII-files with extension '*.def' which can be read with e.g. notepad. Even though the format of these files seems self-explaining it is however strongly advised not to alter them manually. You can design your solar cell and change different layers by clicking on add layer and modify properties such us thickness, band gap

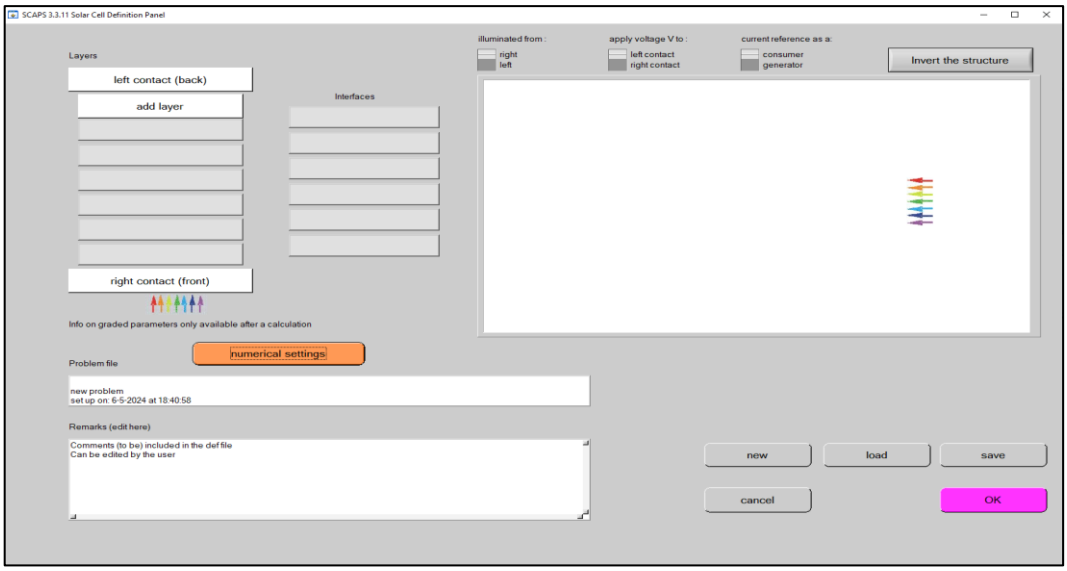

Figure 3.4: SCAPS solar cell definition panel

3.9 Change parameters:

By clicking on a layer, you can alter its thickness and band gap, among other factors.

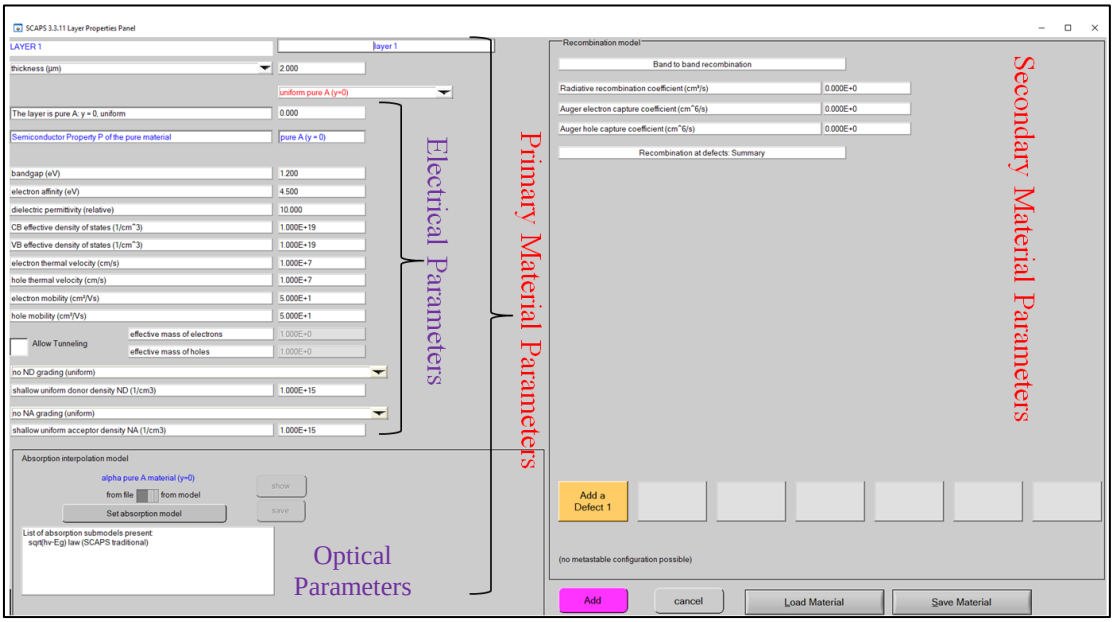

Figure 3.5: Parameters of the layer

3.10 Start the calculation(s):

We have 3 different types of calculation single shot, batch and recorder:

- **Single shot calculation:** when clicking on the button (calculate: single shot) the calculations start. At the bottom of the Panel, you see a status line, e.g. “iv from 0.000 to 0.800 Volt: V = 0.550 Volt”, showing you how the simulation proceeds. Meanwhile, SCAPS stands you a free movie how the conduction and valence bands, the Fermi levels and the whole caboodle are evolving.

When you see the hated divergence message, you're entitled to get into a bad mood, but don't exaggerate. Anyway, you did not lose the I-V points already calculated.

- **Batch calculation:** When you want to explore the influence of one or a few parameters to the solar cell characteristics, you can take profit of the batch option. When you click Batch set-up, a panel opens where you can choose which parameter to vary, over which range, and in which mode (Lin, Log or custom). You can also define more than one parameter, and vary all of them (in a nested way or 'simultaneous'), but be modest to start. A batch calculation is launched when calculate: batch is clicked.

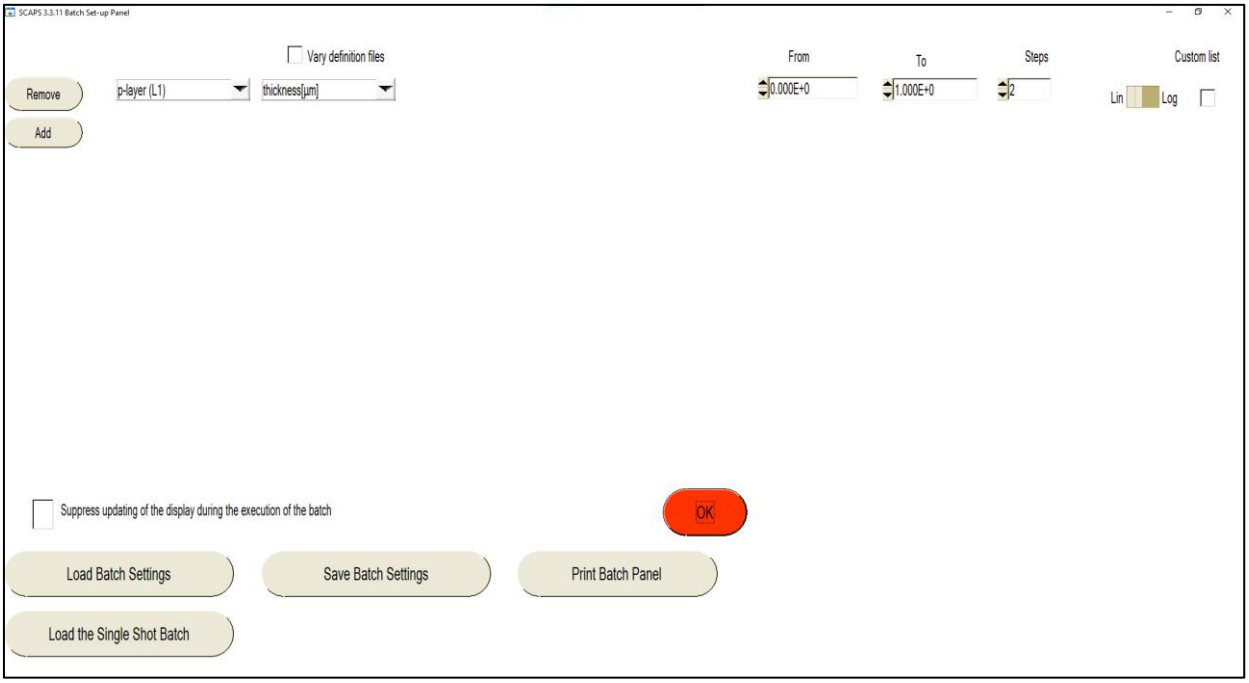

Figure 3.6: Batch set-up panel

3.11 Display the simulated curves:

After the calculation(s), SCAPS switches to the Energy band panel (or the AC-band panel). You can now look at your ease to the band diagrams; carrier densities, current densities, at the last bias point calculated (stop your calculations earlier, or use the pause button on the Action Panel if you want to look at an intermediate state at ease). You can output the results (buttons print, save graphs, show (then the numbers are shown on screen; cut & paste to e.g. Excel is possible), or save (then the numbers are

saved to a file). You can switch to one of the specialized output Panels (if you have already simulated at least one corresponding measurement). We only show the example of the IV Panel

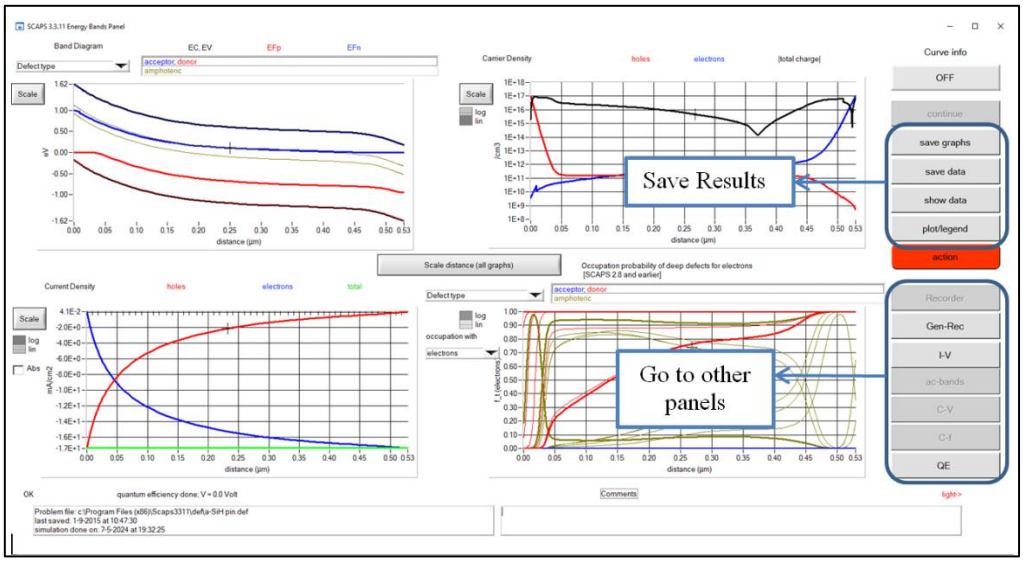

Figure 3.7: SCAPS energy band panel

3.12 Conclusion

In this chapter, we described SCAPS-1D simulation program. We started with introducing the fundamental equations in semiconductors which are used by SCAPS. We explained how to use necessary functions in this program and how to start simulating and finding results.

Chapter 4: Simulation and Results

4.1 Introduction:

The most promising option for third-generation solar cell technology is the Organic Inorganic Perovskite Solar Cell (PSC), which can be economically fabricated and has good electrical and optical features. Recent years have witnessed remarkable advancements in PSC research, leading to improved performance relative to cost.

Simple 1D simulation based study is presented in this work for $CH_3NH_3PbI_3$ (also known as $MAPbI_3$) based PSC with all inorganic metal oxide transport layers in a p–I–n configuration. NiO_x, a high bandgap p-type oxide is chosen as HTM to provide better optical transparency for incoming light. On the other hand, ETMs as TiO_2.

4.2 Describe the structure of a perovskite single junction solar cell:

The schematic diagram of the solar cell, shown in Figure, illustrates the typical p-i-n structure of a. The Thickness of $CH_3NH_3PbI_3$ ($MAPbI_3$) perovskite layer is 350 nm and it's positioned between the HTM and ETM layers, NiOx is used as the HTM in all structures with a thickness of 80 nm. For the ETM layer, two different metal oxides—TiO_2, ZnO—are alternately utilized, each also having a thickness of 80 nm, and their performances are compared.

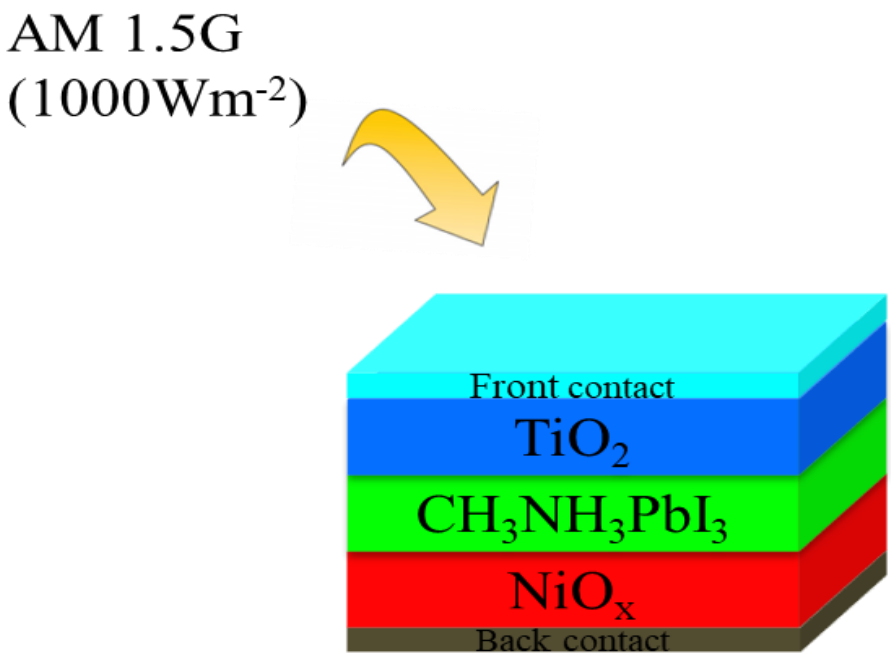

Figure 4.1: Schematic diagram of p-i-n $CH_3NH_3PbI_3$ (MAPbI3) PSC Structure used in the simulation.

4.3 Selection of Material Parameters

Table 4.1: Electrical and optical properties of different layer used in SCAPS [38][39][40].

Characteristics	**NiOx**	**$MAPbI_3$**	**TiO_2**	**ZnO**
Thickness(nm)	80	350	80	80
Bandgap(eV)Eg	3.75	1.56	3.3	3.2
Electron affinity(ev)	2.1	3.9	4.2	4.10
Dielectric permittivity	10.7	10	10	8.1
CB effective density of states(1/cm^3)	2.8×10^{19}	2.76×10^{18}	3.16×10^{18}	4.5×10^{18}
VB effective density of states(1/cm^3)	1.8×10^{19}	3.9×10^{18}	2.5×10^{19}	1×10^{18}
Electron thermal velocity(cm/s)	1×10^{7}	1×10^{7}	1×10^{17}	1×10^{7}
Hole thermal velocity(cm/s)	1×10^{7}	1×10^{7}	1×10^{17}	1×10^{7}
Electron mobility(cm^2/Vs)	12	15	0.1	300
Hole mobility(cm^2/Vs)	25	15	0.1	1
Shallow uniform donor density ND ($1/cm^3$)	0	0	1×10^{19}	1×10^{19}
Shallow uniform acceptor density NA ($1/cm^3$)	1×10^{15}	1×10^{11}	0	0

Figure 4.2: simulated structure of the p-i-n $CH_3NH_3PbI_3$ (MAPbI3) PSC in SCAPS.

4.4 The basic perovskite solar cell results

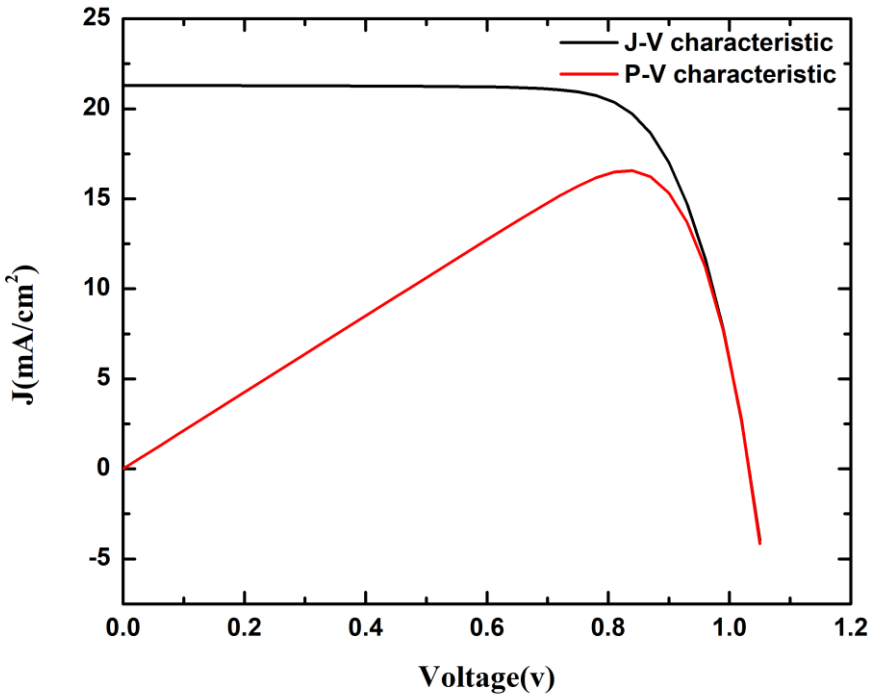

Figure 4.3: J-V and P-V characteristic curves of perovskite solar cell (figure 4.1).

Table 4.2: I-V characteristic resulted from PSC simulation of (figure 4.1).

Parameter	Result with TiO_2
V_{OC} (v)	1.033044
J_{SC} (mA/cm^2)	21.2995813
FF (%)	75.321
Eta (%)	16.5733

4.5 Analysis with the Variation of Absorber ($MAPbI_3$) Thickness

To observe the effect of absorber ($MAPbI_3$) layer thickness on solar cell performance, the thickness is varied from 350 nm to 1000 nm keeping all other parameters same as before for TiO_2 structures.

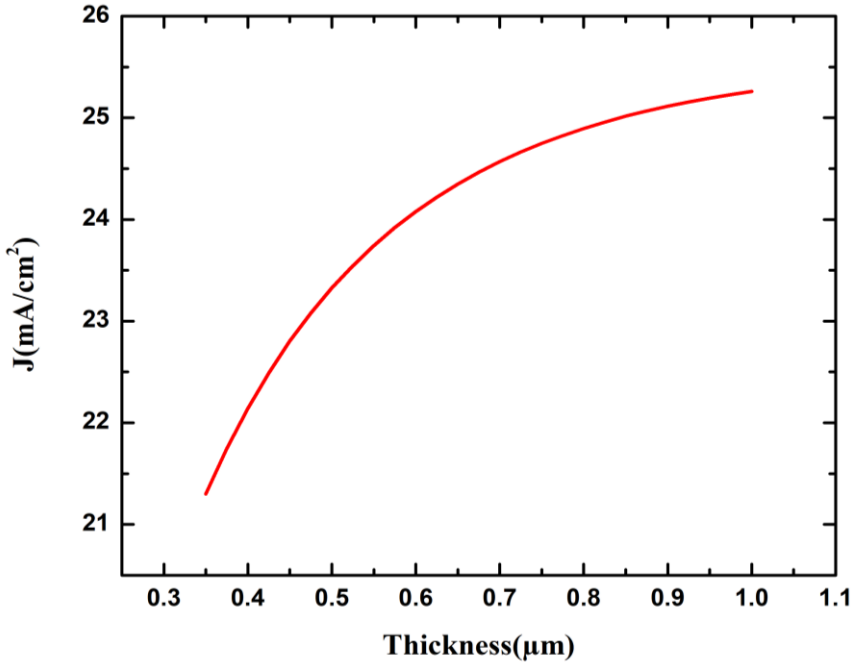

Figure 4.4: J–V characteristics for difference thickness of $MAPbI_3$.

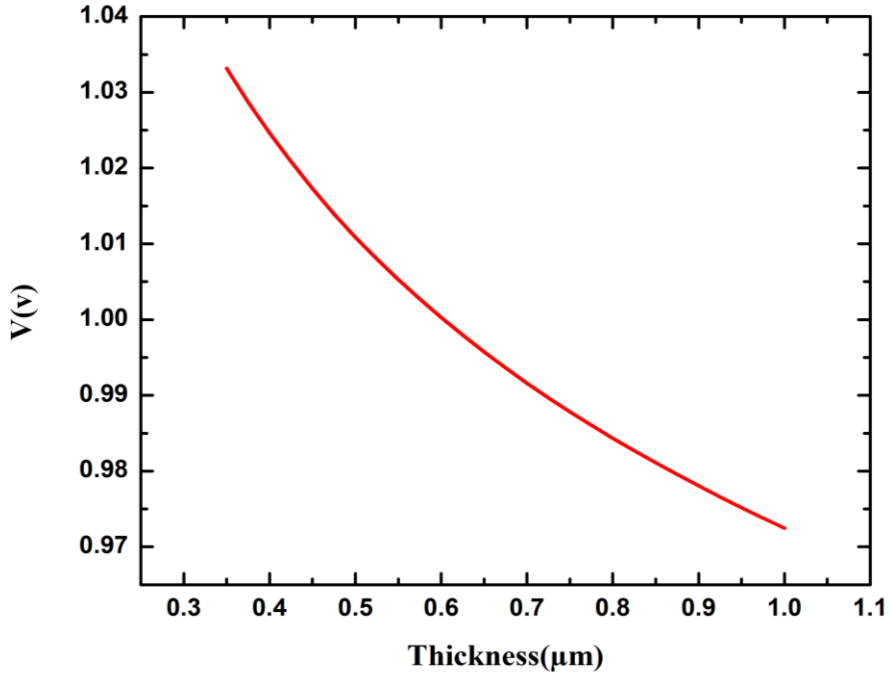

Figure 4.5: Open circuit Voltage as function of thickness of $MAPbI_3$.

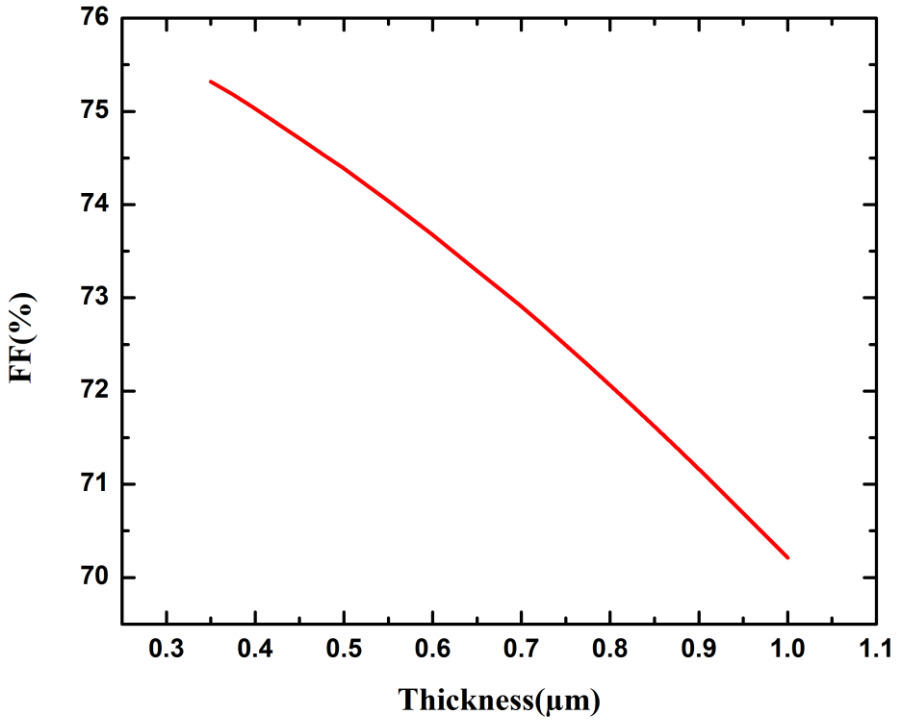

Figure 4.6: Fill factor curve as function of thickness of $MAPbI_3$.

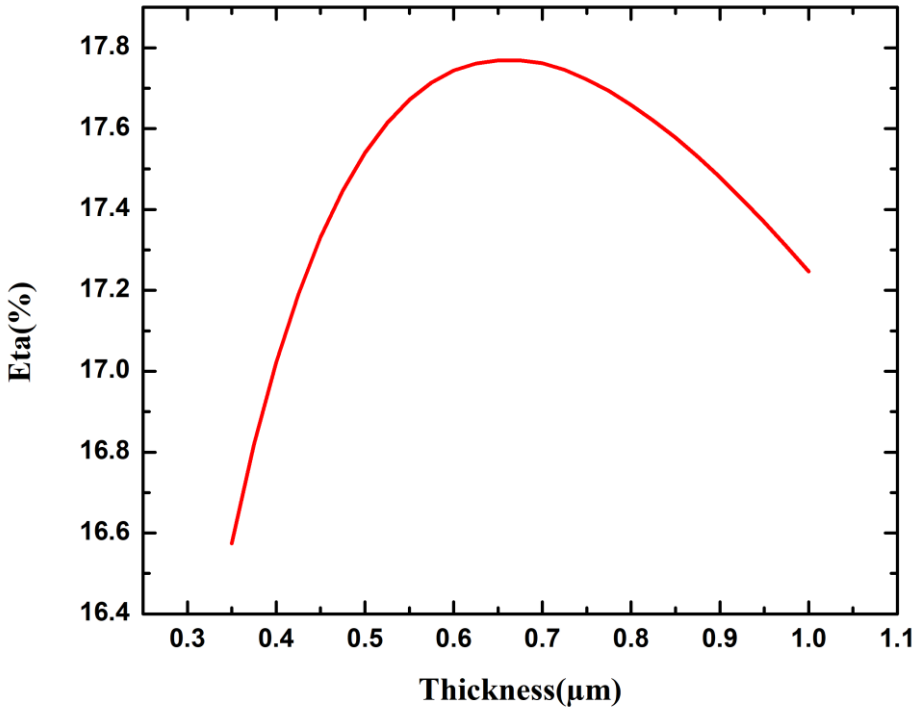

Figure 4.7: Effect of variation of $MAPbI_3$ thickness on Efficiency.

Table 4.3: The effect of changing the thickness of MAPbI3 on solar cell performance.

Thickness(µm)	V_{OC} (V)	J_{SC} (mA/cm^2)	FF (%)	Eta%
0.35	1.03316	21.29958	75.31858	16.57445
0.4	1.02462	22.1426	75.02768	17.02203
0.45	1.01729	22.80321	74.71211	17.33138
0.5	1.01088	23.32573	74.38731	17.54022
0.55	1.00528	23.74253	74.03865	17.67141
0.6	1.00029	24.07741	73.67423	17.74395
0.65	0.99572	24.34837	73.29024	17.76865
0.7	0.99159	24.56857	72.90676	17.76156
0.75	0.98782	24.74828	72.48972	17.72139
0.8	0.98434	24.89532	72.06075	17.65885
0.85	0.98112	25.01575	71.618	17.57745
0.9	0.97806	25.11432	71.16132	17.47959
0.95	0.97518	25.19477	70.69243	17.36866
1	0.97246	25.26007	70.20934	17.24659

(Figure 4.4) showing the increase in short-circuit current density (J_{sc}) with increasing thickness, is from a study on perovskite solar cells, specifically utilizing the $MAPbI_3$ perovskite material as the absorber layer. The upward trend in J_{sc} indicates that thicker perovskite layers, despite slightly lower absorption coefficients, can enhance charge carrier extraction and improve the photocurrent generation capability, which is crucial for achieving higher power conversion efficiencies in perovskite-based photovoltaic devices.

It is observed that (Figure 4.5) shows the open-circuit voltage (V_{oc}) of a perovskite solar cell decreasing as the thickness of the $MAPbI_3$ absorber layer increases, suggesting a trade-off between improved light absorption at higher thicknesses and increased recombination losses that lower the V_{oc}. Optimal thickness is crucial to balance these competing effects for maximizing device performance.

(Figure 4.6) shows the fill factor (FF) curve for a perovskite solar cell as a function of absorber layer thickness. The fill factor decreases linearly from about 75% to 70% as the thickness increases from 0.3 µm to 1.0 µm. This indicates that thicker absorber

layers result in reduced fill factors, likely due to increased recombination losses and decreased charge collection efficiency.

From the result in (figure 4.7) shows that the power conversion efficiency of $MAPbI_3$ perovskite solar cells follows a bell-shaped curve as a function of absorber layer thickness. Efficiency increases with thickness, peaks at around 17.76% for a thickness of 0.6-0.7 μm, and then decreases with further increases in thickness. These trends results from the balance between improved light absorption and short-circuit current in thicker layers, and higher recombination losses and lower open-circuit voltages. The optimal thickness of 0.6-0.7 μm maximizes efficiency by optimizing current collection and minimizing voltage losses, providing key insights for designing high-efficiency $MAPbI_3$-based photovoltaics.

4.6 Comparative study between TiO_2, ZnO of perovskite Transparent Conductive Oxide layers

As the justification of the simulation environment is being established, the simulation is being carried out for two ETMs (TiO_2 & ZnO) keeping the same HTM (NiOx) and the same $MAPbI_3$ thickness 650nm.

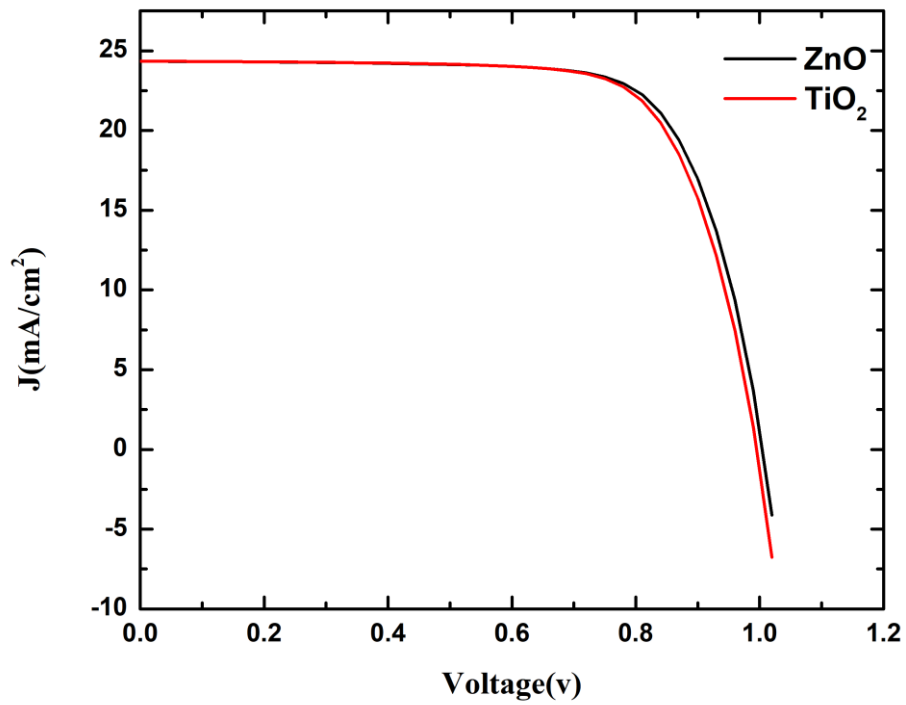

Figure 4.8: I-V characteristic curve for p-i-n PSC for TiO_2 and ZnO at perovskite layer thickness 650 nm

Table 4.4: I-V characteristic resulted from PSC simulation with TiO_2 and ZnO layers

Parameter	Result with TiO_2	Result with ZnO
V_{OC} (v)	0.995677	1.0051
J_{SC} (mA/cm^2)	24.348366	24.344832
FF (%)	73.306	73.6641
Eta (%)	17.7717	18.0259

4.7 Results and discussion

The p-i-n PSC structure for two different ETMs namely TiO_2 and ZnO are analyzed for same absorber ($MAPbI_3$) layer thickness (650 nm), it is observed that, ZnO have superior performance over TiO_2 which is the mostly used ETM in perovskite research so far specially for microscopic structure.

The cell containing ZnO as ETM exhibits higher Eta (0.25% increased than TiO_2)

4.8 Optimization of thicknesses of NiO_x

(Figure 4.8) demonstrates that as the thickness of the NiO_x layer increases, the efficiency of the solar cell decreases. Based on this observation, we have decided to use a NiO_x thickness of 30 nm to achieve an optimal efficiency of 19.6%. This thickness strikes a balance between material usage and maintaining high efficiency.

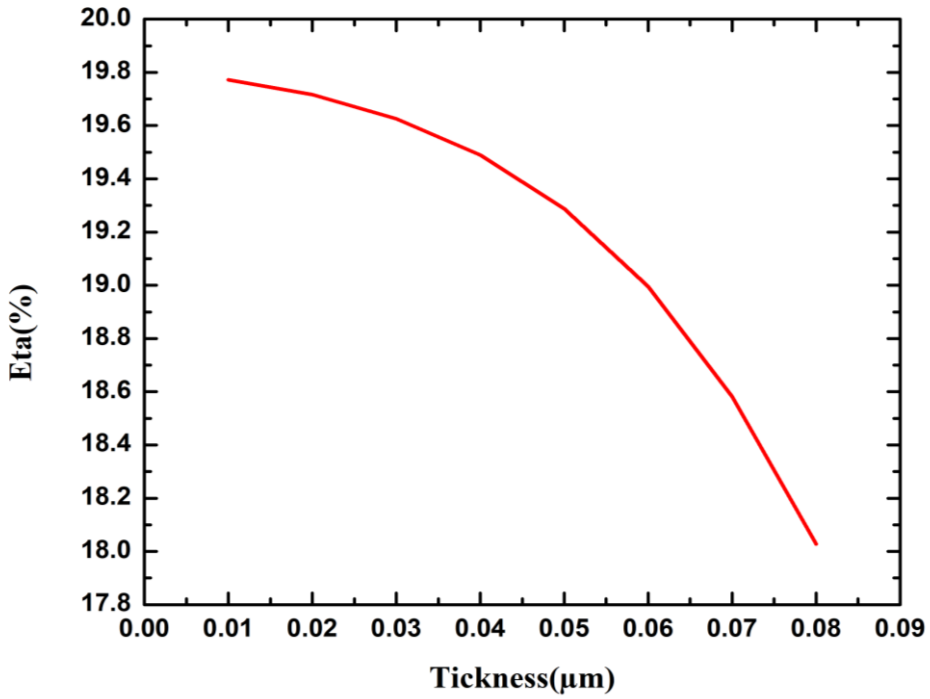

Figure 4.9: Effect of NiO_x thickness on Efficiency.

4.9 Conclusion

In this chapter, the effects of using inorganic transparent oxides metal (TiO_2 ,ZnO) and deferent thickness of $MAPbI_3$ on perovskite solar cell is thoroughly studied using SCAPS 1D program. The main focus is given to seek some transport material properties which are controlling key PSC performances, and optimizing the thickness of the observer to get maximum efficiency.

General Conclusion

In this work, we focused on studying and enhancing the performance of perovskite solar cells by modifying their composition. Perovskite solar cells, composed of multiple layers containing the perovskite compound, are an innovative type of solar cell. To achieve maximum efficiency in converting solar energy to electrical energy, it is essential to improve their properties and components.

Achieving the highest yield requires optimizing factors such as electrical charge conduction, light transmission, and reducing energy loss. The composition and arrangement of different layers in the cell significantly affect these factors. One issue identified in previous studies is the decreased efficiency due to TiO2, which has defects impacting cell performance. Thus, searching for alternatives is crucial.

We proposed using ZnO as a substitute for TiO2. ZnO possesses unique properties making it a strong candidate for improving perovskite solar cell performance. Based on our study, we believe that incorporating ZnO can significantly enhance the efficiency of perovskite solar cells. Therefore, ZnO should receive considerable attention in future research and development.

In summary, this work involved studying and improving perovskite solar cells by altering their structure and using ZnO instead of traditional materials. We believe that this approach may be an effective and promising solution for the future.

Reference

[1] Union of Concerned Scientists. (2019). *How electricity is generated.

[2] International Energy Agency. (2020). *Electricity information: Overview.

[3] World Health Organization. (2018). Air pollution.

[4] Intergovernmental Panel on Climate Change. (2014).

[5] International Renewable Energy Agency. (2020). Renewable energy statistics 2020.

[6] National Renewable Energy Laboratory. (2021). Renewable electricity futures study.

[7] Fraunhofer Institute for Solar Energy Systems. (2021). Photovoltaics report.

[8] National Renewable Energy Laboratory. (2020). Photovoltaic research.

[9] Solar Energy Industries Association. (2021). Solar power.

[10] EnergySage. (2020). The advantages of solar energy.

[11] Callister, W. D., & Rethwisch, D. G. (2020). Materials science and engineering: An introduction (10th ed.). John Wiley & Sons.

[12] Streetman, B. G., & Banerjee, S. K. (2015). Solid state electronic devices (7th ed.). Pearson.

[13] Lutz, G. (2007). *Semiconductor radiation detectors. Springer.

[14] eeeguide.com. (2024, May 25). Energy band diagram of semiconductors, insulators,andmetals.https://www.eeeguide.com/energy-band-diagram-of-semiconductors-insulators-and-metals/

[15] S. M. Sze and M. K. Lee, “Semiconductor devices: phys-ics and technology. 3-rd edition.-New York, John Wiley and Sons, Inc,” 2012.

[16] Husainat, A., Ali, W., Cofie, P., Attia, J., & Fuller, J. (2019). Simulation and analysis of methylammonium lead iodide (CH3NH3PbI3) perovskite solar cell with Au contact using SCAPS 1D simulator. American Journal of Optics and Photonics, 7(2), 33.

[17] Ossila. (2024, May 25). Perovskites and perovskite solar cells: An introduction. https://www.ossila.com/pages/perovskites-and-perovskite-solar-cells-an-introduction

[18] Husainat, A., Ali, W., Cofie, P., Attia, J., & Fuller, J. (2019). Simulation and analysis of methylammonium lead iodide (CH3NH3PbI3) perovskite solar cell with

Au contact using SCAPS 1D simulator. American Journal of Optics and Photonics, 7(2), 33.

[19] Correa-Baena, J. P., Saliba, M., Buonassisi, T., Grätzel, M., Abate, A., Tress, W., & Hagfeldt, A. (2017). Promises and challenges of perovskite solar cells. Science, 358(6364), 739-744.

[20] Chen, J. C. (2021). فيزياء الطاقة الشمسية (M. F. Khodr, Ed.; M. M. Fouad, Trans.).

[21] M.A.M. Al-Alwani et al. Renewable and Sustainable Energy Reviews 65 (2016) 183–213

[22] ned.ipac.caltech.edu. (2024, May 25). Excitation of photoluminescence. https://ned.ipac.caltech.edu/level5/Sept03/Li/Li4.html

[23] G. Barbarino, F. Barbato, and E. Nocerino, "The Semiconductor Multiplication System
for Photoelectrons in a Vacuum Silicon Photomultiplier Tube (VSiPMT) and Related Front End Electronics."

[24] J. Nelson, The Physics of Solar Cells, Imperial College Press, 2003 Sze, S. M. (1981). Physics of semiconductor devices (2nd ed.). Wiley.

[25] Thomas, S. (Ed.). (2019). Nanomaterials for solar cell applications. Elsevier

[26] Practical Handbook of Photovoltaics_ Fundamentals and Applications

[27] Kateb M.N, Mokrani Z. (2011). Conception et simulation électrique d'une cellule solaire en Si par le logiciel Tcad-Silvaco (Master's thesis).

[28] Ossila.(2024,/May/25).Equivalent circuit of solar cell. https://www.ossila.com/pages/equivalent-circuit-of-solar-cell

[29] Karim, S., Machkour, N., Zegrari, M., Aitelmahjoub, A., & Sabiri, Z. (2018). Modeling photovoltaic system using MATLAB/Simulink. Smart Application and Data Analysis for Smart Cities (SADASC'18).

[30] Iowa State University. (2024, May 25). EE 303 Energy systems and power electronics: Photovoltaic energy.
https://wzy.ece.iastate.edu/Courses/EE303/8_Photovoltaics.pdf

[31] Dambhare, M. V., Butey, B., & Moharil, S. V. (2021, May). Solar photovoltaic technology: A review of different types of solar cells and its future trends. In Journal of Physics: Conference Series (Vol. 1913, No. 1, p. 012053). IOP Publishing.

[32] Moon, M. M. A., Rahman, M. F., Hossain, J., & Ismail, A. B. M. (2019). Comparative study of the second generation a-Si: H, CdTe, and CIGS thin-film solar cells. Advanced Materials Research, 1154, 102-111.

[33] N. R. E. Laboratory, "Best Research-Cell Efficiency Chart." NREL Golden, CO, 2023.

[34] Tsutomu Miyasaka - Perovskite Photovoltaics and Optoelectronics_ from Fundamentals to Advanced Applications (2022, Wiley-VCH)

[35] QDsolar. (2024, May 25). QD Solar can deliver much higher efficiencies and energy density. https://qdsolarinc.com/technology/

[36] Burgelman, M., Nollet, P., & Degrave, S. (2000). SCAPS: A simulation program for the electric and optical characteristics of thin-film solar cells. University of Gent.

[37] Khelfaoui-Hala. (2022). Simulation of thin film solar cells using the SCAPS-1D program. University of Mohammed Boudiaf Msila.

[38] Rahman, M. S., Miah, S., Marma, M. S. W., & Sabrina, T. (2019, February). Simulation based investigation of inverted planar perovskite solar cell with all metal oxide inorganic transport layers. In 2019 International Conference on Electrical, Computer and Communication Engineering (ECCE) (pp. 1-6). IEEE.

[39] Haruyama, J., Sodeyama, K., Han, L., & Tateyama, Y. (2016). Surface properties of CH3NH3PbI3 for perovskite solar cells. Accounts of Chemical Research.

[40] BENSALAH M. N. E.I (2022). Simulation et optimisation d'une cellule solaire a base de materiaux perovskite hybride ($CH_3NH_3PbI_{3-X}Cl_X$). Université SAAD DAHLAB de BLIDA